

University of Southern Queensland
Faculty of Health, Engineering & Sciences

**Non-invasive methods for testing the integrity of bulkheads
and/or deckheads during a fire**

A dissertation submitted by

Michael Gall

in fulfilment of the requirements of

ENG4111 and ENG4112 Research Project

towards the degree of

Bachelor of Engineering (Honours) (Mechanical)

Submitted: October, 2016

Abstract

The project aimed to investigate and evaluate a possible non-invasive test method to assess the integrity of bulkheads and/or deckheads during a fire. Currently there is not an accurate method for determining the integrity of a bulkheads and/or deckheads during a fire on-board a ship. This leads to a higher risk being placed on fire fighters.

A literature review was conducted, following which it was determined that Air Coupled Ultrasonics (ACU) was the most viable non-invasive test method for the project. Optimisation of the ACU test method was conducted for use under fire conditions. Aluminium, GFRP and CFRP plates were placed under fire conditions using a LPG bottle and burner. The plates underwent ACU testing at 10°C increments. Results were evaluated in relation to suitability for use of the chosen non-invasive test method, impact of temperature on results and material properties, and structural integrity issues. The results showed the lamb wave velocity greatly changed as the elastic properties of the material changed due to the thermal loading on the plates caused by the fire.

Even though the results showed that the lamb wave velocity greatly changed as the material underwent a significant change in elastic properties, before ACU is suitable for in-service implementation, further research and development is required. Further research and development is required into ultrasonic transducer bandwidth, waveform generator pulse, oscilloscope, depth of penetration and portability to ensure accuracy and reliability in results.

University of Southern Queensland
Faculty of Health, Engineering & Sciences

ENG4111/2 <i>Research Project</i>
--

Limitations of Use

The Council of the University of Southern Queensland, its Faculty of Health, Engineering & Sciences, and the staff of the University of Southern Queensland, do not accept any responsibility for the truth, accuracy or completeness of material contained within or associated with this dissertation.

Persons using all or any part of this material do so at their own risk, and not at the risk of the Council of the University of Southern Queensland, its Faculty of Health, Engineering & Sciences or the staff of the University of Southern Queensland.

This dissertation reports an educational exercise and has no purpose or validity beyond this exercise. The sole purpose of the course pair entitled “Research Project” is to contribute to the overall education within the student’s chosen degree program. This document, the associated hardware, software, drawings, and other material set out in the associated appendices should not be used for any other purpose: if they are so used, it is entirely at the risk of the user.

Dean

Faculty of Health, Engineering & Sciences

Certification of Dissertation

I certify that the ideas, designs and experimental work, results, analyses and conclusions set out in this dissertation are entirely my own effort, except where otherwise indicated and acknowledged.

I further certify that the work is original and has not been previously submitted for assessment in any other course or institution, except where specifically stated.

MICHAEL GALL

0061009722

Acknowledgments

I would like to acknowledge the following people:

John Billingsley for his supervision and guidance.

Ian Raymond for his supervision, guidance and sponsoring the project.

Mathew Ryan for his assistance with experimental testing, circuitry and review and critique of my report.

Keith Mackie for his review and critique of my report.

To my parents and partner, who have patiently supported me during my studies, in particular throughout this past year.

MICHAEL GALL

Contents

Abstract	i
Acknowledgments	iv
List of Figures	xiv
List of Tables	xx
List of Acronyms	xxii
List of Nomenclature	xxiv
Chapter 1 Introduction	1
1.1 Background	1
1.2 Outline of the Project	2
1.3 Problem Outline	2

1.4	Research Objectives	3
1.5	Methodology Summary	4
1.6	Project Contributions	4
1.7	Consequential Effects	5
1.8	Risk Assessment	5
1.9	Project Timeline and Resource Requirements	7
1.9.1	Project Timeline	7
1.9.2	Resource Requirements	7
1.10	Dissertation Outline	7
1.10.1	Chapter 2 - Literature Review	8
1.10.2	Chapter 3 - Methodology	8
1.10.3	Chapter 4 - System Design	8
1.10.4	Chapter 5 - Results and Discussion	9
1.10.5	Chapter 6 - Further Work	9
1.10.6	Chapter 7 - Conclusion and Recommendations	10
 Chapter 2 Literature Review		 11
2.1	Infrared Thermal Sensing	11
2.2	Eddy Current	12

2.3	Acoustic Emission	14
2.4	Ultrasonics	16
2.4.1	Longitudinal Waves	17
2.4.2	Shear Waves	17
2.4.3	Rayleigh Waves	17
2.4.4	Lamb Waves	18
2.4.5	Critique	19
2.5	Low Frequency (Vibration)	20
2.5.1	Global Method	20
2.5.2	Local Method	20
2.5.3	Critique	21
2.6	Dye Penetrant Testing	21
2.7	Magnetic Powder	22
2.8	Radiography	24
2.8.1	X-ray	24
2.8.2	Gamma-ray	24
2.8.3	Neutron Radiography	25
2.8.4	Critique	26

Chapter 3	Methodology	27
3.1	Introduction	27
3.2	Air-Coupled Ultrasonics	30
3.2.1	Acoustic Impedance	31
3.2.2	Transmission Coefficient for a Plate	33
3.2.3	Wave Propagation at Incident in Homogeneous Media	35
3.2.4	Wave Propagation in Non-Homogeneous Media	38
3.2.5	Attenuation	39
3.2.6	Lamb Waves	42
3.2.7	Ultrasonic Velocity and Wavelength with Temperature	43
3.2.8	Doppler Shift	44
3.2.9	Material Properties	45
3.2.10	Material Defects	47
3.3	Aluminium Under Fire	49
3.4	Composites Under Fire	52
Chapter 4	System Design	56
4.1	System Requirements	56
4.2	Air Coupled Ultrasonics	58

4.2.1	Function Generator	58
4.2.2	Ultrasonic Transducer	61
4.2.3	Oscilloscope	64
4.2.4	Piezo Driver	66
4.2.5	Pre-Amplifier	70
4.2.6	Power Source	72
4.3	Bulkhead and Deckhead Materials	77
4.3.1	Aluminium	77
4.3.2	Glass Fibre Reinforced Plastic	78
4.3.3	Carbon Fibre Reinforced Plastic	80
4.4	Fire Simulation	81
4.5	Temperature Reading	84
4.6	Air Coupled Ultrasonics Test Method Schematic	89
 Chapter 5 Results and Discussion		94
5.1	Room Temperature Results	94
5.1.1	Aluminium	95
5.1.2	GFRP	98
5.1.3	CFRP	100

5.2	Fire Condition Results	103
5.2.1	Aluminium	103
5.2.2	GFRP	113
5.2.3	CFRP	120
5.3	Discussion	127
 Chapter 6 Further Work		 131
6.1	Air Coupled Ultrasonics Test Method	131
6.1.1	Ultrasonic Transducer	131
6.1.2	Waveform Generator	132
6.1.3	Oscilloscope	132
6.1.4	Depth of Penetration	133
6.2	In-Service Application	133
6.2.1	Distance	133
6.2.2	Feedback	134
 Chapter 7 Conclusion and Recommendations		 135
 References		 137
 Appendix A Project Specification		 146

Appendix B Risk Assessment	148
Appendix C Timeline	155
Appendix D Resource Requirements Cost	157
Appendix E Ultrasonic Transducer Data Sheet	162
Appendix F Oscilloscope Certificate of Calibration	167
Appendix G Piezo Driver Data Sheet	172
Appendix H Glass Fibre Data Sheet	179
Appendix I Carbon Fibre Data Sheet	181
Appendix J Epoxy Resin Data Sheet	184
Appendix K Arduino M0 Pro Function Generator Code	193
Appendix L Arduino Zero Function Generator Code	196
Appendix M Temperature Calibration Code	197
Appendix N Temperature Readings Code	202
Appendix O Signal Processing Code	207

Appendix P Ambiguity Function	209
-------------------------------	-----

List of Figures

2.1	Infrared Sensing NDT (Lappe 2013).	12
2.2	Eddy Current NDT (Olympus 2016).	13
2.3	Acoustic Emissions NDT (Non Destructive Testing Resource Center 2016).	15
2.4	Rayleigh Wave Mechanical Displacement (David & Cheeke 2012).	18
2.5	Lamb Waves (G Alleman & Groves 2014).	18
2.6	Global Method Low Frequency NDT (Kapadia n.d.).	21
2.7	Fluorescence of Dye Penetrant NDT (International Atomic Energy Agency 1988).	22
2.8	Magnetic Particle NDT (International Atomic Energy Agency 1988).	23
2.9	Radiography NDT (Jobs 2013).	25
3.1	Air-Coupled Ultrasonic System Block Diagram.	31
3.2	Reflection and Transmission at normal incidence for (a) planar interface and (b) layer of thickness d between two bulk media (David & Cheeke 2012).	33

3.3	Transmission Coefficient Aluminium.	35
3.4	Transmission Coefficient GFRP at 3km/s.	35
3.5	Reflection and Transmission at a liquid-solid interface with incidence (David & Cheeke 2012).	36
3.6	Reflection coefficient of an air-aluminium interface (Chimenti 2014). . . .	37
3.7	Phase velocity dispersion curves for a unidirectional fibre reinforced composite plate parallel to the direction of fibre alignment (Rose 2004). . . .	38
3.8	Phase velocity dispersion curves for a unidirectional fibre reinforced composite plate perpendicular to the direction of fibre alignment (Rose 2004). . . .	39
3.9	Lamb Wave Dispersion Curve for Aluminium Plate (Humphries n.d.). . .	42
3.10	Thermal Broadening (University of Colorado 2016).	44
3.11	Pulse-Echo Time of Flight Measurement (Non Destructive Testing Database 2000).	48
3.12	5083 Thermal Expansion with Temperature (P Summers, Allen, Mouritz, Case & Lattimer 2015).	50
3.13	5083 Young's Modulus with Temperature (P Summers et al. 2015). . . .	50
3.14	5083 Ultimate Tensile Strength with Temperature (P Summers et al. 2015). . . .	51
3.15	5083 Yield Strength with Temperature (P Summers et al. 2015).	51
3.16	Material States and Transition with Modulus (Y Bai & Vallee 2008). . . .	53

3.17 Schematic of fire damage through FRP Composite (Gardiner & Mathys 2002).	54
4.1 System Requirements Model.	57
4.2 Arduino M0 Pro.	59
4.3 Arduino M0 Pro 100 KHz Square Wave.	59
4.4 Arduino Zero.	60
4.5 Arduino Zero 100 KHz Square Wave.	61
4.6 100 KHz Ultrasonic Transducer.	62
4.7 100 KHz Directivity in Overall Sensitivity (Multicomp 2010).	62
4.8 TDS3054C.	65
4.9 MX200 Piezo Driver.	66
4.10 50mm Time of Flight.	68
4.11 Operational Amplifier Circuit.	69
4.12 Operational Amplifier Circuit.	70
4.13 Pre-Amplifier Circuit (Silicon Chip Magazine 1994).	71
4.14 Pre-Amplifier.	72
4.15 Dual Power Supply.	73
4.16 Lamb Wave Noise.	74

4.17 Dual Power Supply Noise.	74
4.18 Voltage Regulator Circuit (Texas Instruments 2013).	75
4.19 Voltage Regulator.	76
4.20 Battery Supply.	77
4.21 Aluminium 5083 H116 Plate.	78
4.22 Composite Plates (McConaghy Boats 2016).	79
4.23 Fire Triangle (Elite Fire 2013).	81
4.24 Burner.	83
4.25 Grill.	83
4.26 MAX31855 (Adafruit 2016 <i>b</i>).	85
4.27 Thermocouple Seperation.	86
4.28 Temperature Calibration.	87
4.29 SHT-31D (Adafruit 2016 <i>a</i>).	88
4.30 Schematic Diagram of Experimental ACU Set Up.	89
4.31 Transmit Air Coupled Ultrasonic Set Up.	90
4.32 Receive Air Coupled Ultrasonic Set Up.	91
4.33 Air Coupled Ultrasonic Set Up.	92
4.34 Air Coupled Ultrasonic Set Up.	93

4.35 Air Coupled Ultrasonic Set Up with Aluminium Plate.	93
5.1 Room Temperature Lamb Wave Response Aluminium.	95
5.2 ACU Reflections Model Aluminium.	97
5.3 FFT Room Temperature Aluminium.	98
5.4 Room Temperature Lamb Wave Response GFRP.	98
5.5 FFT Room Temperature GFRP.	100
5.6 Room Temperature Lamb Wave Response CFRP.	100
5.7 FFT Room Temperature CFRP.	102
5.8 Aluminium Testing Under Fire.	103
5.9 Aluminium Lamb Wave Response Under Fire 30 to 100°C.	104
5.10 Aluminium Lamb Wave Response Under Fire 110 to 180°C.	105
5.11 Aluminium Lamb Wave Response Under Fire 190 to 260°C.	106
5.12 FFT Aluminium Under Fire.	107
5.13 Ambiguity Function Aluminium Under Fire.	109
5.14 Aluminium Temperature Readings.	111
5.15 Burnt Lamb Wave Response Aluminium.	112
5.16 GFRP Testing Under Fire.	113
5.17 GFRP Lamb Wave Response Under Fire 30 to 80°C.	114

5.18	GFRP Lamb Wave Response Under Fire 100 to 160°C.	115
5.19	FFT GFRP Under Fire.	116
5.20	GFRP Temperature Readings.	118
5.21	Burnt Lamb Wave Response GFRP.	119
5.22	GFRP Post Fire	119
5.23	CFRP Testing Under Fire.	120
5.24	CFRP Lamb Wave Response Under Fire 30 to 90°C.	121
5.25	CFRP Lamb Wave Response Under Fire 100 to 160°C.	122
5.26	FFT CFRP Under Fire.	123
5.27	CFRP Temperature Readings.	125
5.28	Burnt Lamb Wave Response CFRP.	126
5.29	CFRP Post Fire	126

List of Tables

3.1	Attenuation in Air.	41
4.1	Function Generator Max Frequencies.	58
4.2	Oscilloscope Sample Rates.	64
4.3	MX200 Maximum Frequency (Hz) with capacitive load (Piezo Drive 2016).	67
4.4	Power Requirements.	73
4.5	Aluminium 5083 H116 Thermal Properties (Aerospace Specification Metals Inc 2016).	78
4.6	GFRP Thermal Properties (Colan Australia 2007).	80
4.7	CFRP Thermal Properties (AZOM 2003).	81
4.8	Flame Colour Temperatures (ELGas 2016).	82
4.9	MAX31855 Specifications (Adafruit 2016 <i>a</i>).	85
4.10	IR Temperature Sensor Specifications (Freetronics 2016).	87

4.11	SHT-31D Specifications (Adafruit 2016 <i>a</i>).	88
5.1	Aluminium ACU Fire Test Results.	110
5.2	GFRP ACU Fire Test Results.	117
5.3	CFRP ACU Fire Test Results.	124
C.1	Project Timeline.	155
D.1	Non-Invasive Test Method Resource Costing.	158
D.2	Temperature Evaluation Resource Costing.	159
D.3	Test Materials Costing	160
D.4	Fire Resource Costing.	160
D.5	Work Health and Safety (WHS) Resources Costing.	160
D.6	Miscellaneous Resources Costing.	161
D.7	Calibrated Test Equipment.	161

List of Acronyms

ACU Air Coupled Ultrasonics.

CFRP Carbon Fibre Reinforced Plastic.

COTE Coefficient of Thermal Expansion.

FRP Fibre Reinforced Plastic.

GFRP Glass Fibre Reinforced Plastic.

HAZ Heat Affected Zone.

LPG Liquefied Petroleum Gas.

N/A Not Available.

OFC Oxygen Free Copper.

Op-Amp Operational Amplifier.

PK-PK Peak to Peak.

PWM Pulse Width Modulation.

RMS Root Mean Square.

TOF Time of Flight.

WHS Work Health and Safety.

YCOB Yttrium Calcium OxyBorate.

List of Nomenclature

C_{ijk} Stiffness Tensor.

C_L Load Capacitance.

G Shear Modulus (GPa).

I_{av} Current Limit.

V/us Voltage SLew Rate (V/us).

V_L Longitudinal Velocity (m/s).

V_S Shear Velocity (m/s).

V_{P-P} Voltage Peak-Peak (V).

V_{PL} Plate Velocity (m/s).

α Attenuation.

λ Lamé's First Parameter.

λ Wavelength.

ν Poisson's Ration.

ρ Density (kg/m^3).

σ_{ijk} Stress Tensor.

σ Conductivity (mhom-1).

θ Angle ($^{\circ}$).

ε_{ijk} Strain Tensor.

$^{\circ}\text{C}$ Degrees Celcius.

f Frequency (Hz).

dB Desibels.

KHz Kilo Hertz.

mm Millimeters.

mV Millivolts.

pF PicoFarad.

us Microseconds.

V Volts.

Chapter 1

Introduction

1.1 Background

Currently there is not an accurate method for determining the integrity of a bulkheads and/or deckheads during a fire on-board a ship. When a ship is constructed from materials such as Aluminium, Glass Fibre Reinforced Plastic (GFRP) and Carbon Fibre Reinforced Plastic (CFRP), due to their comparatively low temperature resistance this can be a significant structural integrity risk. Aluminium loses 50% of its original strength at approximately 200°C (Beatrice Faggiano 2004). Therefore, at temperatures even below 200°C, a fire can have a catastrophic effect on the structural integrity of a ship. Consequently, it is of great importance that a fire on a ship be extinguished particularly early if damage or harm is to be prevented or minimised.

Measuring the temperature of a bulkhead and/or deckhead using an infra-red sensor is currently the only analysis technique employed during incidents of fire on a ship. However, a limitation of an infra-red sensor is that it only provides the temperature of the material face with which it is physically aimed at. Information on the material itself, for instance integrity, is not gained and are limited by the accuracy of the sensor.

As a result, a higher risk being placed on fire fighters as they are required to enter an environment during an active fire without being able to assess if the bulkhead and/or deckhead holding the compartment together is structurally sound.

Non-invasive testing is a way to inspect, test or evaluate the properties of a material without causing damage. The project aimed to investigate and evaluate a possible non-invasive test method to assess the integrity of bulkheads and/or deckheads during a fire.

1.2 Outline of the Project

The project began with a review of current non-invasive test methods to assess their advantages and limitations. From the findings of this review the most viable test method was determined. The most suitable non-invasive test method was investigated further to allow for optimisation with respect to the project. Research into Aluminium, GFRP and CFRP material properties and integrity issues under high temperatures and fire was conducted to optimise the test method design to acquire this information. Through testing and evaluation this test method was further developed to optimise the results achieved. The optimised test method design was evaluated for feasibility for in-service use.

1.3 Problem Outline

The project aimed to investigate and evaluate a non-invasive test method to assess the integrity of bulkheads and/or deckheads during a fire.

Through testing and evaluation an optimum design configuration of the chosen non-invasive test method was determined. The material properties and integrity results evaluated through the chosen test method was analysed for their assistance in helping the

end-user understand the incumbent fire. This optimised design was evaluated for feasibility for in-service use.

1.4 Research Objectives

The research objectives were derived from the Project Specification at Appendix A

- Research non-invasive methods for testing integrity of materials during a fire.
 - Covered in Chapter 2.
- Design a potential non-invasive test method to determine integrity of a material.
 - Covered in Chapter 3 and 4.
- Test the chosen non-invasive method on Aluminium and GFRP under fire conditions up to 200°C.
 - Covered in Chapter 5.
- Evaluate the results achieved from the chosen non-invasive test.
 - Covered in Chapter 5.
- Evaluate the feasibility of this chosen non-invasive test method.
 - Covered in Chapter 5.
- As time and resources permit:
 - Test the chosen non-invasive method against CFRP and evaluate results.
 - * Covered in Chapter 5.
 - Re-design the chosen non-invasive test method to be fully portable and suitable for a fire hazardous environment.
 - * Unable to be undertaken due to time and resource constraints.

1.5 Methodology Summary

Due to the large number of non-invasive test methods currently available, a literature review was undertaken to determine the most suitable test method for the project. From this review air-coupled ultrasonic testing was selected for further design development.

Aluminium, GFRP and CFRP material properties and integrity issues under high temperatures and fire was investigated to optimise the design configuration for acquiring this information. This was important to understand, to ensure that the information acquired from the test method is suitable, relevant and most importantly, beneficial to the end-user.

The results of preliminary testing at room temperature were evaluated, allowing for further optimisation of the design configuration before testing under fire conditions was conducted. Aluminium was heated to 260 °C and, GFRP and CFRP were heated to 160 °C using a gas bottle and burner to simulate fire conditions. The materials underwent testing at 10°C temperature increments. The test results were evaluated in relation to:

- suitability of the chosen non-invasive test method;
- impact of temperature on results;
- material properties and integrity issues evaluated;
- suitability of the results to be used as a baseline response at a set temperature; and
- limitations of this non-invasive test method.

1.6 Project Contributions

The anticipated contribution of the project to the literature includes the development of a non-invasive test method suitable for evaluating the integrity of Aluminium, GFRP and

CFRP under fire. The project should also assist in the understanding of the interaction between a fire and Aluminium, GFRP and CFRP material properties and integrity at temperature increments.

1.7 Consequential Effects

During a fire on-board a ship there is currently no accurate method of determining the integrity of a bulkhead and/or deckhead. This leads to a higher risk being placed on fire fighters. Fire fighters are required to enter an environment without knowing if it is structurally sound. The aim of the project being to design and evaluate a non-invasive test method for use during a fire that will evaluate the integrity of a material.

A greater understanding of fire impacts increases the chances of stopping a fire before it is able to cause irreversible damage to the ship, harm and injury to personnel and damage to the surrounding ecosystem. By providing vital information on the integrity of the bulkhead and/or deckhead that is supporting the ships structure, fire fighters will have an understanding on whether this structure is capable of supporting the load, or if it is about to fail. This will likely impact their approach to fighting the fire. If the information that is provided is inaccurate then this will lead to fire fighters entering an environment that is extremely unsafe which could lead to catastrophic consequences, including, personal injury or death.

1.8 Risk Assessment

To ensure that the project was undertaken in a safe and appropriate manner for all parties involved, all hazards must be identified and managed. All hazards identified and the associated risk management are detailed in Appendix B.

From the hazards identified at Appendix B, there were three with a risk level of high or above. These hazards are detailed below to ensure that the associated risk was understood and an appropriate action plan was in place and continuously reviewed.

The first hazard with a risk level of high associated with the project was Respirable fibres. Respirable fibres are fibres less than 3 microns in diameter and greater than 5 microns in length (Department of Justice & Attorney General 2015). Safe Work Australia provides guidance on the time weighted average of 0.5 fibres per mL of air for respirable fibres to minimise upper respiratory tract irritation (Safe Work Australia 2012). It was these fibres that may present a health risk during the experiment. There was a risk of these fibres becoming airborne from the plates burning at high temperatures. To manage this high risk, the experiment was undertaken outdoors to ensure adequate ventilation and the composite plates used in the experiment were undamaged with no exposed frayed fibres.

The second hazard with a risk level of high associated with the project was fumes and smoke. As the plate heats up there was a possibility of the plate burning. As the plate burns it will create smoke and fumes which by breathing in can lead to health issues such as metal fume fever. Metal fume fever can cause such health issues as malaise, myalgias, arthralgias, headache and nausea (Royal Australian College of General Practitioners 2012). To manage this high risk, the experiment was undertaken outdoors to ensure adequate ventilation, diffusion and to minimise possible exposure time.

The third hazard with a risk level of high associated with the project was the use of a motor vehicle. Use of a motor vehicle was required for the procurement of resources to undertake the project and travel to and from the experiment location. To manage this high risk, while using a motor vehicle all road rules were obeyed. Further, the motor vehicle was not be operated by a fatigued driver.

1.9 Project Timeline and Resource Requirements

1.9.1 Project Timeline

To ensure that deadlines were met and progress through the Project Specification was maintained, a timeline detailing approximate start and completion date for each aspect was necessary. This timeline is detailed in Appendix C.

1.9.2 Resource Requirements

A number of resources were required to undertake the project. These are broken into the following categories with the cost breakdown associated detailed in Appendix D:

- Non-invasive test method (Table D.1)
- Temperature Evaluation (Table D.2)
- Test Materials (Table D.3)
- Fire (Table D.4)
- WHS (Table D.5)
- Miscellaneous (Table D.6)
- Calibrated Test Equipment (Table D.7)

Detailed specification and function of the components is provided in Chapter 4.

1.10 Dissertation Outline

An overview for each chapter of the dissertation is detailed below.

1.10.1 Chapter 2 - Literature Review

This chapter provides a comprehensive literature review of non-invasive test methods.

The review highlighted that an ACU non-invasive test method was the most viable method for the hazardous environment of interest to the project.

1.10.2 Chapter 3 - Methodology

This chapter presents the methodology for the key design aspects of the chosen non-invasive test method. Further, it outlines the material properties and integrity issues for Aluminium, GFRP and CFRP under high temperatures and fire conditions.

The key design aspects of ACU were acoustic impedance, transmission coefficient for a plate, wave propagation at incident in homogeneous media, wave propagation in non-homogeneous media, attenuation, lamb waves, ultrasonic velocity with temperature, Doppler shift, material properties and material defects.

A review of material properties under fire showed that the elastic modulus of Aluminium greatly decreases after 200°C and for Composite greatly decrease after Glass Transition Temperature (T_g).

1.10.3 Chapter 4 - System Design

This chapter details the requirements, components and processes required to achieve the project specification.

An ACU test method was designed to transmit a pulsed ultrasonic waveform through the air, impinging on the test material, thereby generating a lamb wave. The ACU test method would also capture this lamb wave response through the air for analysis. Both

symmetric and antisymmetric modes of the lamb wave required capture to ensure the response was able to be fully analysed and provide ample feedback.

1.10.4 Chapter 5 - Results and Discussion

This chapter presents an analysis of the results of testing Aluminium under fire conditions up to 260 °C and, GFRP and CFRP under fire conditions up to 160 °C at 10°C increments using the designed non-invasive test method.

The results showed that ACU utilising commercially available components was suitable for testing under fire conditions. As the plates undergo thermal loading due to fire conditions, the elastic properties of the material begin to change as the material moves away from solid state. This material state change impacts the resulting lamb wave response. The results also showed there were number of limitations due to design which required further research.

1.10.5 Chapter 6 - Further Work

This chapter details further work required to ensure that the design is suitable for in-service applications. It also details other possible testing or design validation requirements for further improvements in the design.

The result showed there were a number of limitations due to design which require further research. These limitations requiring further work were categorised as either ACU design development or in-service application development.

1.10.6 Chapter 7 - Conclusion and Recommendations

This chapter summarises the project, analyses the results achieved, compares the results to the project specification, and provides recommendations.

Chapter 2

Literature Review

This chapter provides a comprehensive literature review of non-invasive test methods.

The review highlighted that an ACU non-invasive test method was the most viable method for the hazardous environment of interest to the project.

2.1 Infrared Thermal Sensing

Infrared sensors work by reading the infrared energy from the target in its field of view. As the target gets hotter, more infrared energy is emitted and detected by the infrared thermometer. There are two types of infrared sensors, first uses a thermopile which produces an electronic signal based on the temperature of the target. The second type uses a quantum detector which creates an electronic signal as the detector is struck by the photon energy radiating from the target (Lappe 2013).

The area for which the temperature is read works off the distance to spot ratio (D:S). For low end IR sensors the D:S ratio can be as low as 1:1, which compared to high end models which can have a ratio of 60:1 (Grainger 2016).

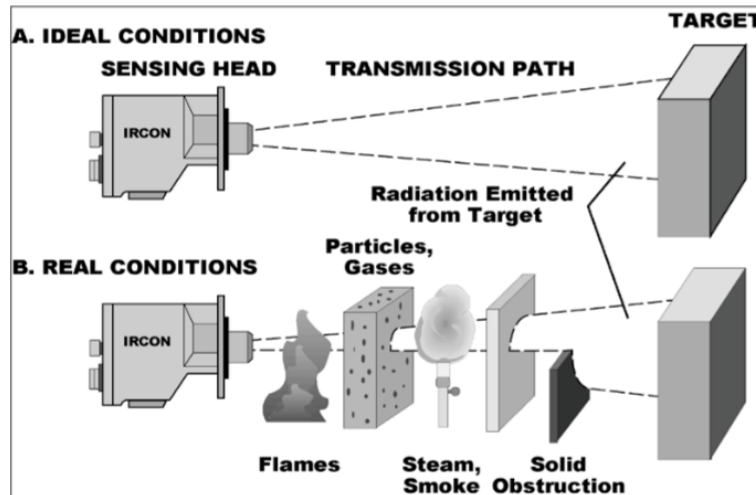


Figure 2.1: Infrared Sensing NDT (Lappe 2013).

To allow the temperature reading of objects from a safe location or through a boundary an infrared inspection window is installed to allow for the transmission of the infrared signal. The inspection window allows for a small field of view where temperature readings are able to be taken from (Robinson 2009).

Oliveira (2004) reported that the presence of inhomogeneities such as holes and cracks are able to be detected due to the local thermal property changes. Further, Cheng & Lu (2011) reported the limitations of these sensors in that they can only measure the surface temperature of the part instead of the state of the entire part.

Due to the limitations of infrared thermal sensing in only providing information at the time of reading, readings in the sensors direct line of site and limitations on the detection of flaws and defects, further analysis and development was not feasible for the project.

2.2 Eddy Current

Eddy current testing is the use of an alternating electric current passing through a coil creating an electric field (Olympus 2016). When the coil is placed near a conductive

material, it induces eddy current flow in the material by electromagnetic induction. This eddy current flow produces its own magnetic field, which modulates the impedance of the exciting coil or a secondary coil that is compared to the original coil impedance. This comparison is measured and analysed for changes in magnitude and phase of the signal to find flaws, determine conductivity, permeability and dimensions of the material. This test method is limited to use with conductive materials and near surface defects (Olympus 2016).

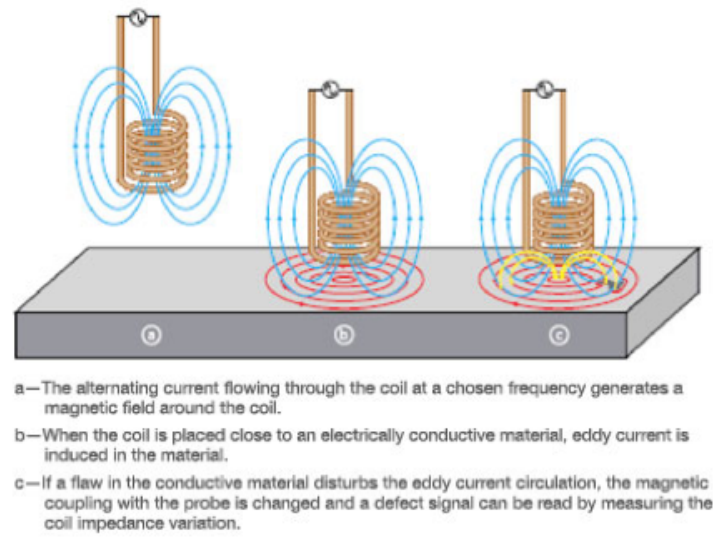


Figure 2.2: Eddy Current NDT (Olympus 2016).

For eddy current testing, the two important parameters that must be controlled are frequency and probe geometry. The frequency is the key parameter when it comes to examining surface or sub-surface defects as it determines the depth of penetration. The depth of penetration is defined as the depth at which the eddy current is 0.37 of its surface value (Olympus 2016). Olympus (2016) provides the equation for which this is calculated:

$$d = (\pi f \mu \sigma)^{-0.5} \quad (2.1)$$

where d is the depth of penetration in m, f is the frequency of the alternating current in Hz, μ is the magnetic permeability in Hm-1 and σ is the electrical conductivity in mhom-1.

The probe geometry is directly related to the shape of the induced eddy-current path. For a circular core probe the induced eddy current path in an electrically conducting isotropic and homogenous material is circular. Larger coils allow for a greater inspection volume since the magnetic field flows deeper into the test piece, whereas, smaller coils are more sensitive to small defects (Olympus 2016).

Z Zhang & Zhao (2016) showed that eddy current has been used for the detection of surface defects in continuous casting slabs up to 1100°C, with the equipment also being suitable for operation in these high temperatures.

Summerscales (1990) examined the use of eddy current testing in composites and noted that it was only suitable in CFRP with a volume fraction of 40% or higher. It was also noted that eddy current testing is not suitable for GFRP (Summerscales 1990). Due to testing only being suitable for conductive materials it was not feasible for use in the project.

2.3 Acoustic Emission

Acoustic emission is the examination of transient elastic waves generated from sudden redistribution of stress in a material (Oliveira 2004). Acoustic emission provide information on the initiation and evolution of damage, it is unable to provide quantitative results about size, depth and overall integrity of a part. Sources of acoustic emissions may be stress release from crack growth, plastic deformation, dislocation movement, phase transformation and friction mechanisms (Non Destructive Testing Resource Center 2016).

There are two types of acoustic emission signals, transient and continuous. Transient

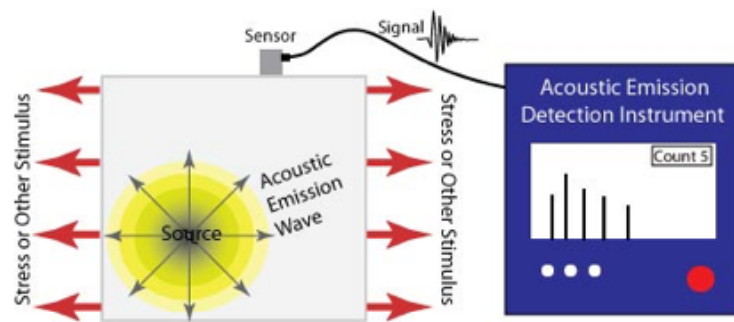


Figure 2.3: Acoustic Emissions NDT (Non Destructive Testing Resource Center 2016).

signals are burst signals that correspond to discrete mechanical events in a material. Such bursts are random in time and have the aspect of damped sinusoid, with starting and end points deviating clearly from background noise (Oliveira 2004). Continuous signals are observed when the acoustic emission activity overlaps and, generally, results from the combination of electronic noise with the environmental acoustic noise in the emissions bandwidth (Oliveira 2004).

Joseph Johnson, Zhang, Wu & Jiang (2014) analysed the feasibility of acoustic emissions for use in high temperatures, they summarised that the limiting factor was the piezo-electric transducer. Joseph Johnson et al. (2014) utilised a Yttrium Calcium OxyBorate (YCOB) single crystals piezoelectric transducer which allowed for use in temperatures up to 1000°C. Portable acoustic emissions controllers are also available for use in high temperature environments with the appropriate piezo and cable however they are limited to only active flaws/defects (Testing & Research 2016).

Acoustic emission is a dynamic process, in that only active events are able to be detected during the occurrence (Non Destructive Testing Resource Center 2016). The event must also be of a load which causes an acoustic event, otherwise it will not be detected (Non Destructive Testing Resource Center 2016). Due to this acoustic emission is not suitable for the project, as the damage that may have already been caused before testing is done would not be evaluated.

2.4 Ultrasonics

Ultrasonics is the use of sound waves at high energy for material inspection (Resource Center n.d.). As the ultrasonic wave propagates through the material it is modified by the boundaries encountered, the material itself and the presence of flaws or defects (Resource Center n.d.). Ultrasonic inspection is capable of being undertaken through contact transducers, wave-guided or medium coupled.

Contact and wave-guided transducers are typically in the range of 500 to 20,000 KHz (International Atomic Energy Agency 1988). The transducer is in direct contact with the material under inspection allowing for higher frequencies. Through the use of such high frequencies small and microstructure flaws and defects are able to be detected.

Medium coupled ultrasonics is a non-contact inspection technique which utilises typically water or less commonly air as a medium for the transfer of an ultrasonic wave from a transducer to the component. Air-coupled ultrasonics operate in the range of 25 to 1,000 KHz due to the limitation of attenuation in air (Kommareddy 2003). Water-coupled ultrasonics cannot be applied to water-sensitive or porous materials and is difficult for in the field applications (Kommareddy 2003).

Ultrasonic inspection is undertaken through either an A-scan, B-scan or C-scan. A-scan involves the transmittance of a signal from a transducer into the material and receipt of the signal by another transducer (Non Destructive Testing Resource Center 2016). A-scan only provides information about the section of material through which the signal travelled. B-scan involves moving the transducer used for an A-scan in a plane parallel to the surface. This permits the estimation of the depth or length of a defect along the axis of transducer movement (Non Destructive Testing Resource Center 2016). C-scan is the most complex scanning method, in that it conducts a scan of the whole material reproducing a colour map showing the extent of defects in plan view (Non Destructive Testing Resource Center 2016).

2.4.1 Longitudinal Waves

Longitudinal waves are a compressional wave where the particle motion is parallel to the direction of energy transfer. The velocity is determined by the elastic properties of the material (David & Cheeke 2012). Longitudinal waves propagate in both liquids and solids.

$$V_L = \sqrt{\frac{C_{11}}{\rho}} \quad (2.2)$$

2.4.2 Shear Waves

Shear waves are a transverse wave where the particle motion is perpendicular to the direction of energy transfer (David & Cheeke 2012). Shear waves typically have a velocity around half of the longitudinal wave velocity in the same material (David & Cheeke 2012). Shear waves only propagate in solids.

$$V_S = \sqrt{\frac{C_{44}}{\rho}} \quad (2.3)$$

2.4.3 Rayleigh Waves

Rayleigh waves also commonly referred to as surface acoustic waves, are waves confined to within a wavelength or so of the surface along which they propagate (David & Cheeke 2012). This type of wave only travels on a surface that is bounded on one side by strong elastic of the solid and on the other side by elastic forces of the gas molecules (International Atomic Energy Agency 1988). The longitudinal and shear velocities are intimately coupled together, meaning they travel at a common velocity. Rayleigh waves is suitable for detecting near surface flaws or defects in complicated shapes as they are

capable of travelling around corners (International Atomic Energy Agency 1988).

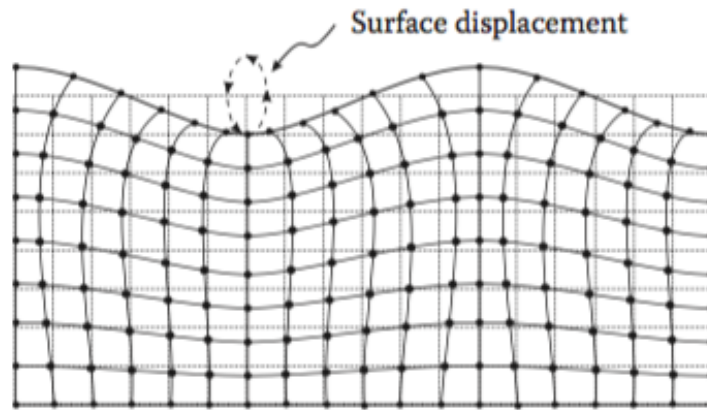


Figure 2.4: Rayleigh Wave Mechanical Displacement (David & Cheeke 2012).

2.4.4 Lamb Waves

If a Rayleigh wave is introduced into a material that has a thickness equal to three wavelengths or less then a Lamb Wave results (International Atomic Energy Agency 1988). Lamb waves propagate in the plane of the structure, bound by its parallel surfaces. There are two types of lamb wave modes, antisymmetric (A_0) and symmetric (S_0) (David & Cheeke 2012).

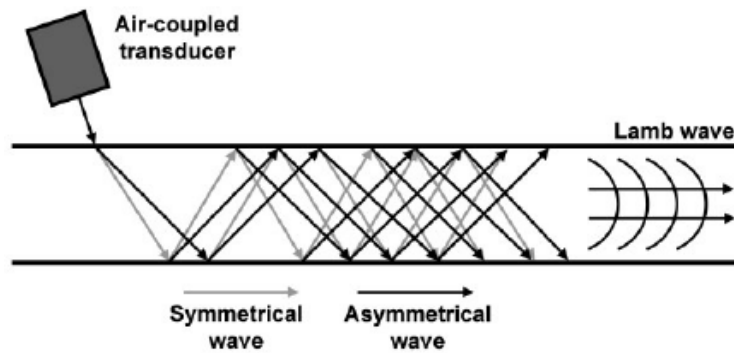


Figure 2.5: Lamb Waves (G Alleman & Groves 2014).

For Symmetric Mode:

$$V_{PL} = 2V_S - \frac{V_S^2}{V_L^2} \quad (2.4)$$

$$V_S\sqrt{2} < V_{PL} < V_L \quad (2.5)$$

For Antisymmetric Mode:

$$V_P = \frac{V_{PL}\beta b}{2\sqrt{3}} \quad (2.6)$$

2.4.5 Critique

F Cegla & Davies (2011) investigated the use of ultrasonics at high temperature and noted it was suitable for use at high temperatures and that laser ultrasonics was the most suitable however due to the very high price laser ultrasonics has limited feasibility.

Currently there are a number of portable ultrasonic detectors on the market however they are limited to flaw and defect detection, provide no information on the materials strength, require skilled technician placement of the transducers and are very limited for a hazardous environment.

This leads to the conclusion that for ultrasonics to be suitable for the project. Further investigation would be required into the material properties obtained through ultrasonics, impact of the hazardous environment on testing, material properties under fire and end-user compatibility would be required. Detailed investigation into ultrasonics is undertaken in Chapter 3.

2.5 Low Frequency (Vibration)

Low frequency vibration methods are those in which bulk disturbances are excited in the structure (Kapadia n.d.). The frequency of vibration is the materials natural or resonance frequency (Kapadia n.d.). Any changes to the structure due to the presence of flaws or defects affect the modal properties of the structure (Pant 2014). Pant (2014) found that damage will decrease the mass and stiffness and increase the damping ratio. L Nelson, Jones & Smith (2008) reported that sensitivity is highly dependent on defect depth and size limiting application to large or shallow defects. L Nelson et al. (2008) demonstrated that low frequency inspection was possible with access to only one side without diminishing results.

There are two types of methods used low frequency, global and local.

2.5.1 Global Method

Global method measures the vibration response of the entire structure from a single point (Kapadia n.d.). The properties measured are modal frequency, modal damping and mode shape (Kapadia n.d.). Kapadia (n.d.) states that the global method is less sensitive than local methods because the influence of a flaw is spread over the whole structure rather than concentrated in the region of testing. Consequently, they are less effective at detecting small, localised defects (Kapadia n.d.).

2.5.2 Local Method

Local method is undertaken through either of two methods. The first method where the excitation is applied at a single point and the response measured at several other locations; and the second is where the excitation is applied and the response measured at each location (Kapadia n.d.).

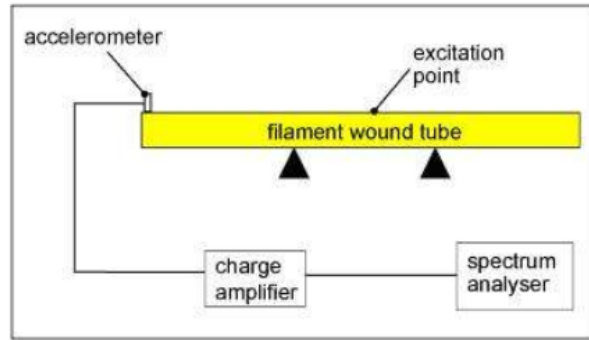


Figure 2.6: Global Method Low Frequency NDT (Kapadia n.d.).

2.5.3 Critique

Low frequency testing would be able to provide information on the integrity of the material, however further investigation would be required into the undertaking of this inspection at high temperatures as only limited information currently exists. Additionally, this test method would require direct contact with the material from the end user, which would raise a safety issue when it is at 200°C and not meet the requirements for portability. Due to this, low frequency is not suitable for the project.

2.6 Dye Penetrant Testing

Dye penetrant testing is a technique used for the detection of surface flaws or discontinuities in non-porous materials (International Atomic Energy Agency 1988). A liquid dye penetrant is applied to the surface of the material for a period of time to allow the flow of the liquid dye penetrant into any surface flaws through capillary action. The excess liquid is wiped off the surface leaving the dye entrapped in the flaw or discontinuity. This provides contrast between materials and the flaw (International Atomic Energy Agency 1988).

Dye penetrant is available in aerosol spray cans making it suitable for portable applica-

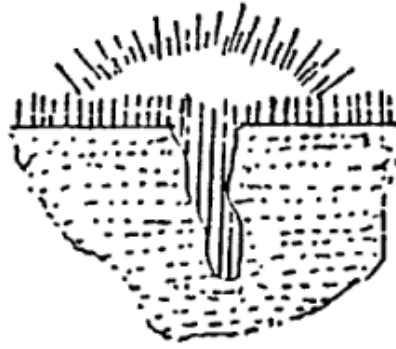


Figure 2.7: Fluorescence of Dye Penetrant NDT (International Atomic Energy Agency 1988).

tions (Khan 1999). Z Zhang & Zhao (2016) states that dye penetrant testing is suitable for use in high temperature environments however, the penetrant can only be in contact with the high temperature artefact for a short period of time without damaging the dye, therefore it requires the test speed to be fast (Z Zhang & Zhao 2016).

Dye penetrant testing has a number of disadvantages, including but not limited to, only surface flaws can be detected, pre-cleaning of the material is critical as contaminants may mask defects, direct access to the surface is required and the flaw must be of sufficient size to allow the ingress of dye penetrant. If the defect is not of sufficient size, then enough dye will not penetrate to bleed out, allowing for detection by the human eye or satisfy the dimensional thresholds of fluorescence.

Due to dye penetrant testing being limited to the detection of surface flaws or discontinuities in non-porous materials it was not deemed feasible for the project.

2.7 Magnetic Powder

Magnetic particle testing is the inspection of surface and just below surface flaws in materials that are able to be easily magnetised. The test piece must first be magnetised, either through the use of a magnet or by passing an electric current, thus inducing a

magnetic field. Any surface or near surface flaw will therefore interrupt the flow of the magnetic field and be visible once magnetic particles are sprinkled on the material (International Atomic Energy Agency 1988).

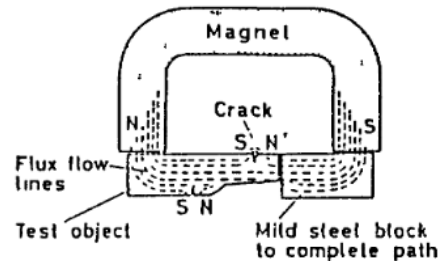


Figure 2.8: Magnetic Particle NDT (International Atomic Energy Agency 1988).

Dry powder magnetic particle inspection is capable of being conducted at temperatures up to 316°C (Inspection for Industry 2012). For temperatures up to 399°C a black coated powder is available (Inspection for Industry 2012). Dry powder is limited by the iron or iron oxide coating that is used to enhance visibility. The iron or iron oxide coating breaks down under high temperatures, thereby limiting the mobility of particles. As the temperature increases there is a decrease in magnetic permeability of the iron particles and a decrease in magnitude of the magnetic poles on opposite sides of the flaws (Inspection for Industry 2012). International (2008) further states that magnetic powder is combustible, albeit the fire hazard is very low.

International (2008) states that through the use of a magnetic slurry/paint examination of vertical or overhead surfaces is possible. Khan (1999) further states that to achieve best results the magnetic field must be orientated perpendicular to the discontinuity. Due to this and the limitation on determining internal material integrity issues magnetic particle testing was not feasible for the project.

2.8 Radiography

Radiography can be used for the inspection of internal flaws or defects (Hashemite University n.d.). There are three common types of radiography, x-rays, γ -rays and neutron radiography (Engineers Handbook n.d.).

2.8.1 X-ray

The inspected component is exposed to X-ray radiation for the detection of flaws or defects. X-rays utilise a photographic film placed on the other-side of the material that captures the differences in intensity from the produced source. The shadow picture produced is known as a radiograph. The absorption of a material undergoing x-rays will increase with increasing atomic number (Oliveira 2004). The effectiveness of X-rays is improved through the use of an opaque penetrating fluid such as hydrogenated hydrocarbons (Oliveira 2004). If sufficient time is allowed from injecting, the fluid will spread into the damaged regions increasing sensitivity to the x-ray. A limitation is that the opaque fluid must be injected into the area of concern, therefore internal delaminations require a hole to be drilled into the material to allow for fluid penetration (Oliveira 2004). Meaning the material must be damaged for the test to be conducted.

2.8.2 Gamma-ray

Gamma(γ)-ray utilise a similar operation method to x-ray however a different source is required. Hashemite University (n.d.) states that γ -rays are the most energetic form of electromagnetic radiation. The difference between the sources is in that the shortest wavelength in the x-ray spectrum is equal to the penetrating power of the γ -ray, but the rest of the wavelengths are far less penetrating (Blom & Gradin 1990). γ -ray has advantages over x-ray, for instance, its portability, requires no electrical supply, smaller,

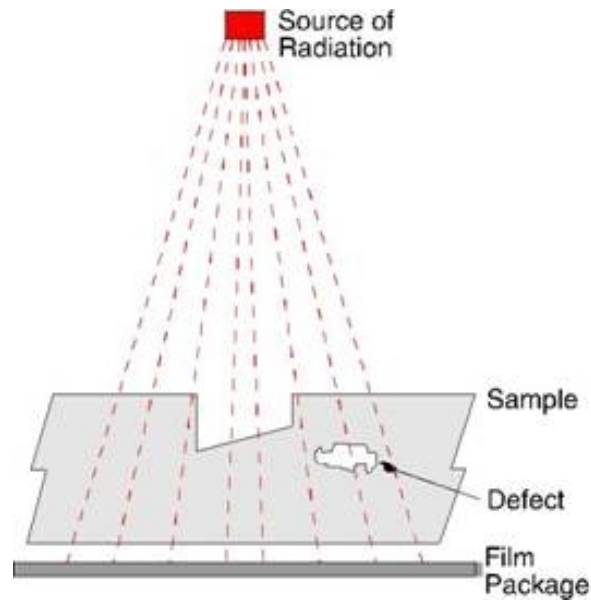


Figure 2.9: Radiography NDT (Jobs 2013).

lighter and more robust equipment. The penetrating power of γ -rays is governed by the isotope selected and elapsed time limiting its tailorability.

2.8.3 Neutron Radiography

Neutron radiography uses flux neutrons, which are absorbed by the material being inspected. Neutron radiography is produced from sources such as nuclear reactors, electron sources or isotopes sources (Svab & Balasko n.d.). The neutron radiation is absorbed more into materials containing hydrogen and least absorbed by materials with a high atomic number. A screen is placed before a x-ray film which is sensitive to the neutron flux and will emit radiation to which the x-ray film is sensitive (Svab & Balasko n.d.).

2.8.4 Critique

International Atomic Energy Agency (2005) states that radiography is suitable for high temperature environments. The limitations of radiography lies in that access to both sides of the material is required, exposure to radiation and must be used in a highly controlled environment. Due to access being restricted to one side of the material, exposure to harmful radiation and the uncontrolled environment testing will be undertaken in, radiography is not suitable for the project.

Chapter 3

Methodology

This chapter presents the methodology for the key design aspects of the chosen non-invasive test method. Further, it outlines the material properties and integrity issues for Aluminium, GFRP and CFRP under high temperatures and fire conditions.

The key design aspects of ACU were acoustic impedance, transmission coefficient for a plate, wave propagation at incident in homogeneous media, wave propagation in non-homogeneous media, attenuation, lamb waves, ultrasonic velocity with temperature, Doppler shift, material properties and material defects.

A review of material properties under fire showed that the elastic modulus of Aluminium greatly decreases after 200° C and for Composite greatly decrease after Glass Transition Temperature (T_g 1).

3.1 Introduction

The test method chosen must not require contact with the material undergoing testing, as this ensures the safety of personnel conducting the testing by keeping personnel a safe

distance from the hot material. Additionally, the test method must be non-invasive and non-impact to ensure the material will not be negatively affected by the test. If the test method chosen required contact with a hot bulkhead and/or deckhead which had reached a plastic state then any excessive force applied by personnel conducting the test could lead to extreme damage to the bulkhead and/or deckhead or at worst personnel falling into the hot material.

From the literature review it was determined that ultrasonic testing was the most suitable non-invasive test method for further design development. Specifically, ACU testing was chosen as the most suitable non-invasive test method for further development as it does not require direct contact with the hazardous material, is non-invasive, and provides the benefits of ultrasonic testing.

The key design aspects of ultrasonics are detailed in Chapter 3.2.

Aluminium, GFRP and CFRP material properties and integrity issues under high temperatures and fire were investigated to optimise the design configuration to acquire relevant information. This information was used to optimise the non-invasive test method by ensuring information acquired was suitable, relevant and most importantly beneficial to the end-user. This information allowed understanding of what happens to our materials under fire, it was also the baseline for which to compare results. This information is detailed in Chapter 3.3 and 3.4.

The results of preliminary testing at room temperature were evaluated, allowing for further optimisation of the design configuration before testing under fire conditions. Signal processing and analysis was undertaken in MATLAB. The testing at room temperature allowed for the determination of the feasibility of the design and determination of what further optimisation or re-design needed to be undertaken. Optimisation of the design was undertaken by examining the reasons why favourable results were not achieved and determining how to overcome this to achieve the desired results.

Due to the cost involved in the procurement of the Aluminium, GFRP and CFRP plates, three plates of each were available for the project. Furthermore, the irreversible damage caused to the plates when placed under fire conditions limits them to being tested once. If a plate was to be tested more than once, the previous damage to the plates would negatively impact the reliability of the results. Therefore, testing at room temperature ensured that the optimal non-invasive test method design was used when the materials were placed under fire conditions and resources were not wasted.

Aluminium was heated to 260°C, while GFRP and CFRP were heated to 160°C. A Liquefied Petroleum Gas (LPG) gas bottle and burner were used to simulate fire conditions. A grill was placed above the burner to break the flame thereby limiting flame high points and ensuring even flame distribution. Secondly, a minimal air gap was placed between the flame and the plate to minimise burning and maximise heat loading.

The materials underwent non-invasive testing at 10°C temperature increments. The test results were evaluated in relation to:

- suitability of the chosen non-invasive test method;
- impact of temperature on results;
- material properties and integrity issues;
- suitability of the results to be used as a baseline response at a set temperature; and
- limitations of this non-invasive test method.

If time permitted a re-design of the chosen non-invasive test method to be fully portable and suitable for a fire hazardous environment would have been undertaken. If resources and time permitted a prototype of this new design was to be built for in-service testing, with verification and validation of results against a calibrated oscilloscope. Due to the time taken to optimise results received at room temperature, no time was available to re-design the test method to be portable.

3.2 Air-Coupled Ultrasonics

Ultrasonics are used in the inspection of metals, fibre-reinforced plastics, concrete and many other materials. Most commonly this technique is undertaken using water as a coupling agent or contact transducers. Both techniques are not suitable or feasible for the hazardous environment for which the project is examining due to requiring direct contact with the bulkhead and/or deckhead which may cause damage. To overcome this ACU testing was deemed the most suitable non-invasive test method for further development. ACU was chosen due to not requiring direct contact with the hazardous material, while providing the benefits of ultrasonic testing.

The non-invasive test method chosen must be feasible with access to only one side of the material, therefore through transmission ultrasonics was not suitable. For the operation of a ACU transducer, a high voltage (V_{P-P}) is required to produce the waveform. Therefore, this limits a transducer to being used for only transmit or receive. Furthermore, due to the size of the transducers a separation angle is required to align them meaning pulse-echo ultrasonics cannot be utilised. Therefore, lamb waves were used for air-coupled ultrasonic testing.

A block diagram of a lamb wave air-coupled ultrasonic test method is shown in Figure 3.1.

The key design aspects of air-coupled ultrasonics requiring further investigation were:

- Acoustic Impedance;
- Transmission Coefficient for a Plate;
- Wave Propagation at Incident in Homogeneous Media;
- Wave Propagation in Non-Homogeneous Media;
- Attenuation;

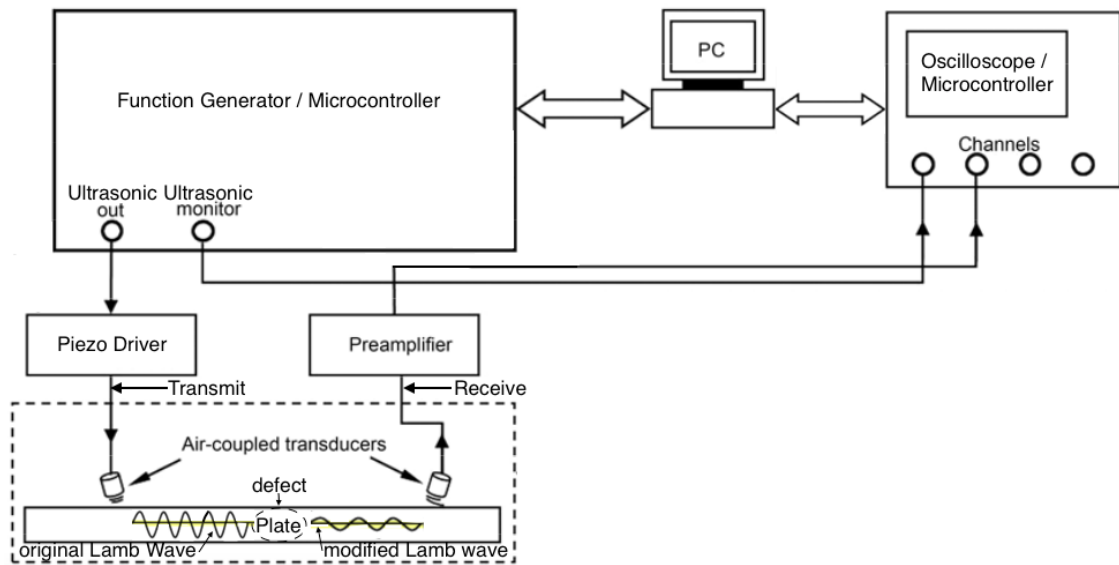


Figure 3.1: Air-Coupled Ultrasonic System Block Diagram.

- Lamb Waves;
- Ultrasonic Velocity with Temperature;
- Doppler Shift;
- Material Properties; and
- Material Defects

The hardware configuration utilised is outlined in Chapter 4.2.

3.2.1 Acoustic Impedance

The material characteristic that defines the amount of energy transmitted is the acoustic impedance. The acoustic impedance of a material is defined as the product of material

density ρ and the velocity of sound V in that material.

$$Z = \rho * V \quad (3.1)$$

When a propagating wave-front hits an interface between two materials, there are partial reflection and transmission coefficients due to the difference in acoustic properties between two media. Figure 3.2 shows the reflection and transmission relationship. The characteristic impedance of the two media is defined as Z_1 and Z_2 . David & Cheeke (2012) specified that since the two media must stay in intimate contact at a perfect interface, the boundary conditions are the continuity of pressure and velocity. The reflection coefficient R , is defined as the fraction of the incident waveform that is reflected back towards the source. Since the acoustic impedance of air is extremely low when compared to most materials, only a small fraction of energy is transmitted into the other medium. Therefore, a high acoustic impedance was present for the project due to the use of air as the coupling medium and aluminium, GFRP and CFRP as the inspection material.

$$R_p = \frac{Z_2 - Z_1}{Z_2 + Z_1} \quad (3.2)$$

The transmission coefficient T_p is given calculated by

$$T_p = \frac{2Z_2}{Z_2 + Z_1} \quad (3.3)$$

$$T_p = 1 - R \quad (3.4)$$

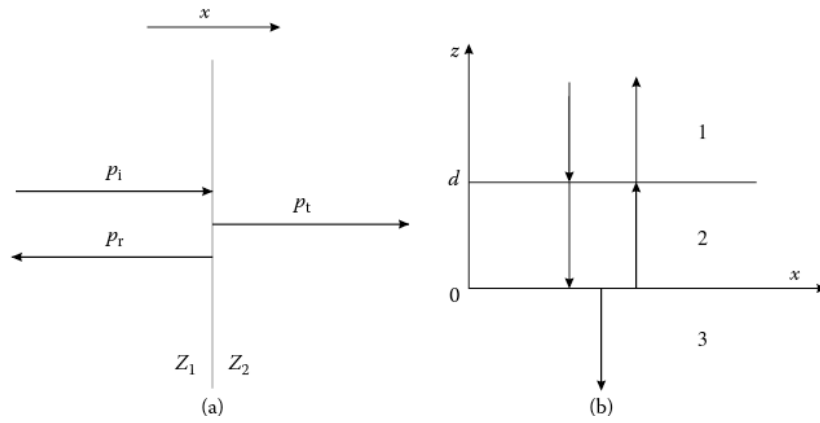


Figure 3.2: Reflection and Transmission at normal incidence for (a) planar interface and (b) layer of thickness d between two bulk media (David & Cheeke 2012).

3.2.2 Transmission Coefficient for a Plate

A plate of thickness d and acoustic impedance Z_2 , inserted between materials of acoustic impedances Z_1 and Z_3 is shown in Figure 3.2 (b). When the propagating wave travelling through material 1 impinges onto material 2, a fraction of the wave is transmitted and the remaining wave is reflected. When the transmitted wave in material 2 hits the material 2/3 interface, a fraction of the wave is reflected again and the remaining wave is transmitted into material 3. The reflected wave from the 2/3 interface travels back to the material 1/2 interface.

Kommareddy (2003) obtained the expression for the amplitude reflection coefficient R_a for a two material interface:

$$R_a = \frac{P_r}{P_i} = \frac{(1 - \frac{Z_1}{Z_3})\cos(k_2d) + j(\frac{Z_2}{Z_3} - \frac{Z_1}{Z_2})\sin(k_2d)}{(1 + \frac{Z_1}{Z_3})\cos(k_2d) + j(\frac{Z_2}{Z_3} + \frac{Z_1}{Z_2})\sin(k_2d)} \quad (3.5)$$

Since the material on both sides of that plate is the same, $Z_1 = Z_3$ the equation for

transmission reduces to:

$$T = \frac{1}{1 + \frac{1}{4}(\frac{Z_2}{Z_1} - \frac{Z_1}{Z_2})^2 \sin^2(k_2 d)} \quad (3.6)$$

Using the ratio for two acoustic impedances $m = Z_1/Z_3$, d for the plate thickness, λ for the wavelength and the relationship from Equation 3.4, Equation 3.6 becomes:

$$T = \frac{1}{\sqrt{1 + \frac{1}{4}(m - \frac{1}{m})^2 \sin^2(\frac{2\pi d}{\lambda})}} \quad (3.7)$$

$$R = \sqrt{\frac{\frac{1}{4}(m - \frac{1}{m})^2 \sin^2(\frac{2\pi d}{\lambda})}{1 + \frac{1}{4}(m - \frac{1}{m})^2 \sin^2(\frac{2\pi d}{\lambda})}} \quad (3.8)$$

If the incident wave is of single frequency, the individual waves are intensified or weakened depending on the phase position. Due to this interface, the transmission and reflection coefficients have a series of maxima and minima. Kommareddy (2003) summarised the relationship between plate thickness and maximum reflection and maximum transmission due to this periodical relationship.

$$\text{Minima of } R \text{ and maxima of } T \text{ occur at } d/\lambda = 0, \frac{1}{2}, \frac{2}{2}, \frac{3}{2} \text{ et seq.} \quad (3.9)$$

$$\text{Maxima of } R \text{ and minima of } T \text{ occur at } d/\lambda = \frac{1}{4}, \frac{3}{4}, \frac{5}{4} \text{ et seq.} \quad (3.10)$$

The dependence of the energy transmission coefficient on the sample thickness is provided in Figure 3.3 for Aluminium and Figure 3.4 for GFRP at 100 kHz and 175 kHz.

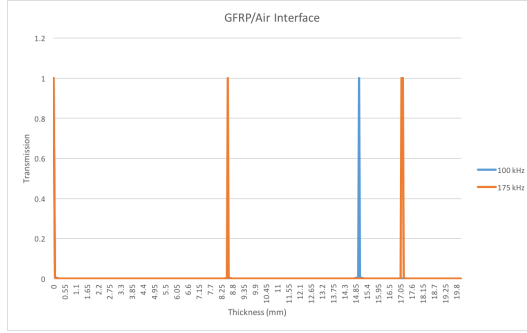


Figure 3.3: Transmission Coefficient Aluminium.

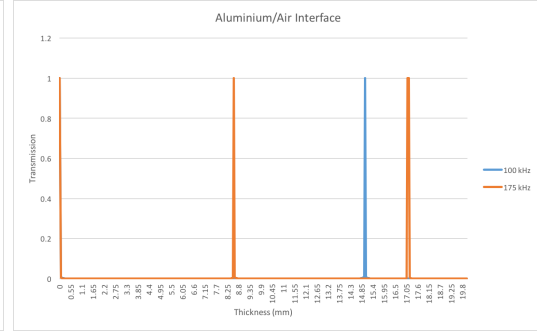


Figure 3.4: Transmission Coefficient GFRP at 3km/s.

3.2.3 Wave Propagation at Incident in Homogeneous Media

When the propagating wave-front hits with incidence, a longitudinal and shear wave component are introduced into the solid due to mode conversion, as shown in Figure 3.5.

The refraction of these waves is governed by Snell's Law:

$$\frac{\sin \theta_i}{v_1} = \frac{\sin \theta_r}{v_1} = \frac{\sin \theta_l}{V_L} = \frac{\sin \theta_s}{V_S} \quad (3.11)$$

where V_L and V_S are the longitudinal and shear wave velocities through the solid respectively.

For wave propagation there exists angle of incidence where the refracted waves become critical, these are known as first and second critical angles (David & Cheeke 2012). At these angles, no energy propagates into the solid, instead propagation occurs along the interface between two media. This is known as interface waves. The reflection coefficient for a given angle of incidence is given as:

$$R = \frac{Z_L \cos^2 2\theta_S + Z_S \sin^2 2\theta_S - Z_1}{Z_L \cos^2 2\theta_S + Z_S \sin^2 2\theta_S + Z_1} \quad (3.12)$$

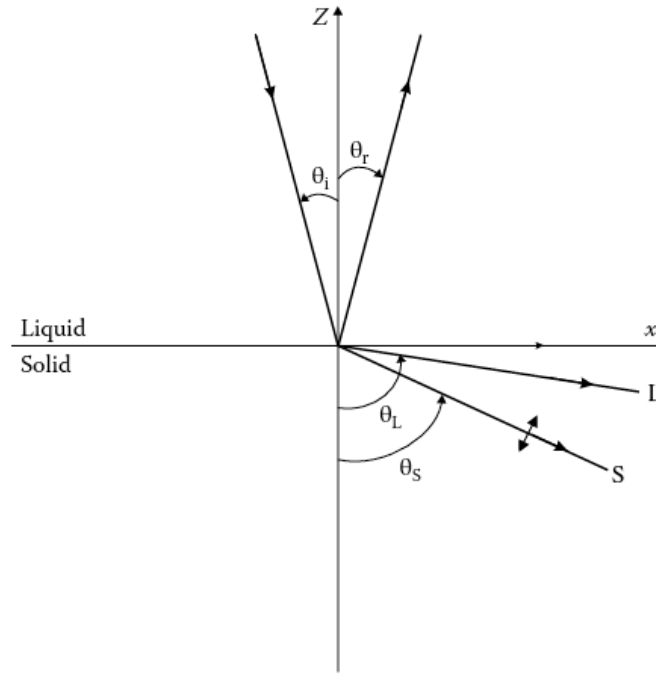


Figure 3.5: Reflection and Transmission at a liquid-solid interface with incidence (David & Cheeke 2012).

From Equation 3.12 the shear and longitudinal wave pressure transmission coefficients can be calculated

$$T_L = \frac{\rho_1}{\rho_2} \frac{Z_L \cos^2 2\theta_S}{Z_L \cos^2 2\theta_S + Z_S \sin^2 2\theta_S + Z_1} \quad (3.13)$$

$$T_S = \frac{\rho_1}{\rho_2} \frac{Z_S \sin^2 2\theta_S}{Z_L \cos^2 2\theta_S + Z_S \sin^2 2\theta_S + Z_1} \quad (3.14)$$

where Z_1 , Z_L and Z_S are given by

$$Z_1 = \frac{\rho_1 v_1}{\cos \theta_i}, \quad Z_L = \frac{\rho_2 v_L}{\cos \theta_L}, \quad Z_S = \frac{\rho_2 v_S}{\cos \theta_S} \quad (3.15)$$

David & Cheeke (2012) simplified the pressure reflection coefficient by defining an effective impedance Z_{eff} for the individual longitudinal and shear impedances.

$$Z_{\text{eff}} = Z_L \cos^2 2\theta_S + Z_S \sin^2 2\theta_S \quad (3.16)$$

$$R = \frac{Z_{\text{eff}} - Z_1}{Z_{\text{eff}} + Z_2} \quad (3.17)$$

Due to the difference in wave-speeds between air and solids, a critical angle exists where all sound will be reflected back into the air. From Equation 3.12 this relationship is plotted for an air-aluminium interface, as shown in Figure 3.6. Therefore, the angle of incidence used must maximise wave transmission.

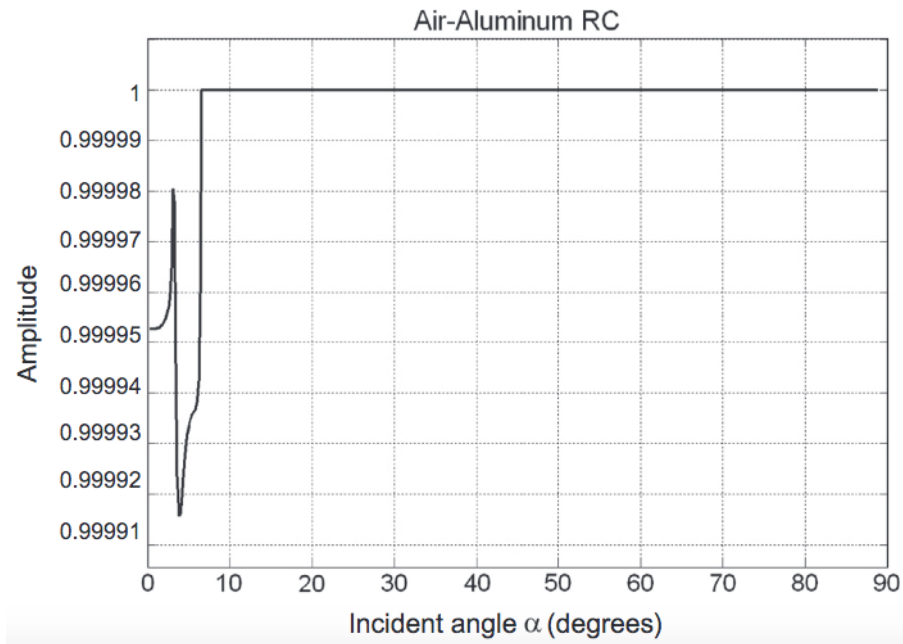


Figure 3.6: Reflection coefficient of an air-aluminium interface (Chimenti 2014).

3.2.4 Wave Propagation in Non-Homogeneous Media

In homogeneous and isotropic media, bulk waves propagate with the same velocity and displacement properties independent of frequency, this is not the case for non-homogeneous or anisotropic media. In non-homogeneous media (e.g. GFRP, CFRP) the structure and dimensions of micro-structured media determine the properties of the propagating waves leading to dispersive solutions and are directionally dependent. Dawson (2010) investigated the influence of angle of incidence relative to the fibre orientation on velocity by plotting the phase velocity dispersion curves for parallel and perpendicular incidence, as shown in Figure 3.7 and Figure 3.8.

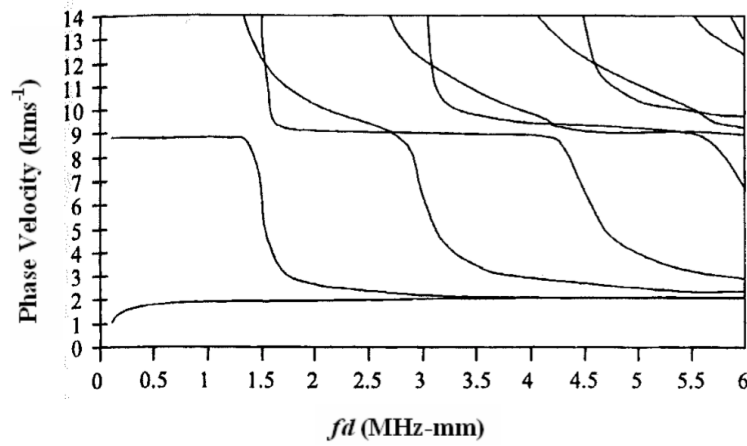


Figure 3.7: Phase velocity dispersion curves for a unidirectional fibre reinforced composite plate parallel to the direction of fibre alignment (Rose 2004).

Wang & Rokhlin (2002) summarised the findings of Rose, Rokhlin & Adler (1987), Hosten (1992) and Lobkis, Chimenti, Zhang & Rudolph (2000), specifically, that non-homogeneous composites may be considered as an effective homogeneous medium when using low frequency ultrasonics. Therefore, the same procedures developed for a homogeneous layer can be used to reconstruct the effective elastic constants from the wave velocity measurements (Wang & Rokhlin 2002).

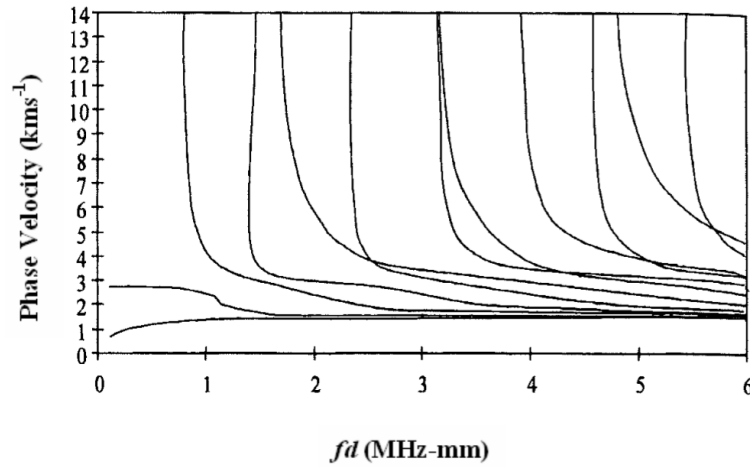


Figure 3.8: Phase velocity dispersion curves for a unidirectional fibre reinforced composite plate perpendicular to the direction of fibre alignment (Rose 2004).

3.2.5 Attenuation

Attenuation is the loss of sound energy as the ultrasonic beam passes through the material (Kommareddy 2003). Attenuation results in the change in amplitude of a travelling wave over a given distance (R Nishanth & Babu n.d.). Attenuation is composed of two components, absorption and scattering. Absorption is the loss of energy due to mechanisms such as dislocation, damping, hysteresis losses and thermoelastic effects. Scattering is the loss of energy due to interaction with the materials polycrystalline structure when the wavelength approaches the grain size.

Attenuation in the material is measured by finding the amplitude difference between the two back-surface signals and dividing by the path travelled. Kumar & Pandey (2010) provided an equation for the determination of attenuation (dB/mm):

$$\alpha = \frac{1}{2X} 20 \log_{10} \left[\frac{1}{(m-n)} \frac{I_n}{I_m} \right] \quad (3.18)$$

where I_m and I_n are the maximum amplitude (voltage) of the m th and n th pulse echoes

respectively and X is the specimen thickness (Kumar & Pandey 2010).

Attenuation is also able to be used as a detection method for early stages of fatigue damage (S Buxbaum & Green 1979). Dislocation motion is a prerequisite to plastic deformation and attenuation is sensitive to dislocation motion and damping, therefore a precise attenuation measurement gives valuable information about the initiation of fatigue damage (S Buxbaum & Green 1979). Green & Joshi (1972) further analysed this theory to show that change in attenuation during a fatigue test provides much better results than the appearance of a reflected signal (echo).

The effects of air as the coupling medium also need to be examined for attenuation. The speed of sound in air is directly related to the temperature in the air as can be seen in Equation 3.19

$$c_r = 331.31 \sqrt{\frac{T}{273.16}} \quad (3.19)$$

Sound energy propagating through air decreases exponentially as a result of the atmospheric absorption, humidity content, temperature and frequency (International Atomic Energy Agency 1988).

$$P = P_O e^{-0.1151\alpha x} \quad (3.20)$$

where P is the final pressure, P_O is the initial pressure, x is the beam path in meters and α is the attenuation coefficient.

The variables in calculating the attenuation coefficient in air are the frequency f in hertz,

temperature T in kelvin, humidity and atmospheric pressure in (kPa).

$$\alpha = 8.686f^2 \left([1.84 \times 10^{-11} \left(\frac{p_a}{p_r} \right)^{-1} \left(\frac{T}{T_r} \right)^{\frac{1}{2}}] + \left(\frac{T}{T_r} \right)^{\frac{5}{2}} (0.01275 [\exp(\frac{-2239.1}{T})]) [\frac{f_{ro}}{f_{ro}^2 + f_{ro}^2}] \right. \\ \left. + 0.1068 [\exp(\frac{-3352}{T})] [\frac{f_{rN}}{f_{ro}^2 + f_{ro}^2}] \right) \quad (3.21)$$

Therefore as the frequency and temperature increase attenuation also normally increases. The attenuation at frequencies of 100 KHz and 175 KHz is provided in Table 3.1, calculated from Equation 3.21.

Temperature	Humidity	Frequency (KHz)	Attenuation (dB/m)
20	60	100	3.282
100	60	100	3.612
150	60	100	8.838
200	60	100	8.802
20	60	175	6.712
100	60	175	8.869
150	60	175	16.159
200	60	175	23.796

Table 3.1: Attenuation in Air.

As can be seen in Table 3.1, the hotter the air the greater the attenuation will normally be. As the plate warms up it will cause the air surrounding the plate to heat up due to convection producing a column of hot air rising vertically called the natural convection current (W Wright, Carpenter & Jansen 1998). To overcome this the distance between the ultrasonic transducer and inspection material must be kept to a minimum while ensuring that the near field is met and the operating temperature limit of the transducer must not to be reached to ensure accuracy of results.

3.2.6 Lamb Waves

Lamb waves were introduced in Chapter 2.4.4. Lamb waves are dependent on the frequency, material thickness, density and elastic properties of the material. The dispersion equation governs this relationship, shown in Equation 3.22. Dispersion is the change in wave speed in a material with respect to frequency (R Nishanth & Babu n.d.).

$$\frac{(k^2 + s^2)^2}{4k^2sq} = \left[\frac{\tanh(dq)}{\tanh(sd)} \right]^{\pm 1} \quad (3.22)$$

where k is the wave number, $s = \sqrt{k^2 - (w/v_T(\theta))^2}$ and $q = \sqrt{k^2 - (w/v_L(\theta))^2}$.

The dispersion equation was used to calculate the symmetric (S_0) and antisymmetric (A_0) velocities at room temperature for Aluminium, shown in Figure 3.9. The symmetric mode corresponds to stretching without bending (David & Cheeke 2012). The antisymmetric mode corresponds to bending without stretching (David & Cheeke 2012).

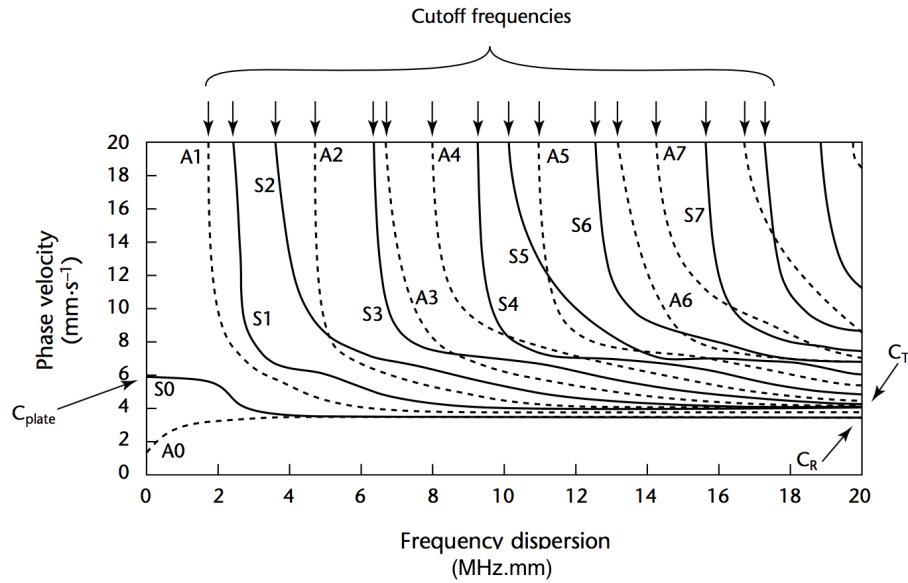


Figure 3.9: Lamb Wave Dispersion Curve for Aluminium Plate (Humphries n.d.).

Therefore, only frequencies where the first symmetric (S_0) and antisymmetric (A_0) mode

are excited, are of interest for the project.

3.2.7 Ultrasonic Velocity and Wavelength with Temperature

Acoustic waves travelling through solid materials are properties of wavelength, frequency and velocity. This relationship is shown in Equation 3.23. This means that wavelength, frequency and velocity are interlinked depending on the condition of the material.

$$\lambda = \frac{V}{f} \quad (3.23)$$

where λ is wavelength in m, V is the velocity is m/s and f is the frequency in Hz.

J Dobson (2014) investigated the thermally induced effect in lamb waves for aluminium plate. The results showed that across the temperature range 20°C to 60°C there was a change in the A_0 mode velocity of 28 m/s. This supports the data in Figure 3.13 that the elastic properties for Aluminium over the temperature range 20°C to 60°C only very slightly, therefore the lamb wave velocity should also only vary slightly.

J Adamowski, Franco & Buiochi (2007) noted that during the calculation of elastic constants, a 0.1°C variation in temperature gradient can result in a 20 ns error in measurement with a 100 mm path, which produces a 2% error in a 1 us time delay (J Adamowski et al. 2007).

As the lamb wave velocity is dependent on the elastic properties, the velocity will change if the elastic properties of the material change. Therefore, as the material elastic properties change due to material solid state moving to smoothing, this will also change the lamb wave velocity. The change in velocity will also change the wavelength due to the relationship shown in Equation 3.23.

3.2.8 Doppler Shift

The Doppler effect is a change in frequency of a wave due to motion relative to its source.

Doppler broadening is a form of Doppler shift due to the thermal motions of the materials atoms. The thermal motion of the absorbing atoms leads to small variations in the absorbed frequency, which changes the wavelength of the transmitted waveform. Different thermal motion of the atoms leads to different Doppler shifts which cumulates to line broadening.

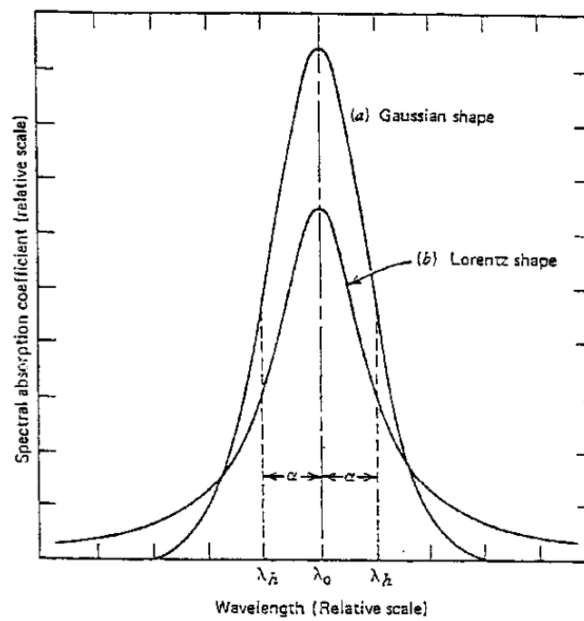


Figure 3.10: Thermal Broadening (University of Colorado 2016).

At room temperature Aluminium, GFRP and CFRP atomic lattice is stable. As the material heats up due to the thermal loading, energy is added into the material. Due to this energy atoms will vibrate more. Bai & Keller (2013) stated that once a composite passes its glass transition temperature the secondary bonds are lost and free volume is formed, allowing molecular motion. This vibration of the atoms may lead to a change in wavelength or frequency. Thermal broadening in the wavelength is shown in Figure 3.10. This would show a correlation between the material solid state moving to smoothing by

energy in the atomic vibration due to thermal loading.

3.2.9 Material Properties

The stress-strain relationship for a material is governed by Hooke's Law:

$$\sigma_{ijk} = C_{ijk}\varepsilon_{ijk} \quad (3.24)$$

where σ_{ijk} is the stress tensor, C_{ijk} is the stiffness tensor and ε_{ijk} is the strain tensor.

The stress-strain relationship for an isotropic homogenous media is expanded to:

$$\begin{bmatrix} \sigma_{11} \\ \sigma_{22} \\ \sigma_{33} \\ \tau_{23} \\ \tau_{13} \\ \tau_{12} \end{bmatrix} = \begin{bmatrix} C_{11} & C_{12} & C_{12} & 0 & 0 & 0 \\ C_{12} & C_{11} & C_{12} & 0 & 0 & 0 \\ C_{12} & C_{12} & C_{11} & 0 & 0 & 0 \\ 0 & 0 & 0 & C_{44} & 0 & 0 \\ 0 & 0 & 0 & 0 & C_{44} & 0 \\ 0 & 0 & 0 & 0 & 0 & C_{44} \end{bmatrix} \begin{bmatrix} \varepsilon_{11} \\ \varepsilon_{22} \\ \varepsilon_{33} \\ \gamma_{23} \\ \gamma_{13} \\ \gamma_{12} \end{bmatrix} \quad (3.25)$$

Equation 2.2 and 2.3 provided the formulas for determining the Longitudinal and Shear velocities for a material from the stiffness tensor. For a homogenous material:

$$C_{11} = \lambda + 2G \quad (3.26)$$

$$C_{44} = G \quad (3.27)$$

$$C_{12} = C_{11} - 2C_{44} \quad (3.28)$$

As shown in Equation 3.26 and 3.27, the ultrasonic velocity is directly affected by the macrostructural and mechanical properties. Therefore, there is a direct correlation to the materials modulus.

$$E = \frac{\rho V_s^2 (3V_L^2 - 4V_s^2)}{(V_L^2 - V_s^2)} \quad (3.29)$$

$$G = \rho V_s^2 \quad (3.30)$$

$$B = \rho \left(V_L^2 - \frac{4V_s^2}{3} \right) \quad (3.31)$$

$$\nu = \frac{(V_L^2 - 2C_s^2)}{(2V_L^2 - 2V_s^2)} \quad (3.32)$$

Lamb wave modes are dependent on the frequency, material thickness, density and elastic properties of the material.

However, composites do not exhibit the same mechanical properties in all directions. The stiffness matrix (C_{ijk}) is dependent on the lay-up and orientation of the individual lamina. The stress-strain relationship for a single monoclinic anisotropic media is expanded to:

$$\begin{bmatrix} \sigma_{11} \\ \sigma_{22} \\ \sigma_{33} \\ \tau_{23} \\ \tau_{13} \\ \tau_{12} \end{bmatrix} = \begin{bmatrix} C_{11} & C_{12} & C_{13} & 0 & 0 & C_{16} \\ C_{12} & C_{22} & C_{23} & 0 & 0 & C_{26} \\ C_{13} & C_{23} & C_{33} & 0 & 0 & C_{26} \\ 0 & 0 & 0 & C_{44} & C_{45} & 0 \\ 0 & 0 & 0 & C_{45} & C_{55} & 0 \\ C_{16} & C_{26} & C_{36} & 0 & 0 & C_{66} \end{bmatrix} \begin{bmatrix} \varepsilon_{11} \\ \varepsilon_{22} \\ \varepsilon_{33} \\ \gamma_{23} \\ \gamma_{13} \\ \gamma_{12} \end{bmatrix} \quad (3.33)$$

For a lamb wave the ultrasonic wave velocity is determined by the plate wave speed, Equation 2.4. The stiffness constants are able to be equated against the density and plate wave speed as shown in Equation 3.34.

$$\rho V_{pl}^2 = C_{11} - \frac{C_{13}^2}{C_{33}} \quad (3.34)$$

Lobkis et al. (2000) evaluated that where the elastic anisotropy leads to ratios between 8 or 10 for C_{11} and C_{33} , accompanied by an even smaller C_{33} the second term in Equation 3.34 can be ignored. Lobkis et al. (2000) summarised by ignoring the second term in Equation 3.34 that the error would never exceed 10%. Lobkis et al. (2000) showed that plate wave speed was wholly dependent on C_{11} .

The elastic modulus is calculated directly from the symmetric lamb wave mode velocity (M Caslini & O'Brien 1987).

$$E = \rho v^2 \quad (3.35)$$

where E is the elastic modulus, ρ is the density and v is the velocity of the S_0 lamb mode.

3.2.10 Material Defects

A defect, flaw or de-lamination in the material will impact a propagating wave by diffraction, reflection, scattering and/or mode conversion. This results in modified detected signals. If the defect is large enough it will reflect the entire propagating wave. A defect or flaw must be larger than one-half the wavelength to stand a chance of being detected as reflection (Kommareddy 2003). As a result, there is limitations on the reflections possible with low ultrasonic frequencies. Consequently, attenuation and backscattering may be more reliable for the detection of material defects and flaws (Green & Joshi 1972).

The location of the defect or flaw is calculated from the Time of Flight (TOF) equation as shown in Equation 3.36 for a pulse echo:

$$s = \frac{Vt}{2} \quad (3.36)$$

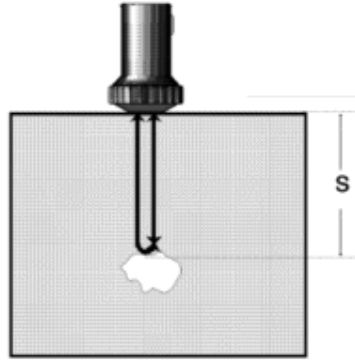


Figure 3.11: Pulse-Echo Time of Flight Measurement (Non Destructive Testing Database 2000).

M Caslini & O'Brien (1987) provides an expression which relates the reduced modulus to crack density for an anisotropic $[0_m, 90_n]$ laminate when using lamb waves:

$$\frac{E}{E_0} = \left[1 + \frac{nE_2}{mE_1} \frac{\tan(\lambda/2D)}{(\lambda/2D)} \right]^{-1} \quad (3.37)$$

where

$$\lambda^2 = \frac{3G_{12}E_0}{h^2E_1E_2} \frac{(n+m)}{(n^2m)} \quad (3.38)$$

In Equation 3.37 and Equation 3.38, E_0 is the modulus for the undamaged composite and E is the modulus for the damaged composite. E_1 , E_2 , and G_{12} are the longitudinal, transverse, and shear moduli, respectively for each individual unidirectional lamina in the plate. D is the crack density, h is the lamina thickness, and m and n are the number

of 0° and 90° layers, respectively, in half thickness of the plate (M Seale & Prosser 1998). Equation 3.37 does not account for damage in the material other than cracks such as charring and temperature degradation which would need to be accounted for in the project.

3.3 Aluminium Under Fire

Aluminium alloy 5083 H116 is commonly used for ship construction making it beneficial for investigation in this study. 5083 H116 is a wrought alloy, strengthened by strain hardening (cold working). It is weldable, exhibits moderate strength and good corrosion resistance. 5083 H116 has major disadvantages, including high thermal conductivity and low melting point.

Structures experience mechanical loading and thermal exposure during a fire. P Summers et al. (2015) reported that damage manifests itself during elevated temperature exposure as large plastic (creep) deformation, grain elongation, dynamic dislocation recovery, precipitate cracking, and cavity formation. These changes accumulate, developing a stress-induced damage state which may cause pre-mature failure of the structure (P Summers et al. 2015).

The effect of temperature on Young's modulus, ultimate tensile strength and yield strength are shown in Figures 3.13, 3.14 and 3.15 respectively.

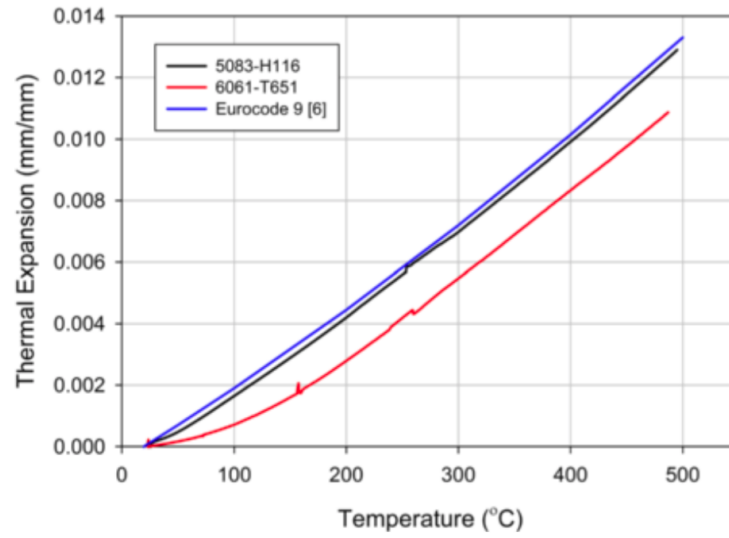


Figure 3.12: 5083 Thermal Expansion with Temperature (P Summers et al. 2015).

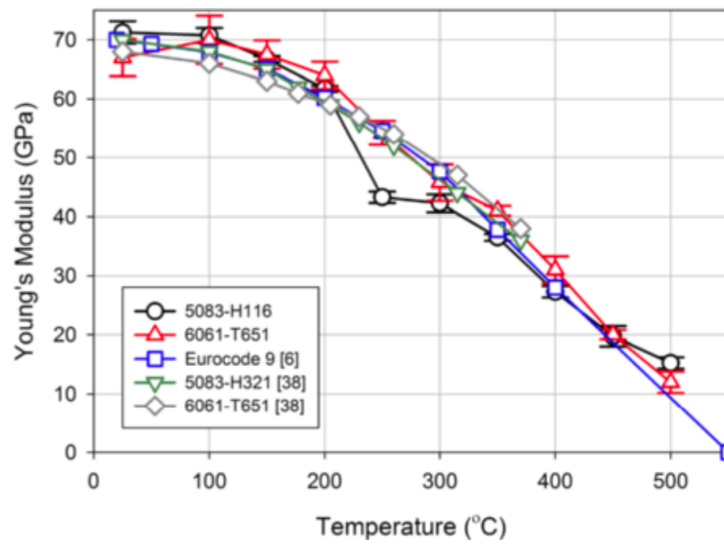


Figure 3.13: 5083 Young's Modulus with Temperature (P Summers et al. 2015).

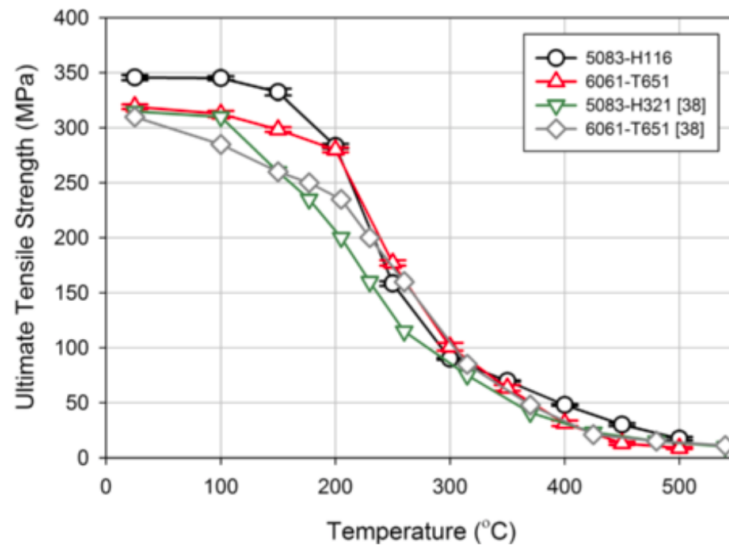


Figure 3.14: 5083 Ultimate Tensile Strength with Temperature (P Summers et al. 2015).

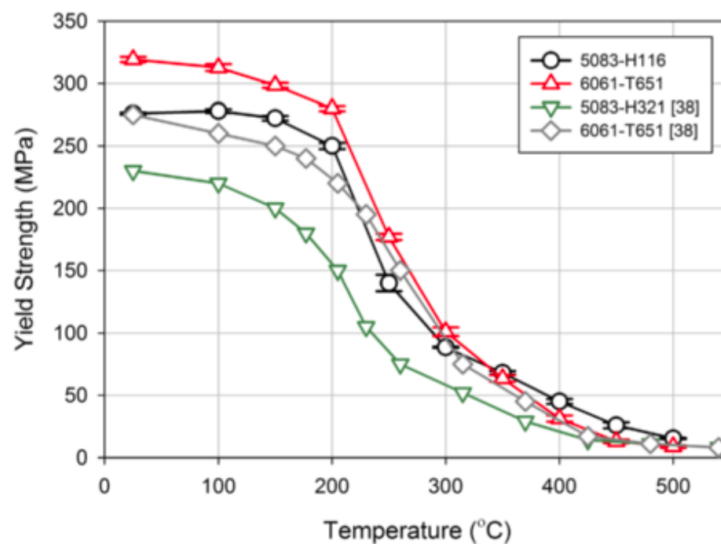


Figure 3.15: 5083 Yield Strength with Temperature (P Summers et al. 2015).

5083 H116 is a strain hardened alloy, therefore, it will lose its mechanical strength when heated for two main reasons, sub-grain coarsening and recrystallisation. When heated to 280-380°C the alloy anneals inducing recrystallisation. Grain growth eventually occurs after long periods of exposure at these temperatures. P Summers et al. (2015) reported that the grain size is 89 μm in the unaffected state and 48 μm following recrystallisation.

The Hall-Petch slope constant determined from this was $0.22 \text{ MPa}\sqrt{m}$, is a similar result to that calculated in Ramesh (2009).

As shown in Figure 3.13, Young's modulus greatly reduces after exposure to temperatures over 200°C .

As shown in Figure 3.15, the yield strength is relatively stable until it begins to decrease after exposure to temperatures of 150°C , this is due to coarsening of the dislocation cell structure (Summers 2014). The alloy is moving away from solid state. The alloy also exhibits ductile shear failure up until 100°C , following which the material transitions to pure ductile failure (Summers 2014).

The exposure of 5083 H116 to water or air results in the spontaneous formation of a thin, strong and adherent aluminium oxide layer. This oxide layer melts at 2050°C , much higher than the melting point of the alloy (Metals 2011). The oxide film is susceptible to the localised breakdown at the exposed surface or at discontinuities due to high dissolution rates from the underlying metal. An example of this is pitting corrosion which occurs due to the rupture of the oxide layer leading to corrosion of the underlying material.

When the alloy is welded, a Heat Affected Zone (HAZ) is formed which undergoes complete annealing and then recrystallisation. Consequently, any prior work hardening that the alloy has undergone is lost and a reduction in hardness is observed.

3.4 Composites Under Fire

GFRP and CFRP are commonly used for ship construction making them beneficial for investigation in this study.

The thermal and mechanical properties of Fibre Reinforced Plastic (FRP) depend on the

type of fibre, resin matrix, fibre volume ratio, modulus of elasticity of the fibres and matrix materials (M El-Badry & Ghali 2000). Carbon fibres oxidise at temperatures above 300°C and melt at temperatures around 4000°C (Bourbigot & Flambard 2002). Glass fibres begin to soften at temperatures above 650°C and melt above 1225°C (Bourbigot & Flambard 2002).

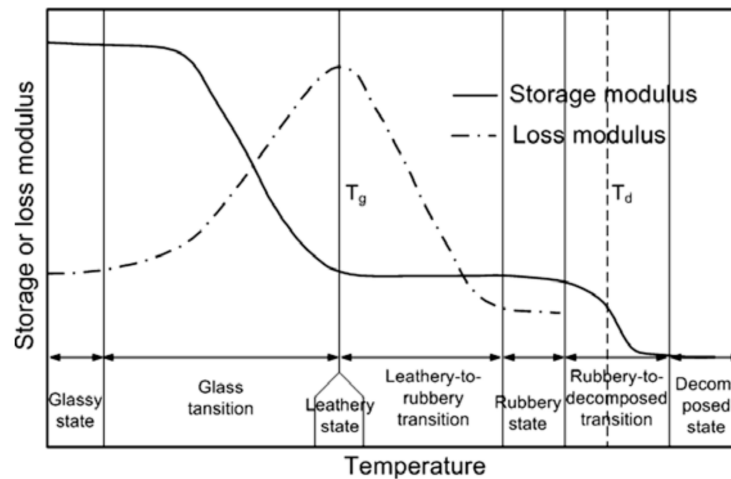


Figure 3.16: Material States and Transition with Modulus (Y Bai & Vallee 2008).

The poor fire resistance and behaviour of composites are due to the behaviour of the resin matrix. H Blontrock & Matthys (1999) stated that the strength and stiffness of FRP composites starts degrading rapidly at a temperature close to the glass transition temperature of the constituent polymer resin. This is due to softening of the resin limiting the transfer of stress between fibres. Bai & Keller (2013) stated that once a composite passes its glass transition temperature the secondary bonds are lost and free volume is formed, allowing molecular motion. As shown in Figure 3.16, the modulus of the composite greatly reduces once the state has moved to glass transition. The temperature of this massive reduction in modulus is the resins T_g . Furthermore, when FRP's are exposed to temperatures above their cure/processing temperature, the result is an initial post-cure. Post cure is followed by degradation due to thermal effect (*CIV8803 Mechanics and Technology of Fibre Composites: Study Book* 2008). Due to this risk, *CIV8803 Mechanics and Technology of Fibre Composites: Study Book* (2008) recommends that

composite be designed so that the glass transition temperature is at least 30°C above the maximum use temperature. Epoxy resins will quickly ignite when exposed to fire temperatures at 300-400°C (*CIV8803 Mechanics and Technology of Fibre Composites: Study Book* 2008). *CIV8803 Mechanics and Technology of Fibre Composites: Study Book* (2008) further noted that moisture absorption results in the decrease of the glass transition temperature.

When a FRP undergoes fire damage, two types of damage occur. The first type of damage is a char region, this is characterised by complete combustion of the resin matrix leaving only the fibre reinforcement. The second is de-lamination and cracking in the unburnt section of the composite (Mouritz & Mathys 1999, Mouritz & Mathys 2000, Mouritz & Mathys 2001). De-lamination and cracking is caused by the Coefficient of Thermal Expansion (COTE) of the resin matrix (Epoxy COTE = $6.0 \times 10^{-5}/^{\circ}\text{C}$) orders of magnitude higher than the Glass fibre (COTE = $5 \times 10^{-6}/^{\circ}\text{C}$). Whereas, carbon fibre (COTE = $0.036 \times 10^{-5}/^{\circ}\text{C}$) has a COTE higher than the Epoxy. Figure 3.17 shows the damage profile to a composite when it undergoes localised fire damage, if the fire was evenly distributed throughout the composite then the damage would also be evenly spread.

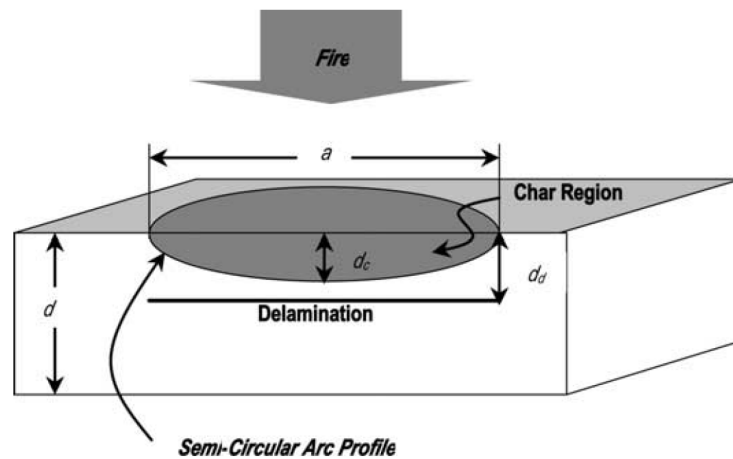


Figure 3.17: Schematic of fire damage through FRP Composite (Gardiner & Mathys 2002).

When a FRP is of thickness greater than 5-10 mm this char region forms a layer of

low thermal conductivity (Gardiner & Mathys 2002), however this layer will act as an insulating layer, slowing heat penetration and evolution of gases from the depth of the composite (*CIV8803 Mechanics and Technology of Fibre Composites: Study Book* 2008). If the material is loaded in compression then the fire induced delamination cracks will cause the material to fail (Gardiner & Mathys 2002).

The strength of the composite is calculated by modelling as two layer material, the strength of the unburnt material and the strength of the char material.

$$S_T = \left(\frac{A - A_c}{A}\right)S_{To} + \left(\frac{A_c}{A}\right)S_{Tc} \quad (3.39)$$

$$S_C = \left(\frac{A - A_c}{A}\right)S_{Co} + \left(\frac{A_c}{A}\right)S_{Cc} \quad (3.40)$$

where A is the total cross sectional area, A_c is the cross-sectional area of the char material, S_o is the compressive or tensile stiffness of the composite and S_c is the compressive or tensile stiffness of the char material.

Gardiner & Mathys (2002) found that the area of the char can be determined through the use of ultrasonics. Gardiner & Mathys (2002) stated that the compressive and tensile strength of the char material is negligible. This means that the strength of the composite is the strength of the unburnt material.

Chapter 4

System Design

This chapter details the requirements, components and processes required to achieve the project specification.

An ACU test method was designed to transmit a pulsed ultrasonic waveform through the air, impinging on the test material, thereby generating a lamb wave. The ACU test method would also capture this lamb wave response through the air for analysis. Both symmetric and antisymmetric modes of the lamb wave required capture to ensure the response was able to be fully analysed and provide ample feedback.

An overall schematic of the air coupled ultrasonic test method is covered in Chapter 4.6.

4.1 System Requirements

A system model encompasses the design requirements for ACU test method. This model is shown in Figure 4.1. The model is broken into three major areas that need addressing in the design, Ultrasonics, Fire and Materials. All items utilised as part of the development of the ACU test method should be commercially available and portable.

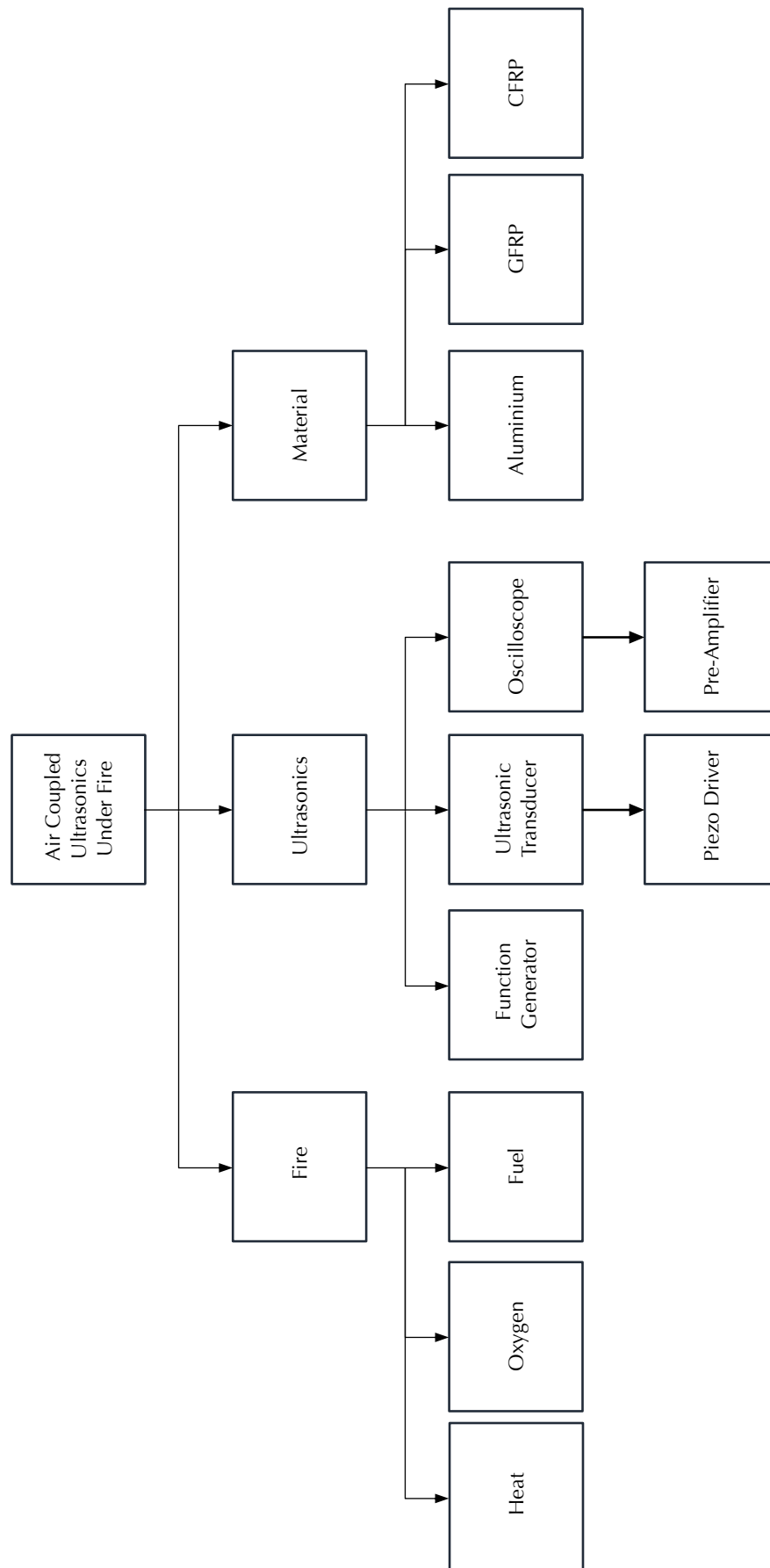


Figure 4.1: System Requirements Model.

4.2 Air Coupled Ultrasonics

4.2.1 Function Generator

A function generator is used to produce different forms of waves at varying frequencies. The waveform required is dependent on the application and the chosen ultrasonic transducer. For the project a pulsed wave was required to be generated from the function generator to maximise transmission, minimise standing wave cancellation and optimise signal analysis.

Table 4.1 details the possible function generators.

Product	Max Frequency (Hz)
Velleman Function Generator	1,000,000
Arduino/Genuino Zero	275,000
Arduino M0 Pro	275,000
Arduino Uno	65,535

Table 4.1: Function Generator Max Frequencies.

Due to their functionality, compact size, power requirements and price, the Arduino Zero and Arduino M0 Pro were chosen.

Arduino M0 Pro

Arduino M0 Pro is a high performance micro-controller which uses a ATSAMD21G18 32-Bit ARM Cortex M0+, allowing for Pulse Width Modulation (PWM). PWM utilises digital control to create a square wave, by switching the supplied voltage between on and off. Therefore, PWM is limited to square waves.

The code at Appendix K was used to produce a 100 KHz square wave with a 50%

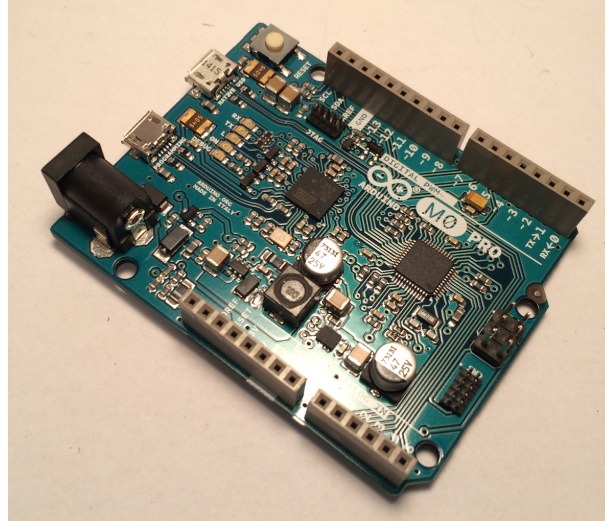


Figure 4.2: Arduino M0 Pro.

duty cycle. The wave was analysed by an oscilloscope as shown in Figure 4.3. The resulting wave varied greatly from the required 100 KHz 50% duty cycle, showing that the produced ultrasonic waveform from the Arduino M0 Pro was unsuitable for use as a function generator.

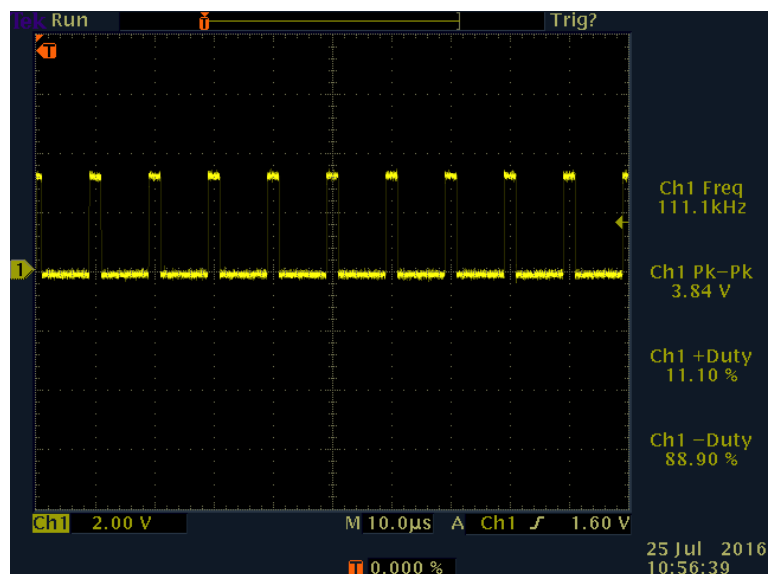


Figure 4.3: Arduino M0 Pro 100 KHz Square Wave.

Arduino Zero

Arduino Zero is similar to the Arduino M0 Pro, but utilises a different interface. The Arduino Zero is a high performance micro-controller which uses a ATSAM21G18 32-Bit ARM Cortex M0+, allowing for PWM. PWM utilises digital control to create a square wave, by switching the supplied voltage between on and off. Therefore, PWM is limited to square waves.

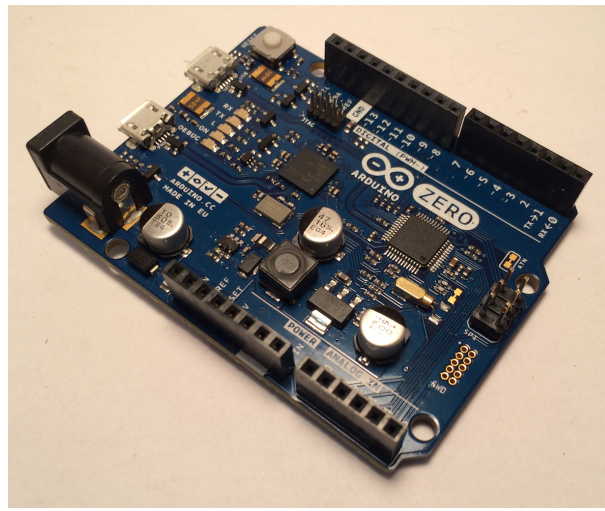


Figure 4.4: Arduino Zero.

The code at Appendix L was used to produce a 100 KHz square wave with a 50% duty cycle. The wave was analysed by an oscilloscope as shown in Figure 4.5. Figure 4.5 shows that the pulsed waveform with 17 cycles, which reads 100 KHz at 50% duty cycle. The produced waveform was suitable for the project. The waveform was limited to 17 cycles to ensure that any overlap in the received response is limited. If a longer pulsed signal was utilised then multiple responses would arrive at the same time making it difficult to analyse.

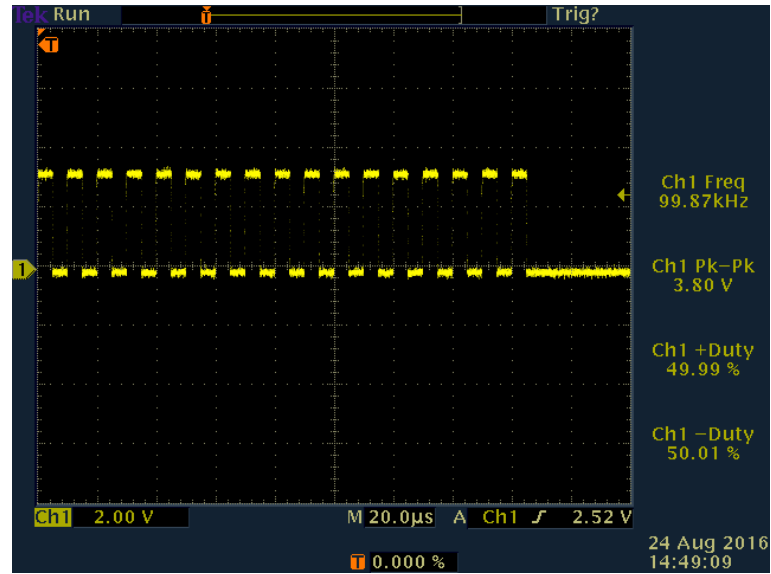


Figure 4.5: Arduino Zero 100 KHz Square Wave.

4.2.2 Ultrasonic Transducer

A piezoelectric ultrasonic transducer was chosen to transmit the waveform. American Piezo (2016) outlined that Jacques and Pierre Curie discovered an unusual characteristic of certain crystalline minerals that when subjected to a mechanical force, the crystals became electrically polarised. This means that if a voltage of the same polarity as the poling voltage is applied to a piezo in the direction of the poling voltage, the element will lengthen and its diameter become smaller. Conversely, if a voltage of polarity opposite that of the poling voltage is applied, the piezo will become shorter and broader. Therefore, when an alternating voltage is applied to the piezo it will lengthen and shorten cyclically at the frequency of the applied voltage. This cyclic motion generates the waveform which is transmitted into the air.

Ultrasonic transducer MCUSD40A100B17RS-70C was selected for the project. It is an ultrasonic transducer with a centre frequency of 100 KHz \pm 8 KHz and a directivity of 9°. An ultrasonic transducer was limited to 100 KHz for two reasons. Firstly, due to the limitation placed on frequency for air coupled ultrasonics, with respect to high losses

through air and attenuation as shown in Table 3.1. The higher the frequency, the higher the transmission losses and attenuation, thereby limiting possible transmission into the test material. Secondly, with a plate thickness of 10 mm, as selected in Chapter 4.3, this results in a high dispersion relationship. If a frequency was used over 200 KHz this would result in antisymmetric and symmetric lamb wave modes with multiple phases, making it difficult to analyse. By utilising 100 KHz, this results in a frequency-thickness of 1 MHz-mm, which from Figure 3.9 has only two lamb wave modes.

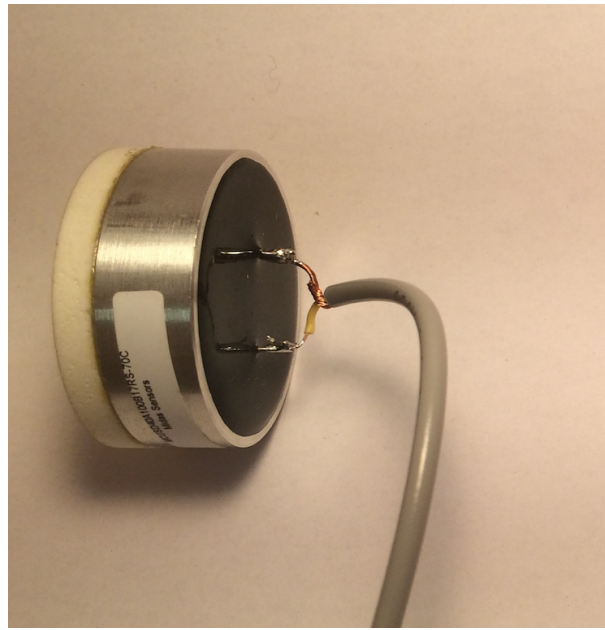


Figure 4.6: 100 KHz Ultrasonic Transducer.

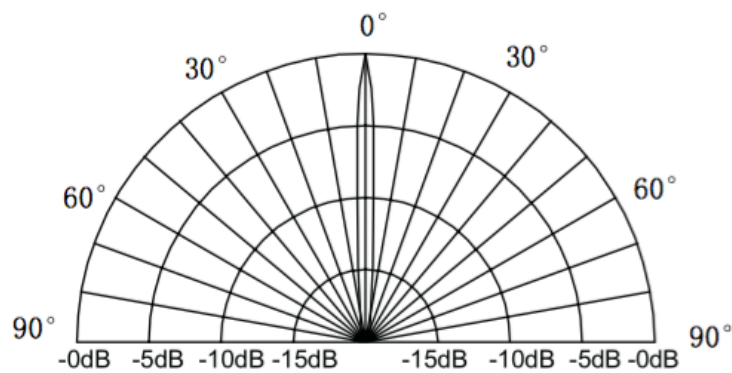


Figure 4.7: 100 KHz Directivity in Overall Sensitivity (Multicomp 2010).

Near field is the field closest to the transducer which has high fluctuations in intensity due to the constructive and destructive interference in the multiple waves originating from the transducer face. The area beyond near field is where the ultrasonic waveform is well behaved and at its maximum strength. Near field is governed by Equation 4.1. Due to the high fluctuations that occur to the signal in this region, the transducer must be positioned at a minimum distance which equates to the end of this field.

$$N = \frac{D^2 F}{4V} \quad (4.1)$$

For a 100 KHz signal produced from the MCUSD40A100B17RS-70C which has a diameter of 40 mm, travelling through air at a temperature of 20°C with a speed of 343 m/s equates to a near field of 116.6 mm. This means that the ultrasonic transducer must be placed at a distance of at least 116.6 mm from the test material. As the temperature of the air increases, the velocity in the air increases. Therefore, as the temperature increase the near field distance reduces, allowing the original near field distance to be suitable for all temperature increments.

Ultrasonic transducers also require an extremely high voltage at low capacitance to overcome the high transmission losses and attenuation that occur as the wave is transmitted through the air. Without a high voltage the ultrasonic transducer would behave as a contact transducer, due to the waveform strength being limited to extremely short distances.

The data-sheet for MCUSD40A100B17RS-70C ultrasonic transducer is attached at Appendix E.

4.2.3 Oscilloscope

Oscilloscopes are used to capture and analyse an electrical signal across a time period. It achieves this by capturing the varying voltage of the signal. By utilising an oscilloscope the received ultrasonic waveform was able to be captured and analysed in MATLAB to see how it varies with time and thereby what impact the fire has on the waveform.

Table 4.2 details the possible oscilloscopes.

Product	Sample Rate (S/s)
Tektronix TDS3054C	5,000,000,000
Arduino/Genuino Zero	350,000
Arduino M0 Pro	350,000
Arduino Uno	76,800

Table 4.2: Oscilloscope Sample Rates.

Nyquist theorem dictates that sampling rate must be at least twice the frequency to ensure the higher frequency components of the signal are captured (Rouse 2005). This means that for a 100,000 Hz signal a minimum sampling rate of 200,000 Hz was required. This, however, is just to meet the minimum requirements. To ensure that sufficient information about the waveform was captured, a sample rate of at least ten times the frequency of the waveform would be beneficial for this experiment. The TDS3054C was the only available oscilloscope capable of meeting that requirement. By utilising the TDS3054C the greatest accuracy in the results captured was guaranteed and it has the benefits of additional inbuilt triggers and multiple channels. The TDS3054C, however, is not portable. The TDS3054C would limit the experiment to test for which it is able to set-up in a non-hazardous area. Due to the higher accuracy that the TDS3054C offers over the other options, not being portable is accepted for experimental testing. For in-field testing an alternative would be required.

The TDS3054C interfaced with a windows computer through the use of the Tektronix

TekXL toolbar. This toolbar integrated with Microsoft Excel allowing for the download of waveform data from the oscilloscope. Due to the limitation of Microsoft Excel this interface was limited to saving 10,000 sample points. Consequently, the maximum sample rate when using this toolbar was 10,000,000 S/s, which is still well above the minimum required rate. With a pulse waveform of 170 μ s as shown in Figure 4.5, the oscilloscope was set up for a time division of 100 μ s. With a time division of 100 μ s the oscilloscope captured a waveform length of 1 ms. Due to the limitation of 10,000 sample points, this equates to a reading every 0.1 μ s.

The oscilloscope was set to trigger on the output signal from the op-amp circuit. Therefore, the delay from the piezo driver needed to be accounted for in the flight time. The output from the op-amp circuit was used as the trigger over the output from the piezo driver to avoid a high voltage being passed through the oscilloscope, as this may damage the equipment.



Figure 4.8: TDS3054C.

The TDS3054C was calibrated which is shown at Appendix F. Although calibrated, the oscilloscope does not read zero when no load is applied. This is due to the oscilloscope having a substantial amount of internal noise which reduces the accuracy of any reading obtained.

4.2.4 Piezo Driver

To allow for the ultrasonic waves to travel through the air, a high voltage was required to overcome the high transmission losses and attenuation. A piezo driver was used to step up the voltage from the function generator to a level that was suitable to be received once attenuation and high reflection as shown in Chapter 3.2.2 were overcome.

The MX200 high voltage amplifier was chosen. The MX200 has differential inputs, with a gain of 20 and slew rate of 60 V/ μ s. Thereby, stepping up the voltage from 3.3 V to 66 V.

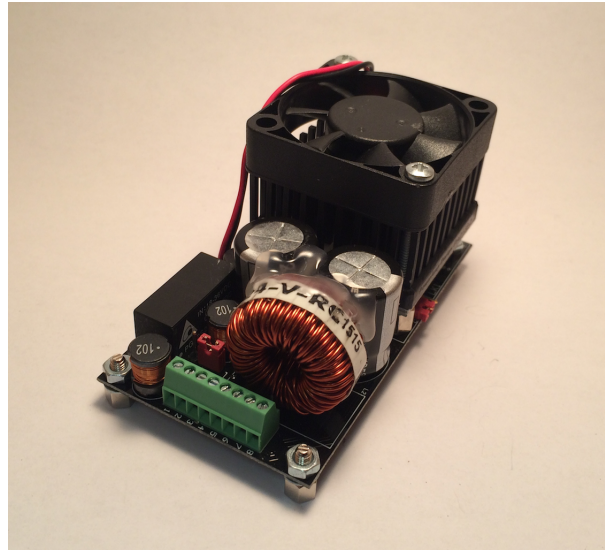


Figure 4.9: MX200 Piezo Driver.

The data-sheet for MX200 piezo driver is attached at Appendix G.

Due to the slew rate, a limiting relationship exists between the output voltage and frequency.

$$f = \frac{I_{av}}{V_{P-P}C_L} \quad (4.2)$$

Load (uF)	100 V	150 V	200 V
0.01	190000	100000	50000
0.03	83333	33333	16667
0.1	19000	10000	5000
0.3	8333	3333	1667
1	2500	1000	500
3	833	333	167
10	250	100	50
30	83.3	33.3	16.7

Table 4.3: MX200 Maximum Frequency (Hz) with capacitive load (Piezo Drive 2016).

Therefore, at an output of 200 V and 900 pF capacitance the frequency was limited to 555 KHz. If a higher voltage was required then a different piezo driver would be required capable of outputting these voltages. This would come at a much greater cost that was not funded under the project. The project was therefore limited to a 200 V Peak to Peak (PK-PK) ultrasonic waveform.

The MX200 output contains two types of noise, a low and a high frequency. The low frequency component was independent of the load capacitance and the high frequency component was inversely related to the load capacitance. The high frequency noise was due to the ripple from the boost converter

During testing at room temperature the function generator was connected directly to the piezo driver. This resulted in a 100 KHz wave with a PK-PK of 66 V. It was during this testing that it was determined that a PK-PK of 66 V was not suitable for testing under fire conditions as the increase in energy in the plate would reflect the lower intensity wave. To resolve this issue, an additional Operational Amplifier (Op-Amp) circuit was connected between the function generator and the piezo driver.

Stepping up the voltage from 10 V to 200 V produced a delay in the system, shown in

Figure 4.10. The delay was calculated through a TOF analysis to be 110 μs . Figure 4.10 shows the TOF for the ultrasonic wave from when it enters the piezo driver to when it is received by an ultrasonic transducer 50 mm from the transmit side. The TOF for an ultrasonic waveform travelling 50 mm through air at 20°C is 145.52 μs . Spurious noise at 180 μs , ultrasonic pulse began at 255 μs and an ultrasonic echo began at 480 μs .

The piezo driver was left running over a 30 minute period to confirm if there was any shift in this delay. Over this 30 minute period the delay due to piezo driver was consistent at 110 μs .

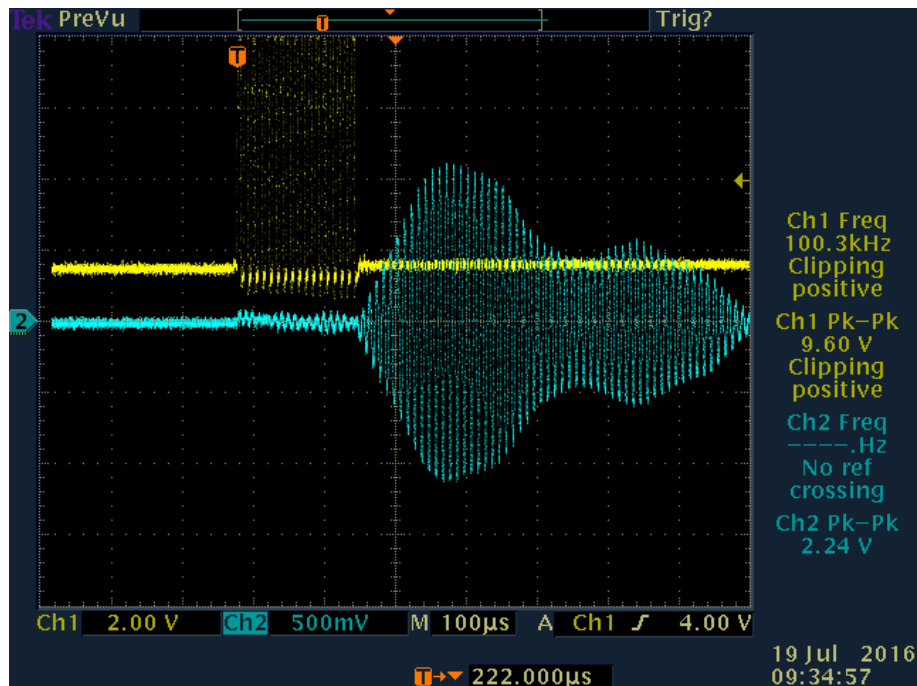


Figure 4.10: 50mm Time of Flight.

Operational Amplifier Circuit

During initial testing the function generator was connected directly to the piezo driver. This resulted in a 100 KHz wave with a PK-PK of 66 V. It was during this testing that it was determined that a PK-PK of 66 V was not suitable for testing under fire conditions

as the resulting received signal was too weak. To resolve this issue an Op-Amp circuit was connected between the function generator and the piezo driver.

An Op-Amp circuit is a direct coupled high gain electronic voltage amplifier. The Op-Amp circuit is shown in Figure 4.12. The Op-Amp circuit has a gain governed by Equation 4.3.

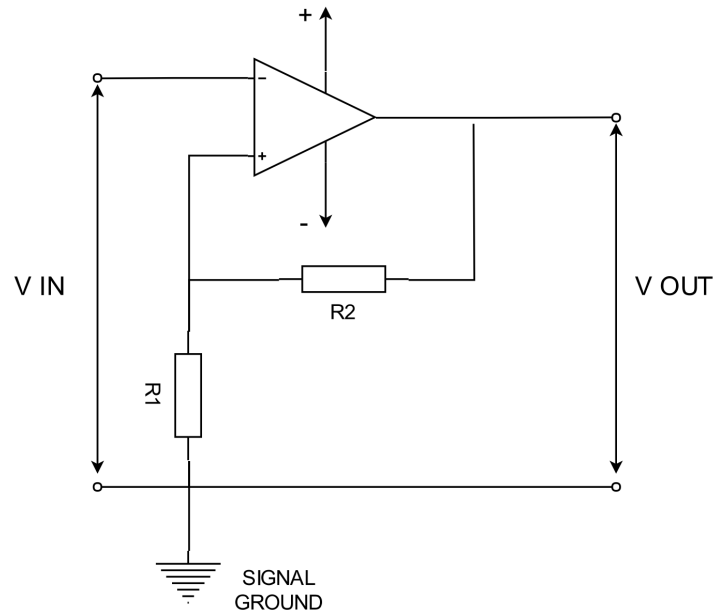


Figure 4.11: Operational Amplifier Circuit.

$$AV = 1 + \frac{R2}{R1} \quad (4.3)$$

An output voltage of 10 V was optimal to maximise the possible voltage from the MX200. To obtain an output voltage of 10 V $R1$ and $R2$ equate to 10,000 ohms and 18,000 ohms respectively. The output voltage from the Op-Amp circuit was tested which showed as 10 V. The output from the piezo driver was therefore 200 V.

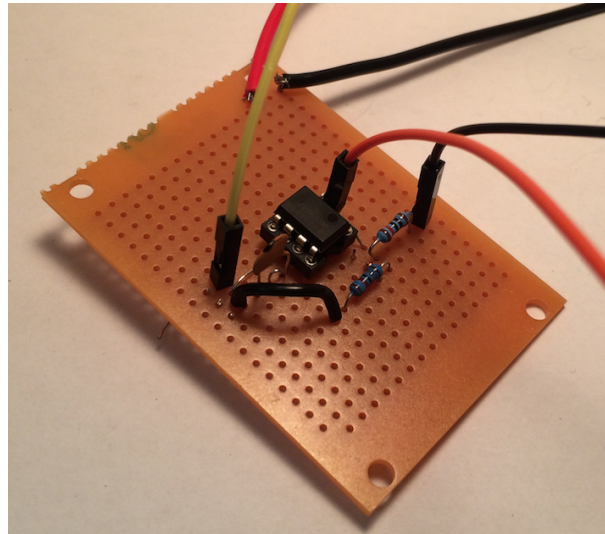


Figure 4.12: Operational Amplifier Circuit.

4.2.5 Pre-Amplifier

Due to the high attenuation that occurs to an ultrasonic wave as it travels through the air and high reflection as shown in Chapter 3.2.2 a pre-amplifier was required. A test at room temperature was conducted with a straight sight signal transmitted between two ultrasonic transducers placed 116 mm apart. The resulting signal was measured on the oscilloscope, which showed a PK-PK of 200 mV for a continuous waveform. Such a low amplitude would not be suitable once transmission into the test material was introduced. Due to the high reflection coefficient that occurs at this interface, the amplitude of the wave received would not allow suitable discrimination. A pre-amplifier steps up the amplitude of the signal received allowing it to be distinguished and analysed by the oscilloscope.

The Silicon Chip Australia PreChamp pre-amplifier was chosen. The PreChamp pre-amplifier circuit is shown in Figure 4.13, which provides a gain of 40dB.

The PreChamp acts as a high and low pass filter through the use of capacitors rolling

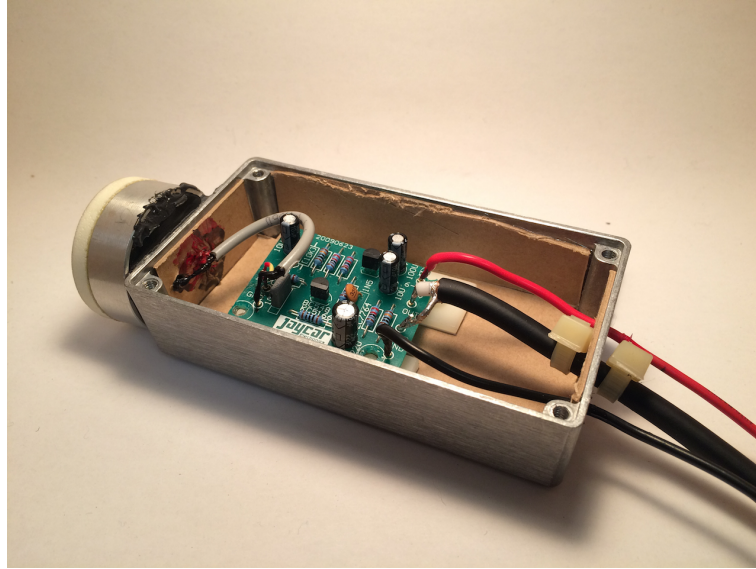


Figure 4.14: Pre-Amplifier.

pre-amplifier was also placed inside an aluminium case to prevent any interference from the turbulent and hot air. Single core Oxygen Free Copper (OFC) screened audio cable was used to carry the signal from the pre-amplifier to the oscilloscope to ensure noise introduction was minimised, while allowing a long cable. The pre-amplifier is shown in Figure 4.14.

4.2.6 Power Source

The power requirements for each of the components utilised as part of the ACU system were examined. These power requirements are outlined in Table 4.4.

As can be seen in Table 4.4, two supply rails of 24 V and 12 V were required. As two voltage rails were required a dual power supply most suitably met the power requirements.

Component	Voltage (V)
Piezo Driver	24
Arduino/Genuino Zero	7-12
Pre-Amplifier	6-12
Op-Amp Circuit	12

Table 4.4: Power Requirements.

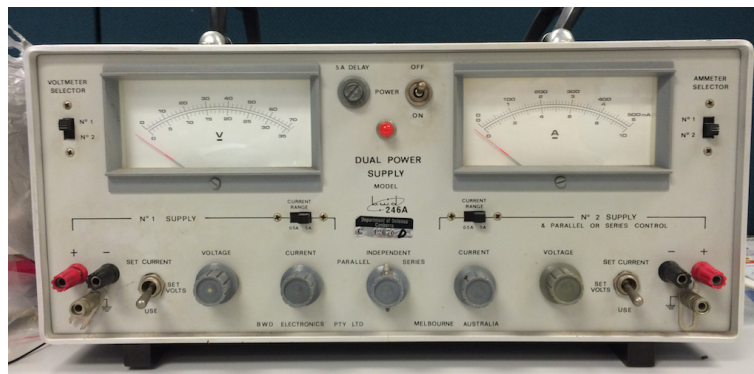


Figure 4.15: Dual Power Supply.

Power Supply

The BWD Electronics 246A was chosen to meet the power requirements. The BDW 246A is a dual DC power supply with a voltage range of 0-70 V and a current range of 0-10 A. The BWD 246A is shown in Figure 4.15.

Initial testing at room temperature showed an exorbitant amount of gaussian random noise was introduced into the received signal. This noise can be seen in the resulting lamb wave shown in Figure 4.16. A component analysis was conducted that showed the gaussian random noise was introduced into the op-amp circuit and function generator through the BWD 246A.

The BWD246A was connected directly to the oscilloscope for testing. Figure 4.17 shows that when the BWD 246A was set to an output voltage of 24 V it produced 1.30 V PK-PK

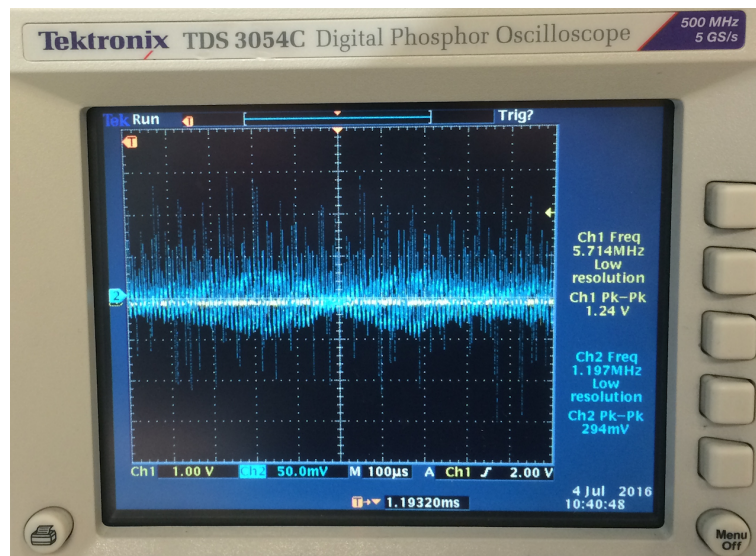


Figure 4.16: Lamb Wave Noise.

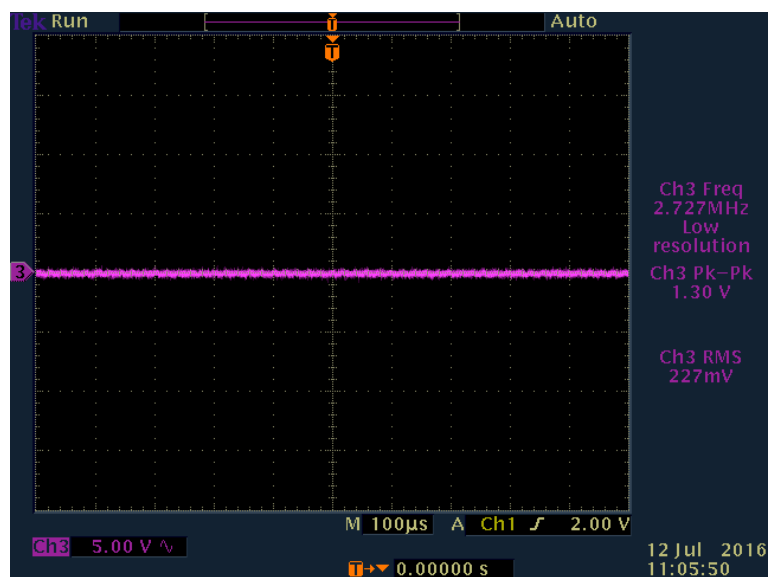


Figure 4.17: Dual Power Supply Noise.

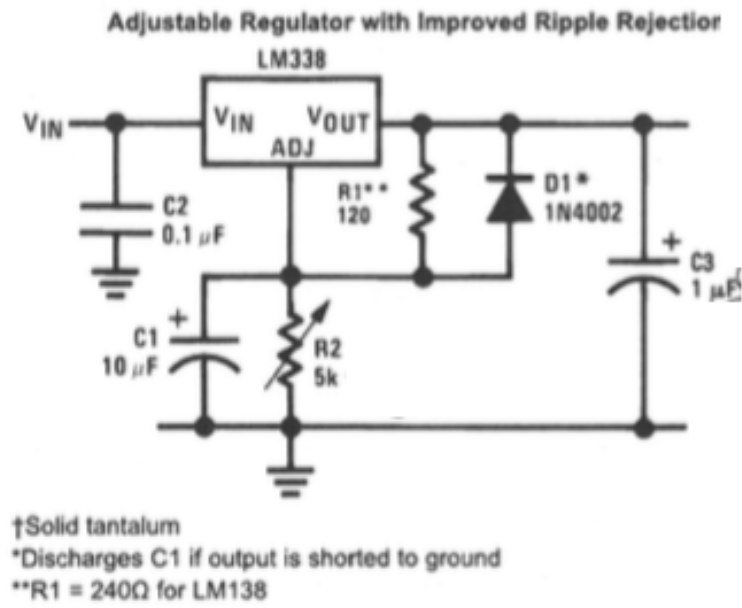


Figure 4.18: Voltage Regulator Circuit (Texas Instruments 2013).

at 227 mV Root Mean Square (RMS). The gaussian random noise was due to ripple in the BWD 246A. Ripple was due to the incomplete suppression of the AC waveform powering the power supply. To overcome this issue a voltage regulator was placed between the power supply and the voltage rails.

The LM338 5-Amp regulator from Texas Instruments was placed between the power supply and voltage rails. A voltage regulator was utilised to maintain a constant voltage level thereby removing any ripples. LM338 was capable of a 75 dB ripple rejection ratio at 10 V (Texas Instruments 2013). The output voltage was set by adjusting R1 and R2 using Equation 4.5. By setting R1 and R2 for the output voltage it remains constant regardless of changes to the input voltage or load conditions.

$$V_{OUT} = 1.25V(1 + \frac{R_2}{R_1}) + I_{ADJ}(R_2) \quad (4.5)$$

A circuit diagram for the voltage regulator is shown in Figure 4.18.

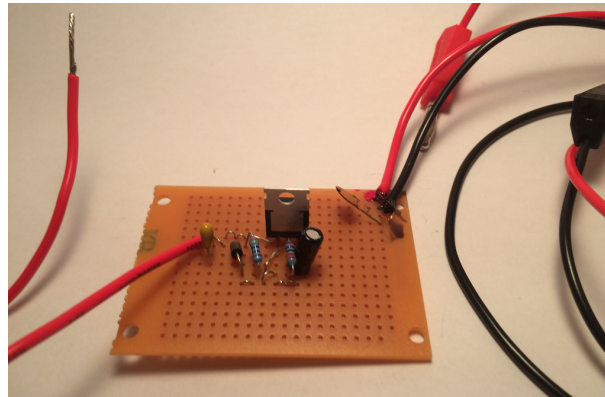


Figure 4.19: Voltage Regulator.

Due to the high accuracy required when analysing the ultrasonics, the voltage regulator did not limit the ripple to a suitable level. For ultrasonic testing the ideal ripple would be 0% which was not possible with the BWD 246A unless complete grounding was used, which would limit this application to a laboratory environment. To guarantee the high quality signal required batteries were utilised.

Batteries

7.2 Amp Hour 12 V sealed lead acid batteries were able to provide the suitable constant voltage supply without noise for both supply rails. By wiring two 12 V sealed lead acid batteries in series, a 24 V supply rail with 7.2 amp hour was produced. Figure 4.20 shows the 24 V battery set up.

The batteries underwent minor modification to ensure they were suitable for the hazardous environment while maintaining portability.

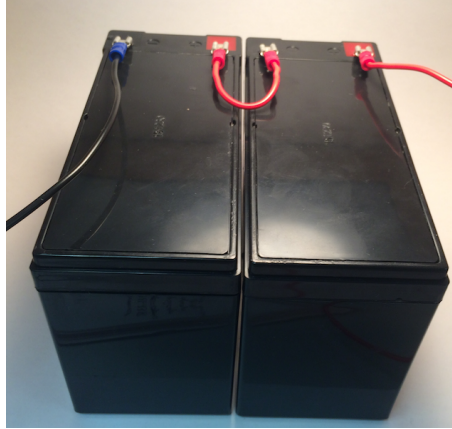


Figure 4.20: Battery Supply.

4.3 Bulkhead and Deckhead Materials

Aluminium, GFRP and CFRP were chosen for the project as they are common ship building materials with comparatively low temperature resistance when compared to steel.

To ensure that the materials exhibited the same characteristics and behaviours as a bulkhead and deckhead would under fire onboard a ship, the size of the plates was of critical importance. The plates were all 500 mm wide by 500 mm deep. Having all plates this size ensured that as they undergo thermal loading they will behave in a similar manner to a bulkhead and deckhead due to its free body area. The thickness for all plates was 10 mm as this is a standard thickness for Aluminium, GFRP and CFRP bulkheads onboard a ship.

4.3.1 Aluminium

Aluminium alloy 5083 H116 is commonly used for ship construction making it beneficial for investigation in this study. 5083 H116 is a wrought alloy, strengthened by strain hardening (cold working). 5083 H116 contains 4-4.9% magnesium, 0.4-1% manganese

and 0.05-0.25% chromium as its main constituents. This chemical composition results in a high resistance to corrosion making it attractive for maritime applications.



Figure 4.21: Aluminium 5083 H116 Plate.

Thermal properties for 5083 H116 are provided in Table 4.5.

Property	Metric
Density	2667 g/m ³
Coefficient of Thermal Expansion, linear 250 °C	26 $\mu\text{m}/\text{m}^\circ\text{C}$
Specific Heat Capacity	0.9 J/g $^\circ\text{C}$
Thermal Conductivity	117 W/mK
Melting Point	591 - 638 °C

Table 4.5: Aluminium 5083 H116 Thermal Properties (Aerospace Specification Metals Inc 2016).

4.3.2 Glass Fibre Reinforced Plastic

GFRP is commonly used for ship construction making it beneficial for investigation in this study. GFRP was composed of two elements a glass fibre and a resin. The glass fibre chosen was MX4500 E-Glass and the resin was Ampreg 22 Epoxy resin.

The data-sheet for MX4500 E-Glass composite reinforcement is attached at Appendix H. The data-sheet for Ampreg 22 Epoxy is attached at Appendix J.



Figure 4.22: Composite Plates (McConaghy Boats 2016).

The composite was manufactured utilising a hand lay-up vacuum bagged method. The volume fraction for this manufacturing method was 40%. The density for glass fibre is $2.54 \frac{g}{cm^3}$, density for Ampreg 22 epoxy is $1.147 \frac{g}{cm^3}$, resulting in a weight fraction of 59.6%. This equates to a glass fibre thickness of 0.1799 mm and an epoxy thickness of 0.27 mm per ply.

The overall lay-up for the GFRP was $[(45,-45)]_{22T}$. An overall thickness of approximately 10 mm.

Thermal properties for GFRP are provided in Table 4.6.

Property	Metric
Fibre Density	2.54 g/cm^3
Fibre Coefficient of Thermal Expansion	5×10^{-6} m/mK
Fibre Melting Point	1225 °C
Epoxy T_g 1	63.2°C
Epoxy Ultimate T_g	108.7°C

Table 4.6: GFRP Thermal Properties (Colan Australia 2007).

4.3.3 Carbon Fibre Reinforced Plastic

CFRP is commonly used for ship construction making it beneficial for investigation in this study. CFRP was composed of two elements a carbon fibre and a resin. The carbon fibre chosen was XC41124K carbon fibre and the resin was Ampreg 22 Epoxy resin.

The data-sheet for XC41124K Carbon Fibre composite reinforcement is attached at Appendix I. The data-sheet for Ampreg 22 Epoxy is attached at Appendix J.

The composite was manufactured utilising a hand lay-up vacuum bagged method. The volume fraction for this manufacturing method was 40%. The density for carbon fibre is $1.6 \frac{g}{cm^3}$, density for Ampreg 22 epoxy is $1.147 \frac{g}{cm^3}$, resulting in a weight fraction of 48.1%. This equates to a carbon fibre thickness of 0.2562 mm and an epoxy thickness of 0.3856 mm per ply.

The lay-up for the CFRP was $[(45,-45)]_{15T}$. An overall thickness of approximately 10 mm.

Thermal properties for CFRP are provided in Table 4.7.

Property	Metric
Fibre Density	1.6 g/cm^3
Fibre Coefficient of Thermal Expansion	2.1×10^{-6} m/mK
Fibre Melting Point	4000 °C
Epoxy T_g 1	63.2°C
Epoxy Ultimate T_g	108.7°C

Table 4.7: CFRP Thermal Properties (AZOM 2003).

4.4 Fire Simulation

To produce a fire, oxygen, heat and a fuel must all be present in an appropriate mixture. This is referred to as the fire triangle as shown in Figure 4.23. Without any one of these three elements a fire is not possible.



Figure 4.23: Fire Triangle (Elite Fire 2013).

A LPG gas bottle was used to provide the fuel element. LPG is a group of flammable hydrocarbon gases including propane, butane or a mixture of these gases, that are liquefied through pressurisation (ELGas 2016). However, in Australia LPG is only available in Propane (ELGas 2016).

A burner was used to control the production of the fire. The burner regulated the mixture of the fuel and oxygen element of the fire triangle. This ensured an appropriate mixture occurs. A Gasmate 3 Ring Cast Iron Burner was used to produce the flame and control the mixture. The Gasmate mixes the LPG and air as they enter the Venturi tube, ensuring the flame produced at the burner was optimal. The Gasmate also provided a large burner area for the flame, ensuring it is not concentrated in one area of the plate.

The colour of the flame produced by the gas and burner regulates the fire conditions. When incomplete combustion occurs the flame burns sooty red or yellow. A yellow colour is due to incandescence of very fine soot particles that are produced in the flame. A blue flame indicates the flame is fully developed, complete combustion, clean and no sooting is present. To produce a blue flame when using LPG as the fuel an air-to-gas volume ratio of about 24:1 is required (ELGas 2016).

Flame Colour	Degree
Blue	1980°C
Red	1000°C
Yellow	1000°C

Table 4.8: Flame Colour Temperatures (ELGas 2016).

A blue flame was required for this experiment to optimise fire conditions.

A grill was placed above the burner to break the flame thereby limiting high points and ensuring even flame distribution. Secondly, a minimal air gap was placed between the flame and the plate to minimise direct flame contact, burning and maximise heat transfer. By removing high points it ensured that the flame was evenly distributed across the whole burner area. Secondly, the addition of the air gap removed direct contact between the fire and the plates, allowing the plates to heat up due to the thermal loading caused by the fire. This thermal loading provided a more suitable test material rather than the plates being directly burnt and distorted from a point flame.



Figure 4.24: Burner.

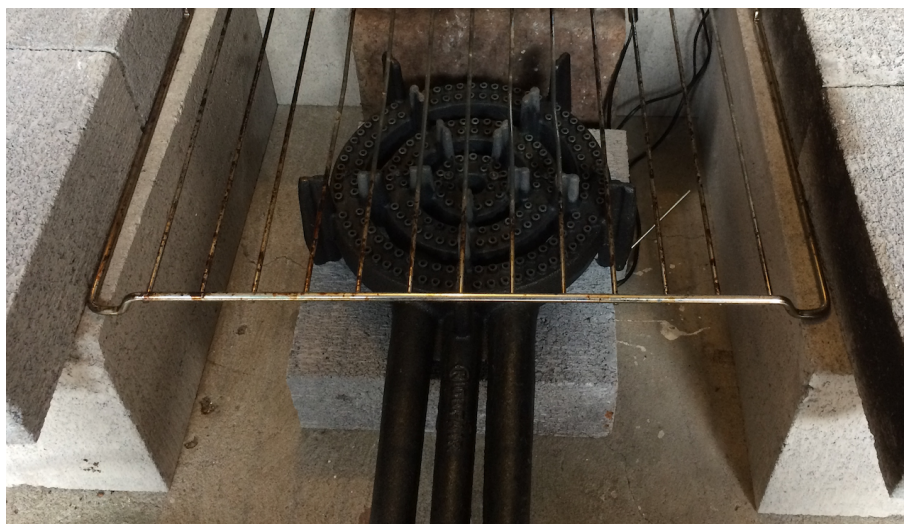


Figure 4.25: Grill.

The burner and grill were encased by concrete blocks. The concrete blocks provided a suitable test bed on which to rest the materials and an environment barrier to control the behaviour of the fire. Concrete blocks were placed on three sides, creating a closed environment from floor to test material as shown in Figure 4.25. By creating a closed environment on three sides of the fire, this ensured that maximum thermal loading was applied to the test material and not lost to the surrounding environment. If fire and heat were lost to the external environment it would impact the behaviour of the material due to uneven thermal loading. The fourth side was left open to ensure the fire was not suffocated and left an opening that allowed the positioning of the burner. The opening also allowed for a view port to record the behaviour of the fire and how it was interacting with the test material. Furthermore, the opening was a safety measure so the behaviour of the fire was known at all times to ensure it is able to be extinguished if the fire damaged components or equipment in surrounding environment.

4.5 Temperature Reading

As the test materials undergo fire conditions it was vital to know the interaction between the fire and the material. Recording the temperature of different elements was vital to this understanding. The temperature of the following elements was necessary:

- ultrasonic transducers;
- test material surface temperature on non-fire side;
- test material surface temperature on fire side; and
- fire enclosure air temperature.

As a number of temperature readings were required to be recorded across a period of time, an Arduino Uno with a data logger was utilised to record this information. The

devices used to capture temperature readings must be compatible with an Arduino Uno. The code used for the Arduino uno data logger is attached at Appendix N.

Thermocouples are a very durable and accurate temperature sensor. Thermocouples however, are very sensitive and they require an amplifier with a cold-compensation reference. The MAX31855 is a thermocouple amplifier that was chosen to use with the thermocouples. The performance specifications for the MAX31855 is provided at Table 4.9. The MAX31855 is compatible with an Arduino Uno allowing for data recording.

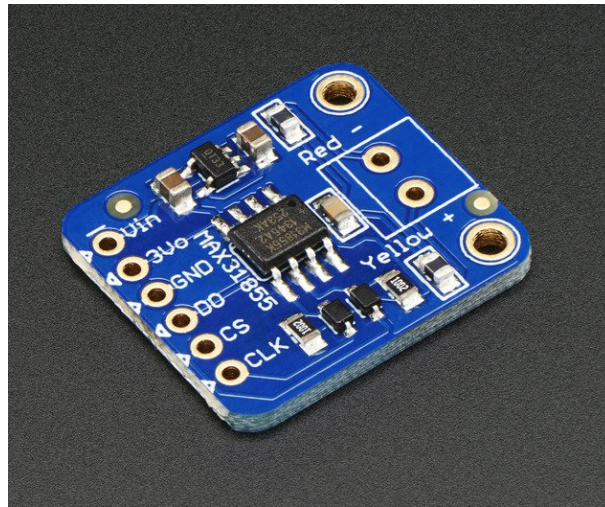


Figure 4.26: MAX31855 (Adafruit 2016*b*).

Parameter	Value
Thermocouple	K Type
Temperature	-200 to 1350°C
Resolution	2 to 6°C
Cold Compensation	Yes

Table 4.9: MAX31855 Specifications (Adafruit 2016*a*).

For the temperature readings inside the fire enclosure, a thermocouple with a high temperature resistance was required. The QM1282 K-type thermocouple was utilised to record these readings due to its ability to record temperatures up to 1200°C. The QM1282

is able to interface with the MAX31855.

During the experiment it was found that the QM1282 was not able to withstand the high temperatures specified. The metal probe used to take the temperature readings was able to withstand the temperatures however the connection to the wire which carries the signal was soldered together. As the temperatures in the fire enclosure reached over 400°C this solder connection failed. The probe that was inside the flames carried the heat down the probe to this solder connection, which then heated up until the solder melted. This separation between the probe and the wire is shown in Figure 4.27.

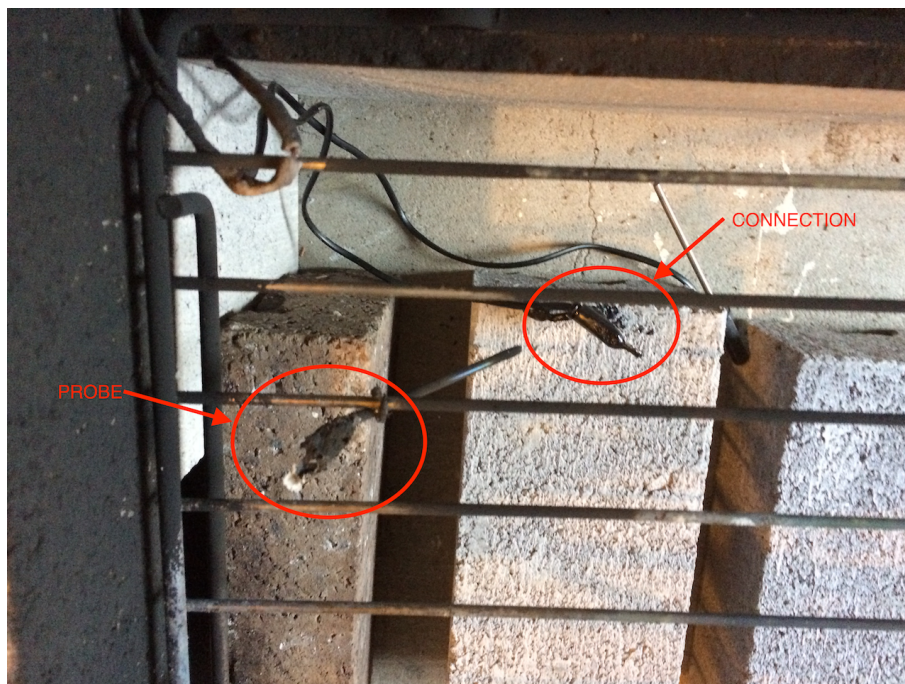


Figure 4.27: Thermocouple Separation.

The surface temperature across an area of the non-fire side of the plate would be suitable. An InfraRed temperature sensor captures the average temperature across the in sight area of the plate. The IR Temperature Sensor from Freetronics was chosen due to its intergration with an Arduino uno. The performance specifications for the IR temperature sensor is provided at Table 4.9.

Parameter	Value
Ambient Temperature	-10 to 50°C
Temperature	-33 to 220°C
Accuracy	2°C
Resolution	0.0625°C

Table 4.10: IR Temperature Sensor Specifications (Freetronics 2016).

Due to the upper limit for the IR temperature sensor being the upper limit for temperatures reached during the project a calibration was undertaken. Calibration was undertaken against a K-type thermocouple on a steel plate heated by a LPG bottle and burner. The code at Appendix M was utilised for calibration recordings.

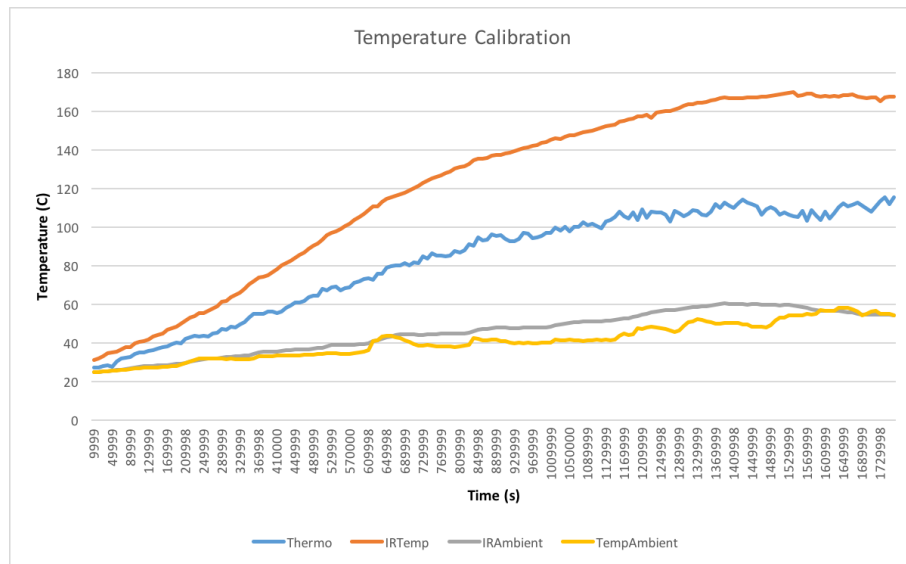


Figure 4.28: Temperature Calibration.

As can be seen from Figure 4.28, the difference between the thermocouple reading and the InfraRed reading was quite substantial once the temperature passes 80°C. The difference between the two sensors once the temperature passes 80°C was maintained at 30%. Due to this high difference the InfraRed sensor was not suitable for the high temperature readings required for the project. A k-type glass braid insulated thermocouple was used

to record the test material surface temperature on non-fire side.

The air temperature at the ultrasonic transducer was not directly exposed to the fire, it only experienced the temperature fluctuations the external environment underwent. The Adafruit SHT31-D is a temperature and humidity sensor. By gathering not just the temperature reading but also the humidity a more accurate determination of the properties of the air through which the ultrasonic wave was being transmitted. The performance specifications are provided at Table 4.11.

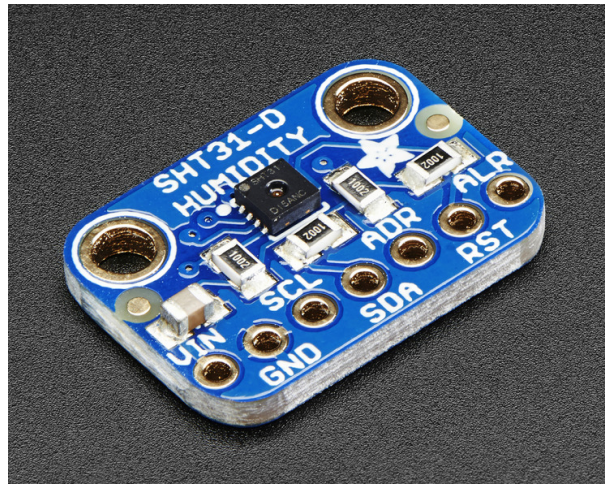


Figure 4.29: SHT-31D (Adafruit 2016*a*).

Parameter	Value
Humidity	0 to 100
Humidity Resolution	0.01
Temperature	-40 to 125°C
Temperature Resolution	0.015

Table 4.11: SHT-31D Specifications (Adafruit 2016*a*).

4.6 Air Coupled Ultrasonics Test Method Schematic

The experimental set-up for the ACU is shown in Figure 4.30.

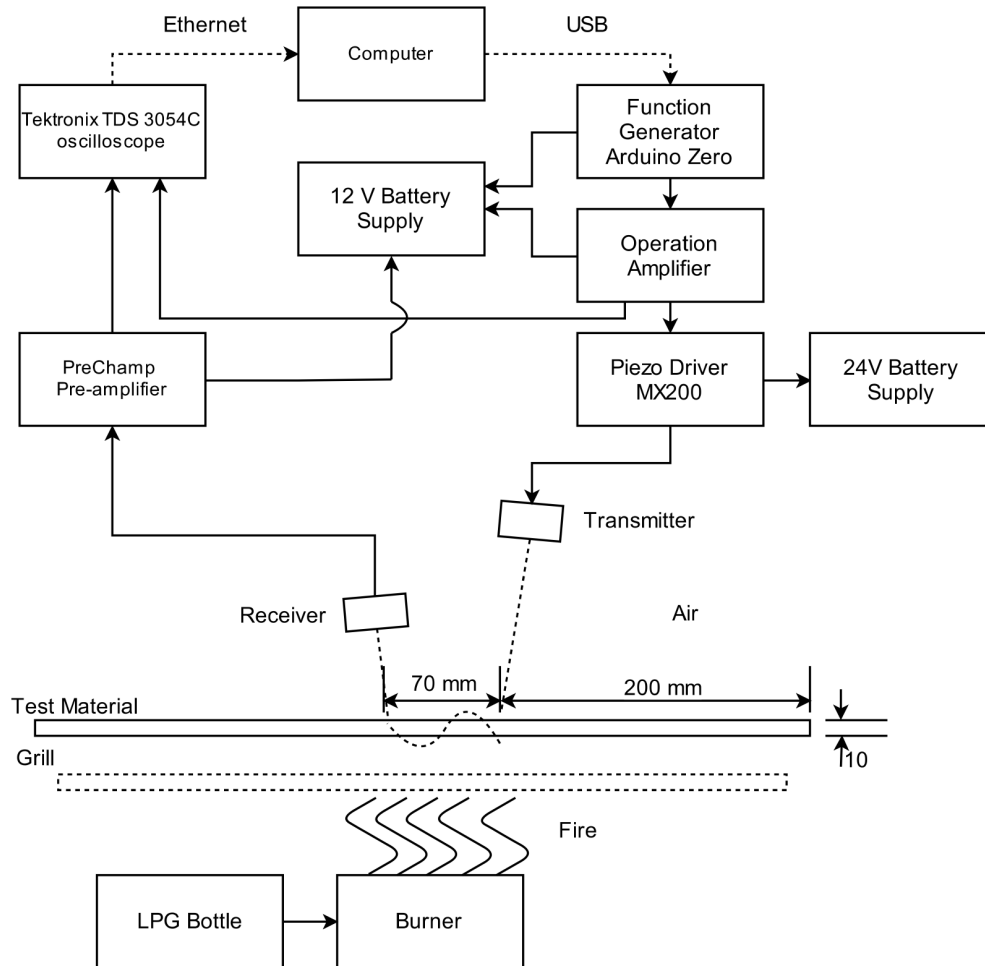


Figure 4.30: Schematic Diagram of Experimental ACU Set Up.

Figure 4.31 shows the configuration for the transmit side of the ACU. The ultrasonic transducer was mounted to the base of an aluminium case. The piezo driver and op-amp circuit were placed inside an aluminium case to minimise any impact from the surrounding environment and to prevent exposure to the hazardous fire conditions. The

function generator was placed on top of the aluminium case due to the limitation of space inside the case. An external reset button was connected to the function generator to allow the reset of the pulsed waveform shown in Figure 4.5 and remove any requirement for human contact direct with the transmit case. Human contact on the transmit components could introduce vibrations or move components which would introduce anomalies into the results.

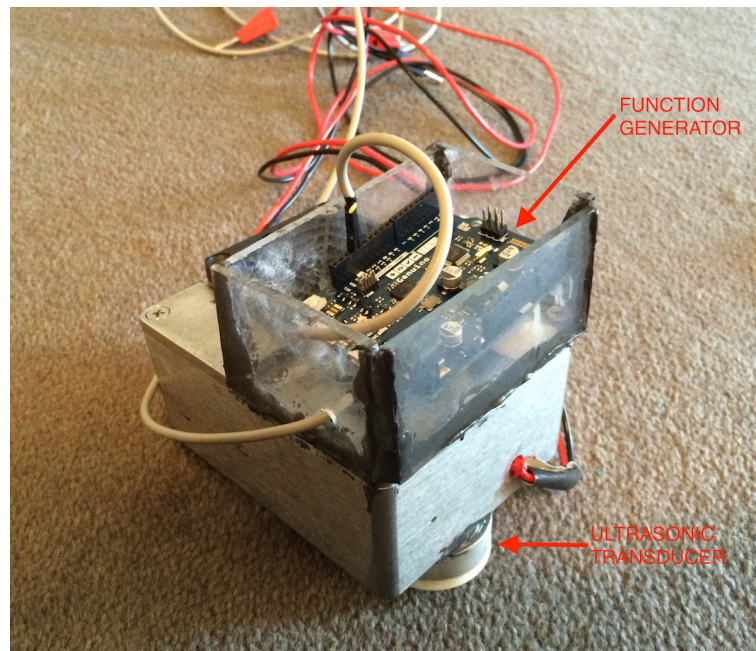


Figure 4.31: Transmit Air Coupled Ultrasonic Set Up.

Figure 4.32 shows the configuration for the receive side of the ACU. The ultrasonic transducer was mounted to the end of an aluminium case. The pre-amplifier was mounted inside the aluminium case. The wires connecting the ultrasonic transducer to the pre-amplifier were of minimal length and protected by the case, minimising noise and interference.

Figure 4.33 and Figure 4.34 shows the configuration of the fire enclosure. Concrete blocks create a fire enclosure on three sides while the fourth side were left open. The grill is shown above the burner with minimal air gap before the plate.

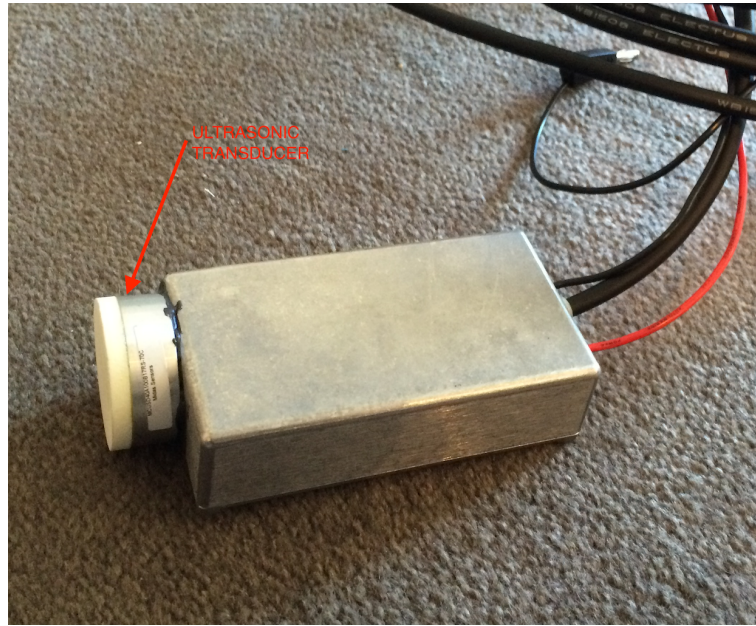


Figure 4.32: Receive Air Coupled Ultrasonic Set Up.

Figure 4.35 shows the configuration of the ACU in relation to the test material. As determined in Chapter 3.2.3, the angle of incident that provides maximum transmission for an aluminium plate is 5° . The transmit ultrasonic transducer was placed at 117 mm from the surface of the test material due to near field, at a -5° angle from the vertical. The receive ultrasonic transducer was placed 52 mm from the test material at an angle of 5° from the vertical. The distance between the outer edges of the two ultrasonic transducers was 45 mm. Therefore, the centre of the two ultrasonic transducers was 85 mm apart. At this spacing the transmit and receive ultrasonic transducers are not in direct line of sight with a full reflection wave off the test material, therefore the receive ultrasonic transducer will only capture lamb wave responses.

The test material was placed so that it was free standing on the concrete blocks to ensure that it did not undergo any applied stress other than due to thermal loading. Thereby, ensuring stress free boundary conditions.

The transmitted ultrasonic waveform entered the test material 200 mm from the edge of

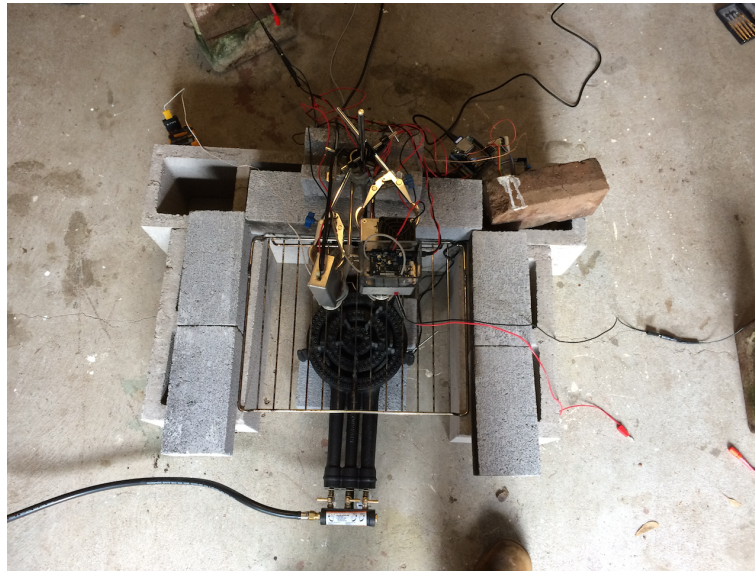


Figure 4.33: Air Coupled Ultrasonic Set Up.

the plate in the path of travel. If the ultrasonic waveform entered the material directly on centre then there was a possibility for standing wave cancellation due to the lamb wave reflections from the end of the plates. This standing wave cancellation was only possible if the lamb waves are in phase with each other due to entering and travelling the same distance. In the real life application for this equipment, the likelihood of the ultrasonic waveform entering directly in the centre of the plate leading to standing wave cancellation is minimal. Conducting the experiment as close to the real life application as possible provided the most effective feedback to ensure the end user requirements were being met. The transmitted ultrasonic waveform enters 210 mm from the non-path of travel edge.

Since the distance between the transmit and receive side of the ACU did not change for all tests, therefore TOF variation is directly related to temperature changes.

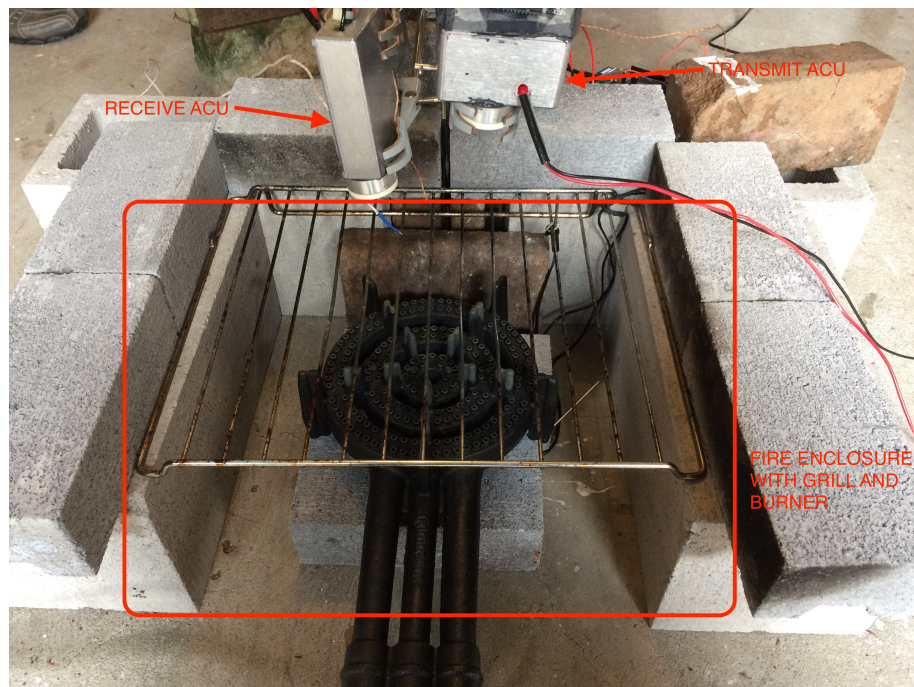


Figure 4.34: Air Coupled Ultrasonic Set Up.

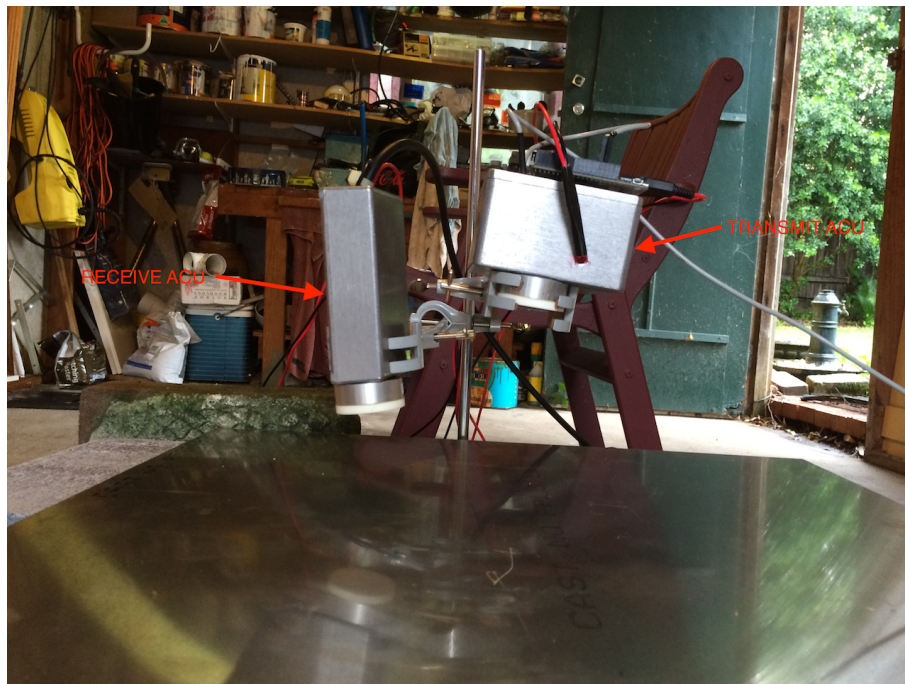


Figure 4.35: Air Coupled Ultrasonic Set Up with Aluminium Plate.

Chapter 5

Results and Discussion

This chapter presents an analysis of the results of testing Aluminium under fire conditions up to 260 °C and, GFRP and CFRP under fire conditions up to 160 °C at 10° C increments using the designed non-invasive test method.

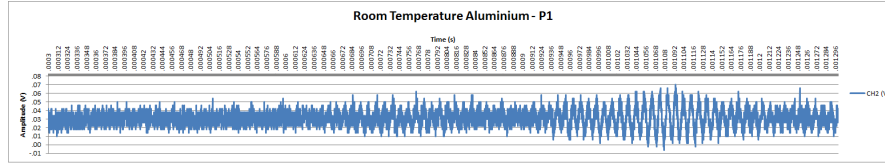
The results showed that ACU utilising commercially available components was suitable for testing under fire conditions. As the plates undergo thermal loading due to fire conditions, the elastic properties of the material begin to change as the material moves away from solid state. This material state change impacts the resulting lamb wave response. The results also showed there were number of limitations due to design which required further research.

5.1 Room Temperature Results

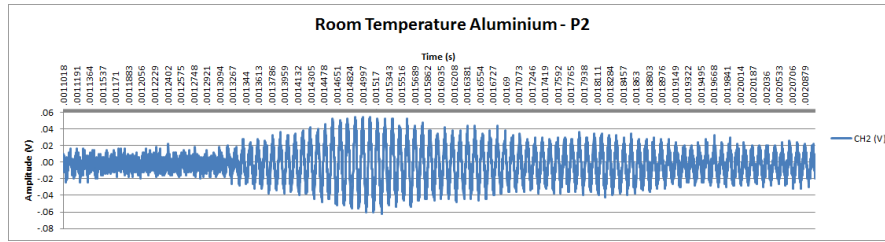
This chapter presents the results of testing at room temperature. These results are used as the baseline for which testing under fire conditions was compared. The testing was undertaken using the ACU test model described in Chapter 4.6.

5.1.1 Aluminium

Figure 5.1 shows the ACU response for Aluminium alloy 5083 H116 at room temperature.



(a) $t = 200 \text{ us to } 1200 \text{ us}$



(b) $t = 1100 \text{ us to } 2100 \text{ us}$

Figure 5.1: Room Temperature Lamb Wave Response Aluminium.

A symmetric lamb wave response was not received, see Figure 5.1. A symmetric lamb wave response should arrive at 610 us noting the high velocity shown in Figure 3.9. The symmetric mode is weaker than the antisymmetric mode due to the vibration of the lamb wave being weaker in this mode. To receive the symmetric lamb wave response, the standing 10 mv PK-PK noise seen in Figure 5.1 needs to be removed. This noise was due to the use of ACU and the noise that naturally occurs in the air. Secondly, it was due to the internal noise of the oscilloscope.

Six antisymmetric lamb wave responses were received. Even though the ultrasonic waveform pulse was 170 us there was still overlap between the received waveforms due to the spurious noise at the start and end of each wave. Secondly, due to the multiple reflections and transmission modes that occur.

The first antisymmetric lamb wave response registered at 632 us. During the testing the

temperature of the air was 17°C with a humidity of 90%, which equates to a speed of sound in air of 342.53 m/s. The TOF for the air was 493 us. The delay for the piezo driver was 110 us. The TOF in aluminium for an antisymmetric lamb wave with velocity of 2400 m/s as shown in Figure 3.9, was 33 us for 70 mm travel path. The total TOF was equal to that of the registered lamb wave.

The second lamb wave response registered at 936 us. The second lamb wave response was due to the reflection off the receive ultrasonic transducer, travelling back to the aluminium plate, reflecting off the plate and travelling back to the ultrasonic transducer. The distance travelled through the air was 273 mm compared to the first wave with a distance of 169 mm. The TOF for the air was 797.01 us. The delay for the piezo driver was 110 us. The TOF for aluminium plate was 33 us.

The third lamb wave response registered at 1320 us. The third lamb wave response was due to the reflection off the aluminium plate, travelling back to the transmit ultrasonic transducer, reflecting off the ultrasonic transducer and travelling back to the plate. The distance travelled through the air was 403 mm compared to the first wave with a distance of 169 mm. The TOF for the air was 1177 us. The delay for the piezo driver was 110 us. The TOF for aluminium plate was 33 us.

The fourth lamb wave response registered at 1480 us. The fourth lamb wave response was due to ultrasonic waveform hitting the plate creating a lamb wave that travelling to the edge of the plate, bounces off the edge travelling back towards the receive ultrasonic transducer. The distance travelled through in the plate was 470 mm compared to the a distance of 70 mm for the standard lamb wave. The TOF for the air was 1177 us. The delay for the piezo driver was 110 us. The TOF for aluminium plate was therefore 195 us.

The fifth lamb wave response registered at 1620 us. The fifth lamb wave response was the third lamb wave response that has reflected off the receive ultrasonic transducer, travelling back to the aluminium plate, reflecting off the plate and travelling back to the

ultrasonic transducer. The distance travelled through the air was 507 mm compared to the first wave with a distance of 169 mm. The TOF for the air was 1480 us. The delay for the piezo driver was 110 us. The TOF for aluminium plate was 33 us.

The sixth lamb wave response registered at 1785 us. The sixth lamb wave response was fourth lamb wave response that has reflected off the receive ultrasonic transducer, travelling back to the aluminium plate, reflecting off the plate and travelling back to the ultrasonic transducer. The distance travelled through the air was 507 mm compared to the first wave with a distance of 169 mm. The TOF for the air was 1480 us. The delay for the piezo driver was 110 us. The TOF for aluminium plate was 195 us. The lamb wave response timings are of the assumption that no dispersion has occurred.

Figure 5.2 shows a schematic of the lamb wave transmission paths.

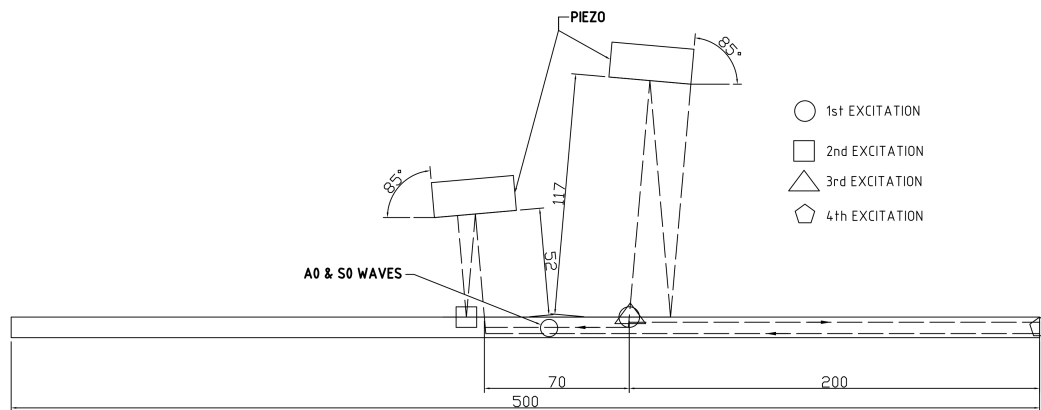


Figure 5.2: ACU Reflections Model Aluminium.

The received waveforms underwent an FFT to determine the received frequency. Figure 5.3 shows this FFT. A spike in the FFT response occurred at 100 KHz which was the frequency that the waveform was transmitted. This showed that the waveform has not undergone any frequency shift during transmission. Harmonics are registered at 590 and 890 KHz. From Equation 3.23 the wavelength was calculated to be 24 mm. Therefore,

the wavelength for the ultrasonic waveform travelling through Aluminium at solid state was 24 mm. The code at Appendix O was used to undertake signal processing.

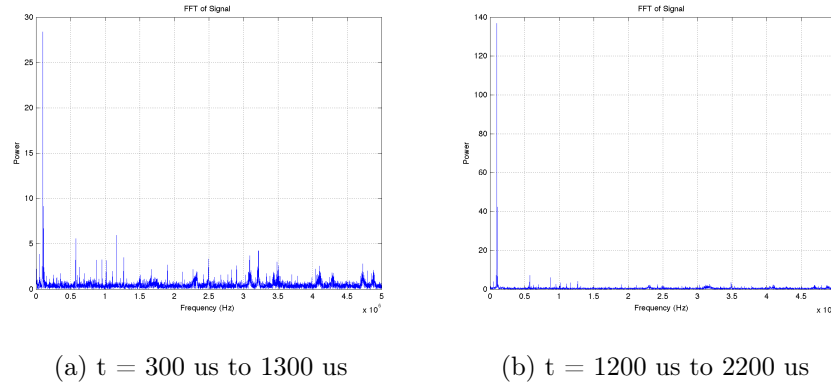


Figure 5.3: FFT Room Temperature Aluminium.

5.1.2 GFRP

Figure 5.4 shows the ACU response for GFRP at room temperature.

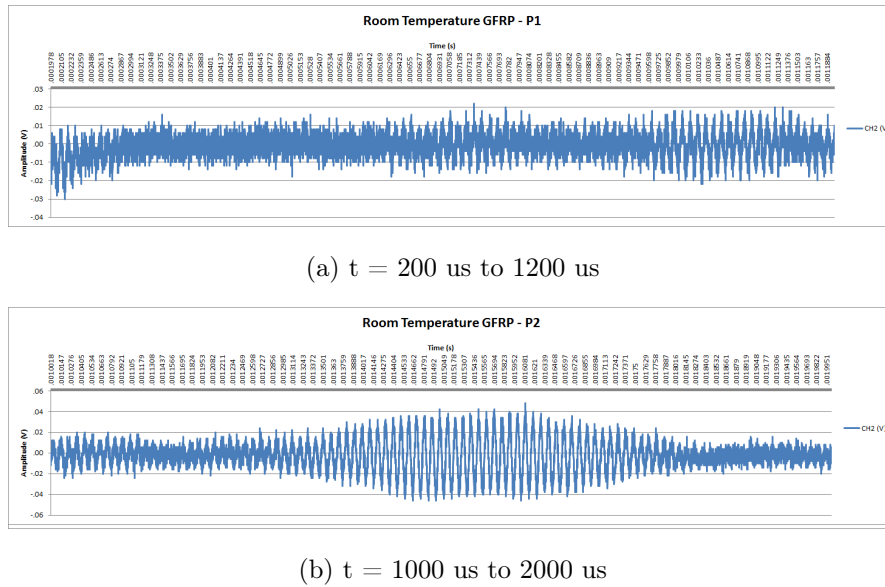


Figure 5.4: Room Temperature Lamb Wave Response GFRP.

Similar to the Aluminium ACU response at room temperature, no symmetric lamb wave response was received, as shown in Figure 5.4.

Five antisymmetric lamb wave responses are received. The first antisymmetric lamb wave response registered at 628 us. The TOF for the air was 493.387 us. The delay for the piezo driver was 110 us. The TOF in GFRP for an antisymmetric lamb wave with velocity was 2800 m/s, determined through calibration was 25 us. The total TOF was equal to that of the registered lamb wave.

The second lamb wave response registered at 932 us. The TOF for the air was 797.01 us. The delay for the piezo driver was 110 us. The TOF for GFRP plate was 25 us.

The third lamb wave response registered at 1310 us. The TOF for the air was 1176.54 us. The delay for the piezo driver was 110 us. The TOF for GFRP plate was 25 us.

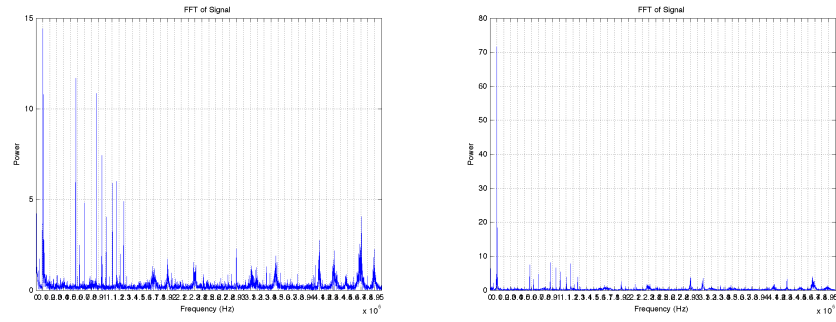
The fourth lamb wave response registered at 1454 us. The TOF for the air was 1176.54 us. The delay for the piezo driver was 110 us. The TOF for GFRP plate was therefore 167.86 us.

The fifth lamb wave response registered at 1615 us. The TOF for the air was 1480.16 us. The delay for the piezo driver was 110 us. The TOF for GFRP plate was 25 us. The lamb wave response timings are of the assumption that no dispersion has occurred.

As the placement for the GFRP was the same as that for the Aluminium plate the reflections model was the same as shown in Figure 5.2.

The received waveforms underwent an FFT to determine the received frequency. Figure 5.5 shows this FFT. A spike in the FFT response occurred at 100 KHz which was the frequency that the waveform was transmitted. This showed that the waveform has not undergone any frequency shift during transmission. Harmonics are registered at 590 and 890 KHz. From Equation 3.23 the wavelength was calculated to be 28 mm. Therefore, the wavelength for the ultrasonic waveform travelling through GFRP at solid state was

28 mm. The code at Appendix O was used to undertake signal processing.



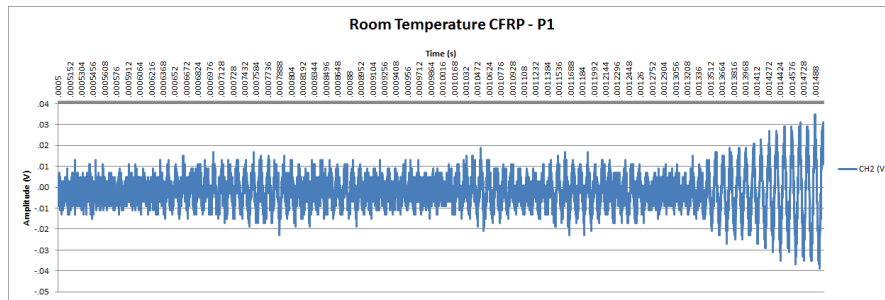
(a) $t = 200 \text{ us to } 1200 \text{ us}$

(b) $t = 1000 \text{ us to } 2000 \text{ us}$

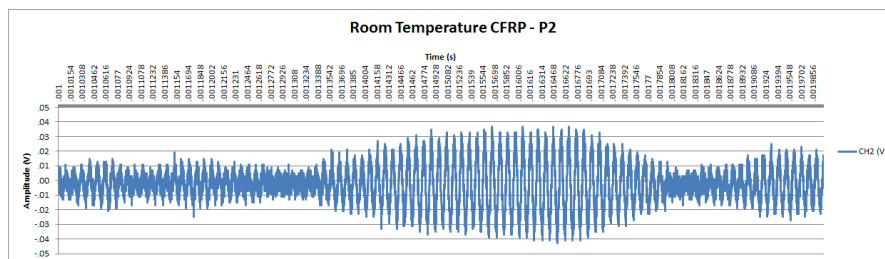
Figure 5.5: FFT Room Temperature GFRP.

5.1.3 CFRP

Figure 5.6 shows the ACU response for CFRP at room temperature.



(a) $t = 500 \text{ us to } 1500 \text{ us}$



(b) $t = 1000 \text{ us to } 2000 \text{ us}$

Figure 5.6: Room Temperature Lamb Wave Response CFRP.

As was shown in the Aluminium ACU response no symmetric lamb wave response was received in Figure 5.6.

Seven antisymmetric lamb wave responses are received. The first antisymmetric lamb wave response registered at 636 us. The TOF for the air was 493.387 us. The delay for the piezo driver was 110 us. The TOF in CFRP for an antisymmetric lamb wave with velocity was 2200 m/s, determined through calibration was 33 us. The total TOF was equal to that of the registered lamb wave.

The second lamb wave response registered at 939 us. The TOF for the air was 797 us. The delay for the piezo driver was 110 us. The TOF for CFRP plate was 33 us.

The third lamb wave response registered at 1129 us. The third lamb wave response was plate edge reflection that has reflected off the receive ultrasonic transducer, travelling back to the CFRP plate, reflecting off the plate edge and travelling back to the ultrasonic transducer. The TOF for the air was 797 us. The delay for the piezo driver was 110 us. The TOF for CFRP plate was 223 us.

The fourth lamb wave response registered at 1321 us. The TOF for the air was 1177 us. The delay for the piezo driver was 110 us. The TOF for CFRP plate was 34 us.

The fifth lamb wave response registered at 1508 us. The TOF for the air was 1177 us. The delay for the piezo driver was 110 us. The TOF for CFRP plate was 223 us.

The sixth lamb wave response registered at 1624 us. The TOF for the air was 1480 us. The delay for the piezo driver was 110 us. The TOF for GFRP plate was 34 us.

The seventh lamb wave response registered at 1814 us. The seventh lamb wave response was the fifth lamb wave response that has reflected off the receive ultrasonic transducer, travelling back to the aluminium plate, reflecting off the plate and travelling back to the ultrasonic transducer. The TOF for the air was 1480 us. The delay for the piezo driver was 110 us. The TOF for CFRP plate was 224 us.

As the placement for the CFRP was the same as that for the Aluminium plate, the reflections model was the same as shown in Figure 5.2.

The received waveforms underwent an FFT to determine the received frequency. Figure 5.7 shows this FFT. A spike in the FFT response occurred at 100 KHz which was the frequency that the waveform was transmitted. This showed that the waveform has not undergone any frequency shift during transmission. Harmonics are registered at 590 and 890 KHz. From Equation 3.23 the wavelength was calculated to be 22 mm. Therefore, the wavelength for the ultrasonic waveform travelling through CFRP at solid state was 22 mm. The code at Appendix O was used to undertake signal processing.

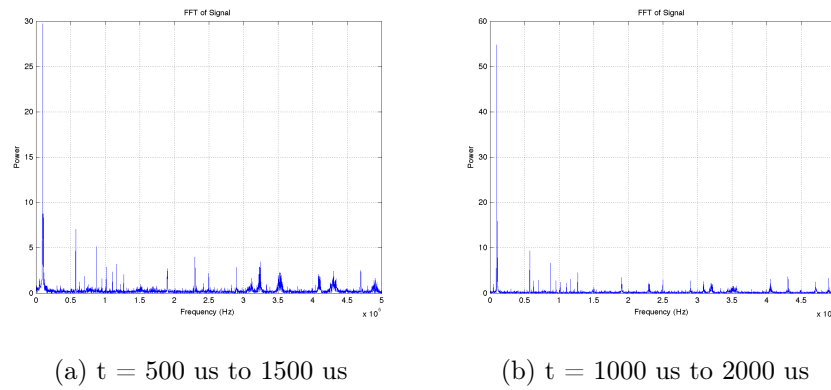


Figure 5.7: FFT Room Temperature CFRP.

5.2 Fire Condition Results

This chapter presents the results of the testing under fire conditions. Testing was undertaken using the ACU model described in Chapter 4.6. Testing was conducted on two separate occasions to ensure results for each material were consistent across multiple tests. For each test a new undamaged plate was used.

A TOF analysis was conducted on the lamb wave response to determine the velocity in the plate and the air. The differences in time domain between consecutive pulses relates to the velocity in the plate and air velocity as the distance travel was consistent through all tests. Assuming no dispersion has occurred.

5.2.1 Aluminium

Aluminium alloy 5083 H116 ACU test under fire conditions is shown in Figure 5.8. Figure 5.9, 5.10 and 5.11 shows the lamb wave response for Aluminium under fire conditions at 10°C increments. Table 5.1 summarises the results of the ACU test for 5083 H116 under fire conditions.

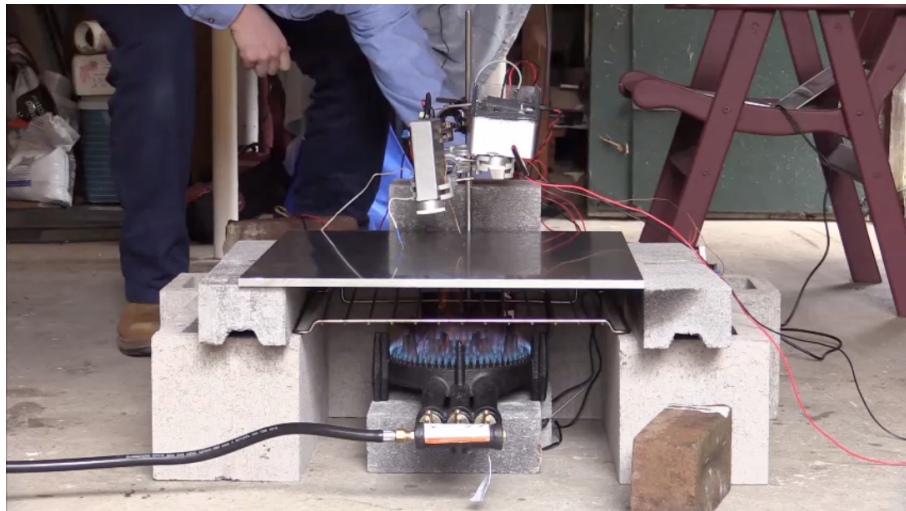


Figure 5.8: Aluminium Testing Under Fire.

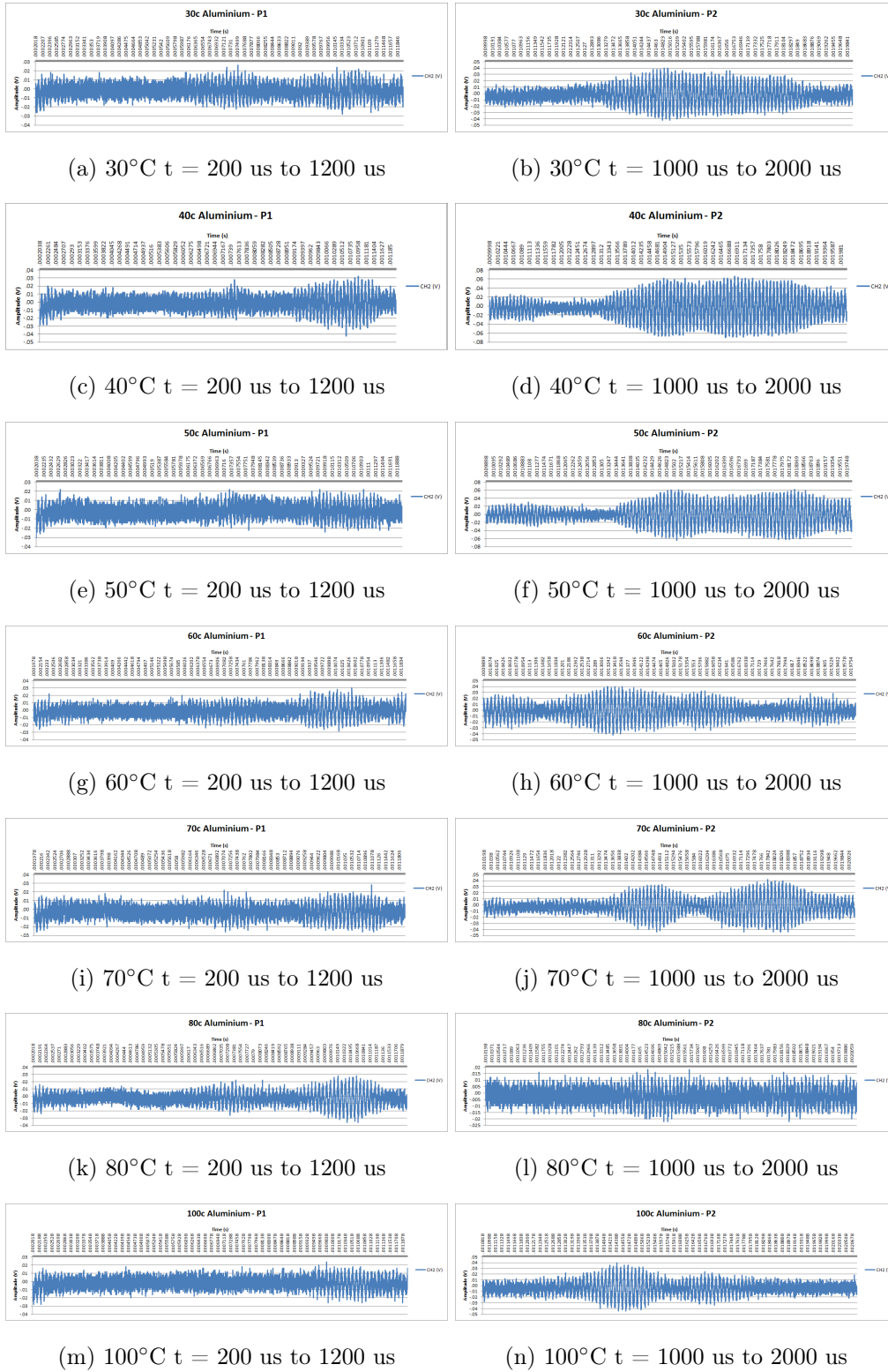


Figure 5.9: Aluminium Lamb Wave Response Under Fire 30 to 100°C.

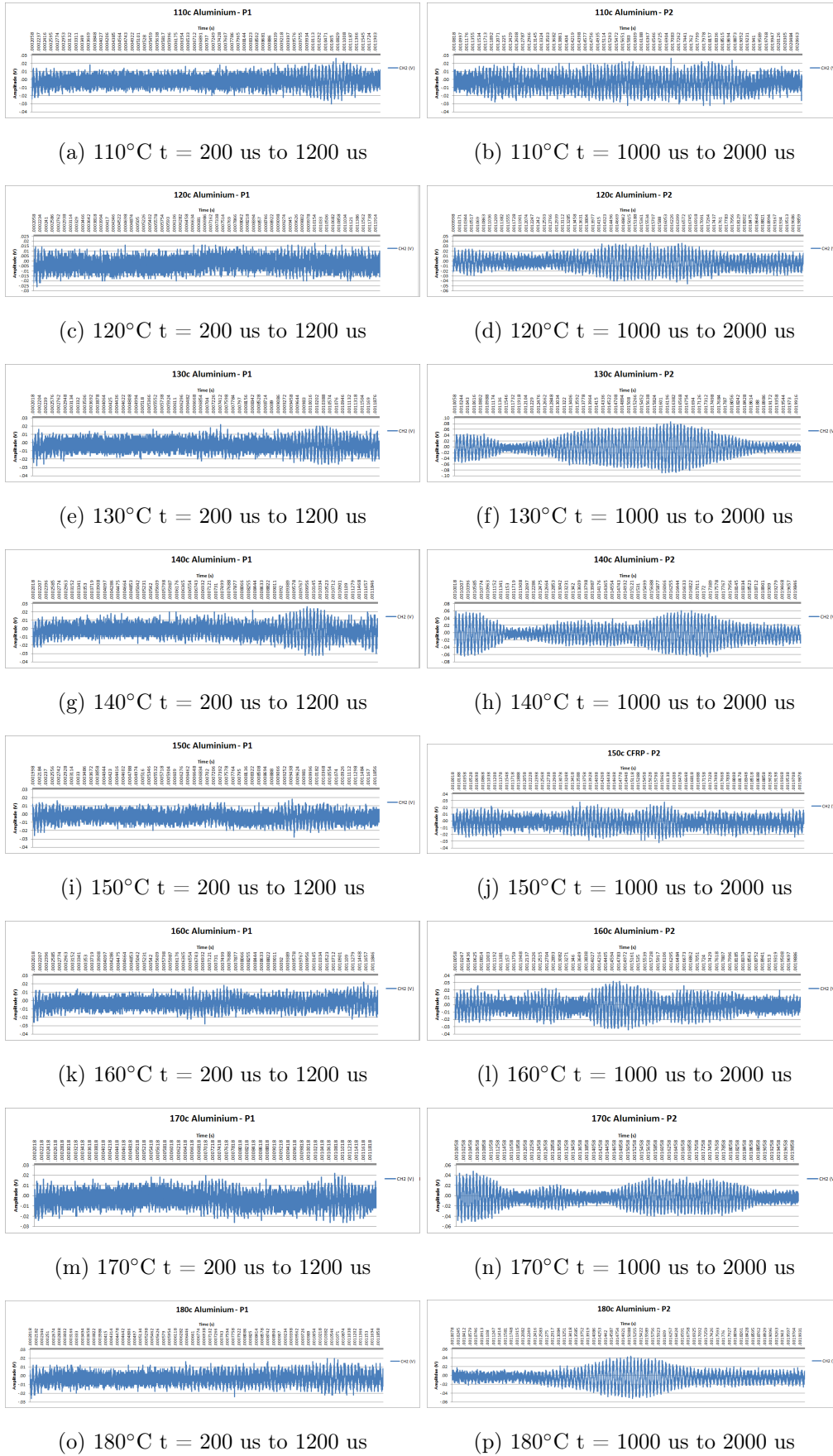


Figure 5.10: Aluminium Lamb Wave Response Under Fire 110 to 180°C.

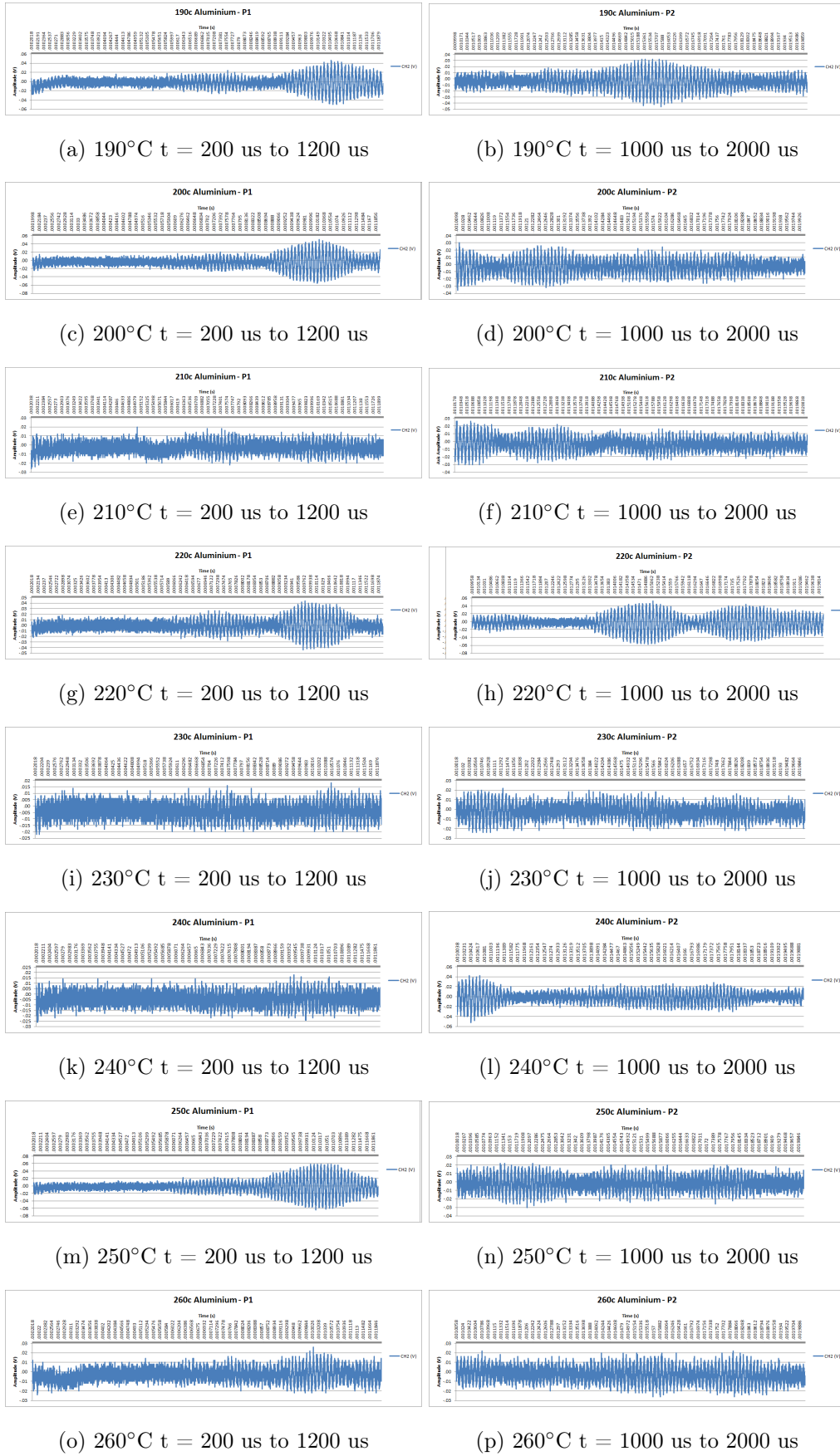
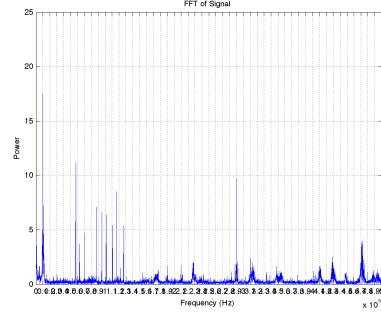
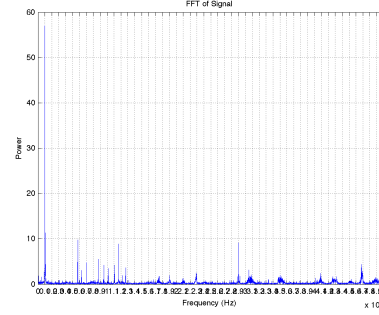


Figure 5.11: Aluminium Lamb Wave Response Under Fire 190 to 260°C.

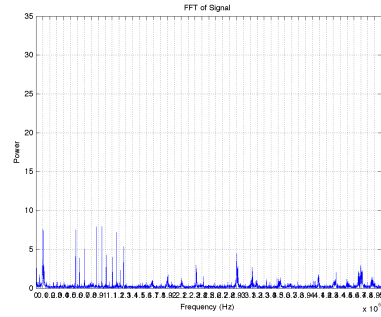
Testing of the 5083 H116 plate under fire conditions was conducted up to 260 °C. At plate outer surface temperature of 260°C the temperature in the plate peaked. Therefore, to continue testing the thermal loading applied to the plate would need to be increased.



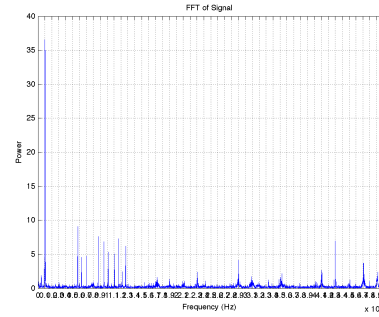
(a) 30°C t = 200 us to 1200 us



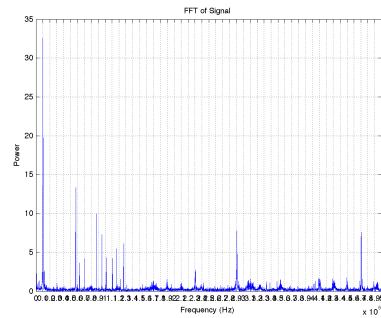
(b) 30°C t = 1000 us to 2000 us



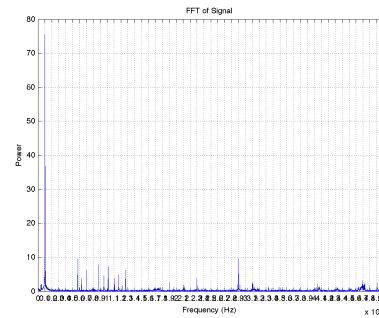
(c) 150°C t = 200 us to 1200 us



(d) 150°C t = 1000 us to 2000 us



(e) 220°C t = 200 us to 1200 us

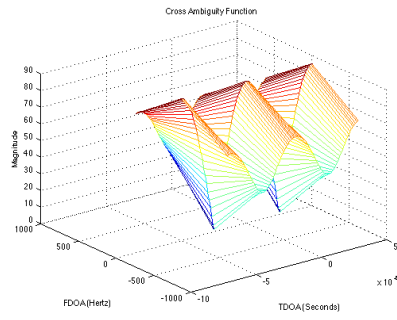


(f) 220°C t = 1000 us to 2000 us

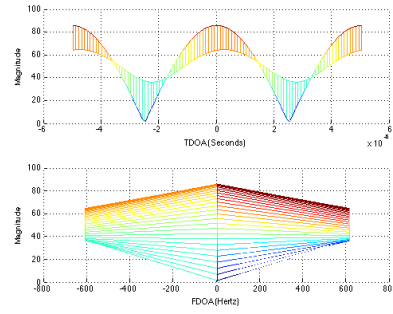
Figure 5.12: FFT Aluminium Under Fire.

All signals underwent an FFT to determine the centre frequency. The FFT response at 30°C, 150°C and 220°C is shown at Figure 5.12. All FFT's showed a spike at 100 KHz and harmonics at 590 and 890 KHz. The code at Appendix O was used to undertake signal processing.

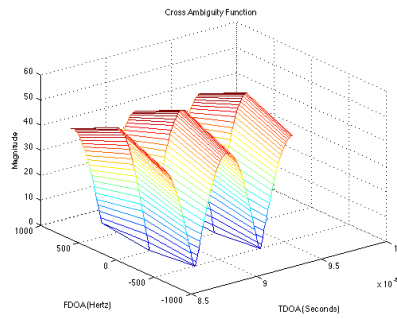
As no frequency change was observed in the FFT's, the lamb wave response was analysed through the ambiguity function to confirm that there was no Doppler shift. The ambiguity function would analyse the received lamb wave response and compare it to the transmitted waveform to show any distortion in the waveform. When the lamb wave response at 220°C was run through the ambiguity function a result was unable to be analysed. The received signal was not able to be correlated to the transmitted signal. This means that the signals were always out of phase. The results of the ambiguity function at room temperature and 220°C are shown in Figure 5.13. The results of the ambiguity function differ in the time domain due to the phase not being able to be correlated. The code at Appendix P was used for the ambiguity function.



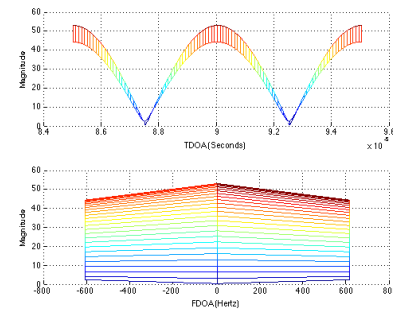
(a) 17°C Cross Ambiguity Function



(b) 17°C Side Views Cross Ambiguity Function



(c) 220°C Cross Ambiguity Function



(d) 220°C Side Views Cross Ambiguity Function

Figure 5.13: Ambiguity Function Aluminium Under Fire.

At room temperature the lamb wave response was a result of six signals. As the plate underwent fire conditions the strongest lamb wave response received is normally of two signals, the reflection off the transmit ultrasonic transducer with a plate edge reflection, which a room temperature arrives at 1480 us. Secondly, a reflection off the transmit ultrasonic transducer with a plate edge reflection and reflection off receive transducer, which at room temperature arrives at 1785 us. This shows that as the plate heats up the lamb wave modes are stronger with a longer travel path in the plate.

Temperature	Air Velocity	Plate Velocity	Frequency	Wavelength
17°C	343 m/s	2400 m/s	100 KHz	24 mm
30	343	2400	100	24
40	343	2400	100	24
50	345	2350	100	23.5
60	360	2350	100	23.5
70	345	2350	100	23.5
80	345	2325	100	23.25
90	No Test	Not Available (N/A)	N/A	N/A
100	345	2300	100	23
110	Reflection	N/A	N/A	N/A
120	350	2300	100	23
130	355	2300	100	23
140	360	2250	100	22.5
150	365	2250	100	22.5
160	365	2250	100	22.5
170	365	2200	100	22
180	365	2200	100	22
190	370	2200	100	22
200	370	2200	100	22
210	Reflection	N/A	N/A	N/A
220	375	2200	100	22
230	Reflection	N/A	N/A	N/A
240	375	2100	100	21
250	375	1900	100	19
260	375	1800	100	18

Table 5.1: Aluminium ACU Fire Test Results.

A full reflection result occurred due to the thermal energy applied to the plate resulting in a high atomic energy which impeded the lamb wave vibration.

Table 5.1 shows that the aluminium plate does not undergo a major change in antisymmetric lamb wave velocity until the overall plate temperature reaches above 200°C. Due to the lamb wave modes being dependent on the elastic properties of the material, the lamb wave velocity should not undergo a major change until a temperature was reached which severely impacted these properties. This confirmed the material properties with temperature shown in Figure 3.13, as the elastic properties of Aluminium are linear up until 200°C. Therefore, the plate velocity should be linear up until this point, as the results show. Between room temperature and 200°C there was an 8% change in velocity. From 200°C to 260°C there was a 18% change. Due to the thermal loading the resulting wavelength has decreased from 24 mm at room temperature to 18 mm at 260°C. This shows a correlation between the materials solid state moving to smoothing.

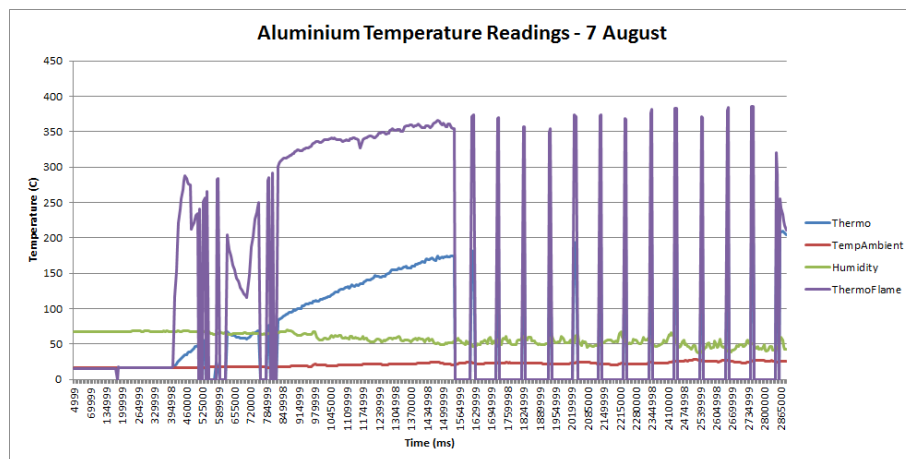
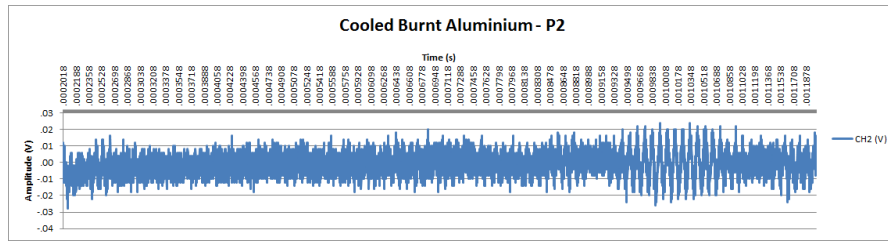


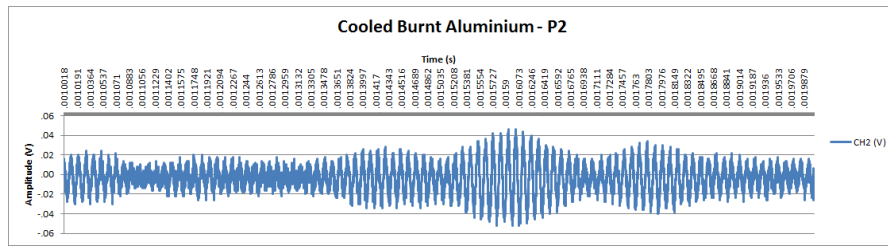
Figure 5.14: Aluminium Temperature Readings.

A follow up test was conducted on the Aluminium plate once it was cooled and the fire enclosure had returned to room temperature. The results of this test are shown in Figure 5.15. The resulting plate velocity was calculated to be 1800 m/s, which equates to a wavelength of 18 mm. The same response was received during the test at 260°C. This shows that on cooling the plate has not returned to the same state that it was prior

to the test. The test has permanently impacted the elastic properties of the plate.



(a) $t = 300 \text{ us to } 1300 \text{ us}$



(b) $t = 1200 \text{ us to } 2200 \text{ us}$

Figure 5.15: Burnt Lamb Wave Response Aluminium.

5.2.2 GFRP

Figure 5.16 shows the CFRP plate undergoing an ACU test. Figure 5.17 and 5.18 shows the lamb wave response for CFRP under fire conditions at 10°C increments. Table 5.2 summarises the results of the ACU test for GFRP under fire conditions.



Figure 5.16: GFRP Testing Under Fire.

Testing of GFRP plate under fire conditions was conducted up to 160 °C. Testing ceased at 160°C due to the intensity of the flame causing overshoots which were close to causing damage to components.

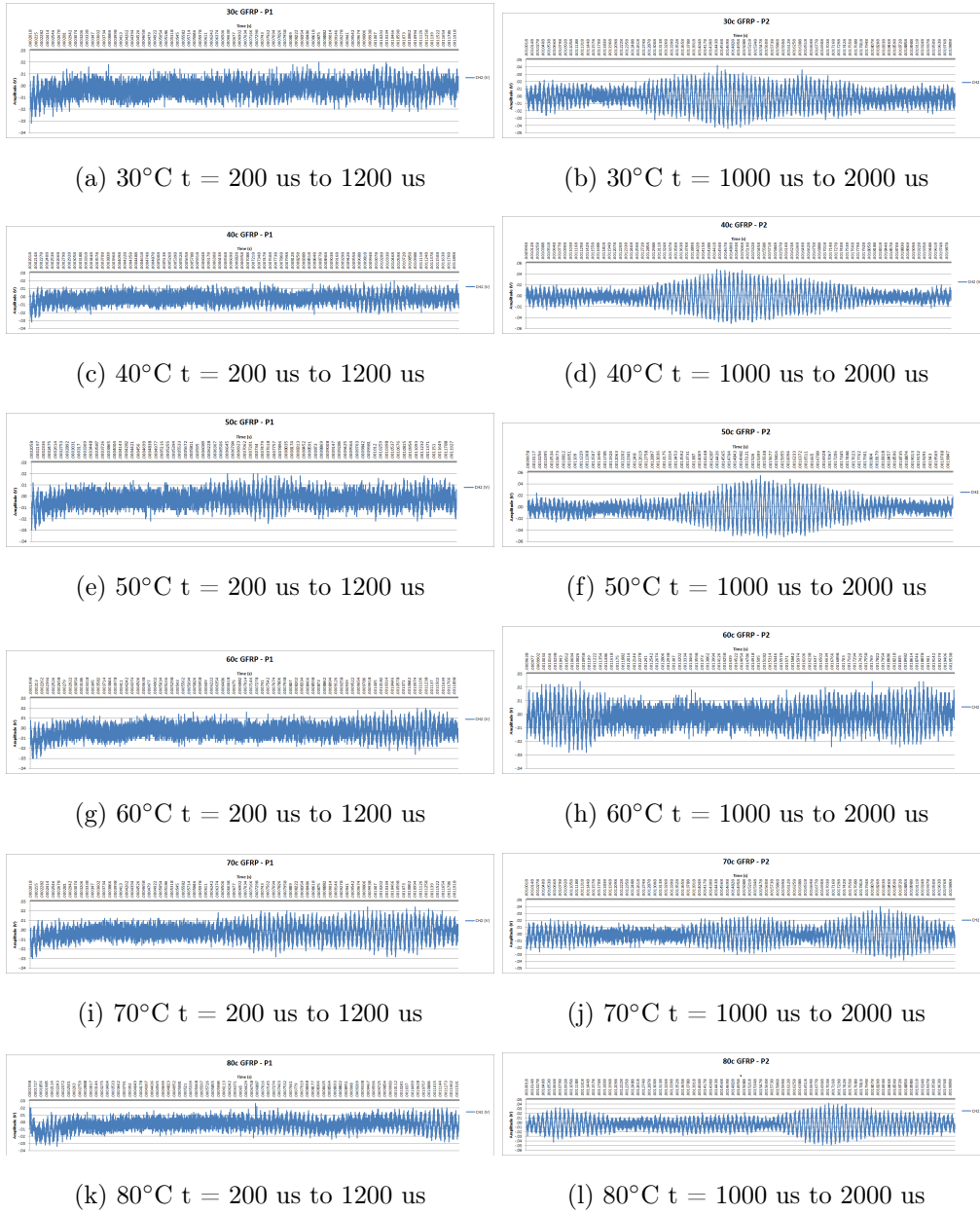


Figure 5.17: GFRP Lamb Wave Response Under Fire 30 to 80°C.

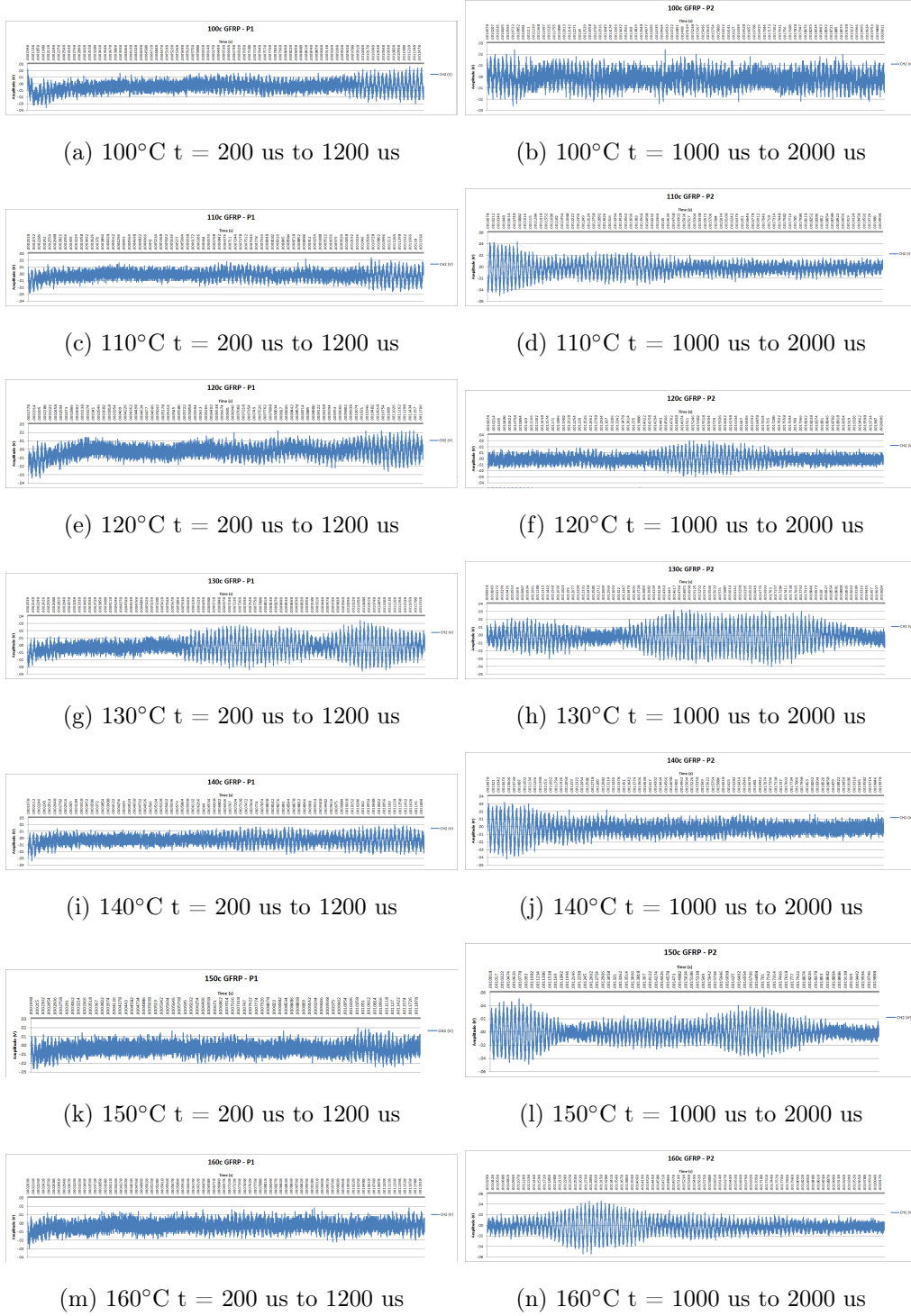
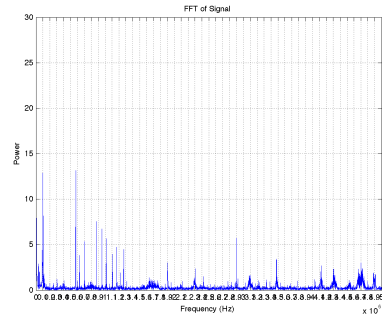
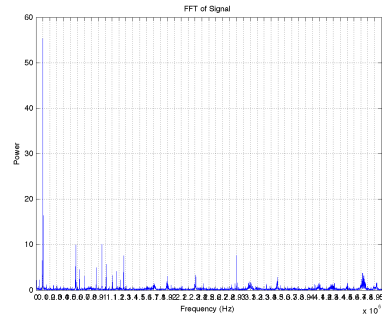


Figure 5.18: GFRP Lamb Wave Response Under Fire 100 to 160°C.

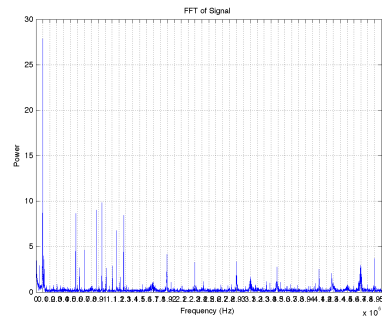
All signals underwent an FFT to determine the centre frequency. The FFT response at 30°C, 700°C and 140°C is shown at Figure 5.19. All FFT's showed a spike at 100 KHz and harmonics at 590 and 890 KHz. The code at Appendix O was used to undertake signal processing.



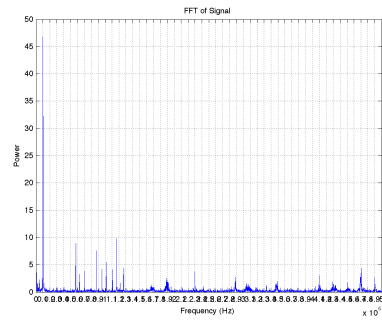
(a) 30°C t = 200 us to 1200 us



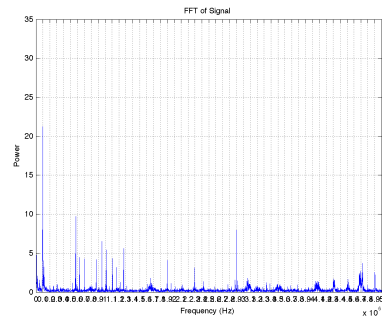
(b) 30°C t = 1000 us to 2000 us



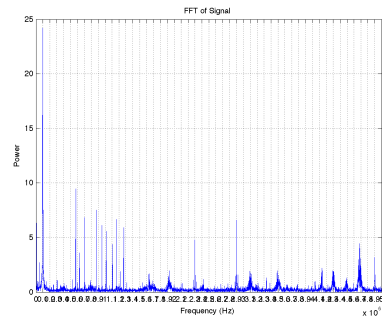
(c) 70°C t = 200 us to 1200 us



(d) 70°C t = 1000 us to 2000 us



(e) 140°C t = 200 us to 1200 us



(f) 140°C t = 1000 us to 2000 us

Figure 5.19: FFT GFRP Under Fire.

At room temperature the lamb wave response was a result of five signals. As the plate underwent fire conditions the strongest lamb wave response received is normally of two signals, the reflection off the transmit ultrasonic transducer, which a room temperature arrives at 1310 us and secondly a reflection off the transmit ultrasonic transducer with reflection off receive transducer, which at room temperature arrives at 1610 us. This shows that as the plate heats up the lamb wave modes are stronger with a shorter travel path in the plate. This lamb wave response is the opposite to the response in Aluminium.

Temperature	Air Velocity	Plate Velocity	Frequency	Wavelength
17°C	343 m/s	2800 m/s	100 KHz	28 mm
30	343	2800	100	28
40	343	2800	100	28
50	345	2700	100	27
60	Reflection	N/A	N/A	N/A
70	360	2450	100	24.5
80	345	2300	100	23
90	No Test	N/A	N/A	N/A
100	Reflection	N/A	N/A	N/A
110	370	2220	100	22.5
120	360	2200	100	22
130	370	2100	100	22
140	Reflection	N/A	N/A	N/A
150	360	2100	100	21
160	375	2000	100	20

Table 5.2: GFRP ACU Fire Test Results.

At an outer surface temperature of 60-70°C the epoxy catches fire and increases the thermal load applied to the plate. At this temperature, the results show a sudden change in antisymmetric velocity and a full reflection response. A full reflection result occurs in response to the thermal energy applied to the plate, and the resulting high atomic energy

which impedes the lamb wave vibration. Flame bursting, as shown in Figure 5.16, is the reason for a sudden air velocity increase.

Between room temperature and 50°C there was an 4% change in velocity. From 50°C to 160°C there was a 22% change. The resulting wavelength decreased from 28 mm at room temperature to 20 mm at 160°C. As noted in Table 4.6 the T_g for Ampregg 22 is 63.2°C, which was when the composite moves to glass transition. This sharp change in lamb wave velocity shows a correlation between the materials solid state moving to glass transition due to thermal loading and breakdown of the secondary bonds. The lamb wave velocity is linear until the composite transitions to a new state.

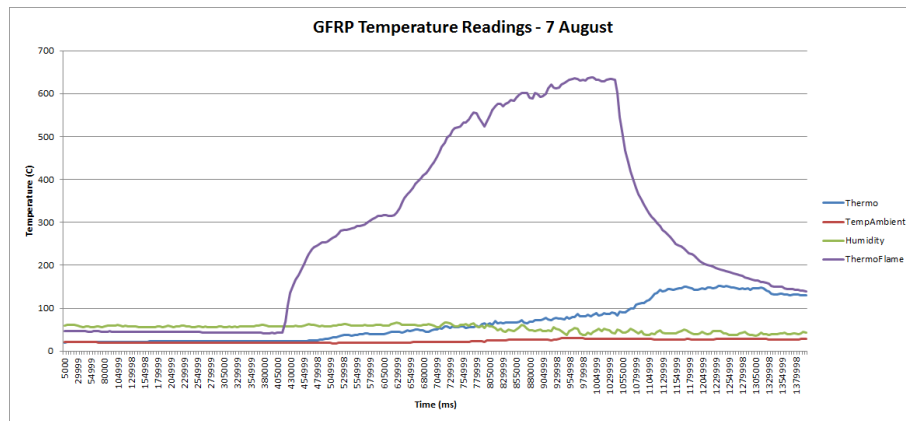


Figure 5.20: GFRP Temperature Readings.

A follow up test was conducted on the GFRP plate once it was cooled and the fire enclosure returned to room temperature. The test was conducted on both the fire damage side and the non fire side of the plate. The results are shown in Figure 5.21. The fire damaged side of the plate had a resulting plate velocity of 2000 m/s, which equates to a wavelength of 20 mm. The non-fire side of the plate has a low amplitude response which is difficult to analyse. The results show that the ultrasonic waveform was able to travel down the exposed glass fibres, which forms with a lamb wave response. On the non-fire side of the plate the epoxy on the surface charred due to the heat transfer through the plate which resulted in a poor penetration of the wave. The charred surface of the GFRP plate is shown in Figure 5.22a and the fire surface is shown in Figure 5.22b.

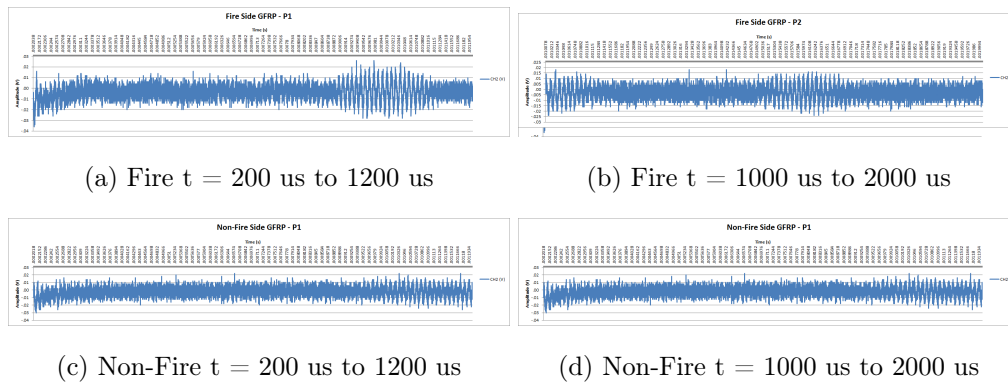


Figure 5.21: Burnt Lamb Wave Response GFRP.



(a) GFRP Charred Surface.

(b) GFRP Fire Surface.

Figure 5.22: GFRP Post Fire

5.2.3 CFRP

Figure 5.23 shows the CFRP plate undergoing ACU test. Figure 5.24 and 5.25 shows the lamb wave response for CFRP under fire conditions at 10°C increments. Table 5.3 summarises the results of the ACU test for CFRP under fire conditions.



Figure 5.23: CFRP Testing Under Fire.

Testing of the CFRP plate under fire conditions was conducted up to 160 °C. Testing ceased at 160°C as the temperature of the plated peaked and stabilised due to the thermal barrier created by the exposed carbon fibre. Therefore, to continue testing the thermal loading applied to the CFRP plate would need to be increased.

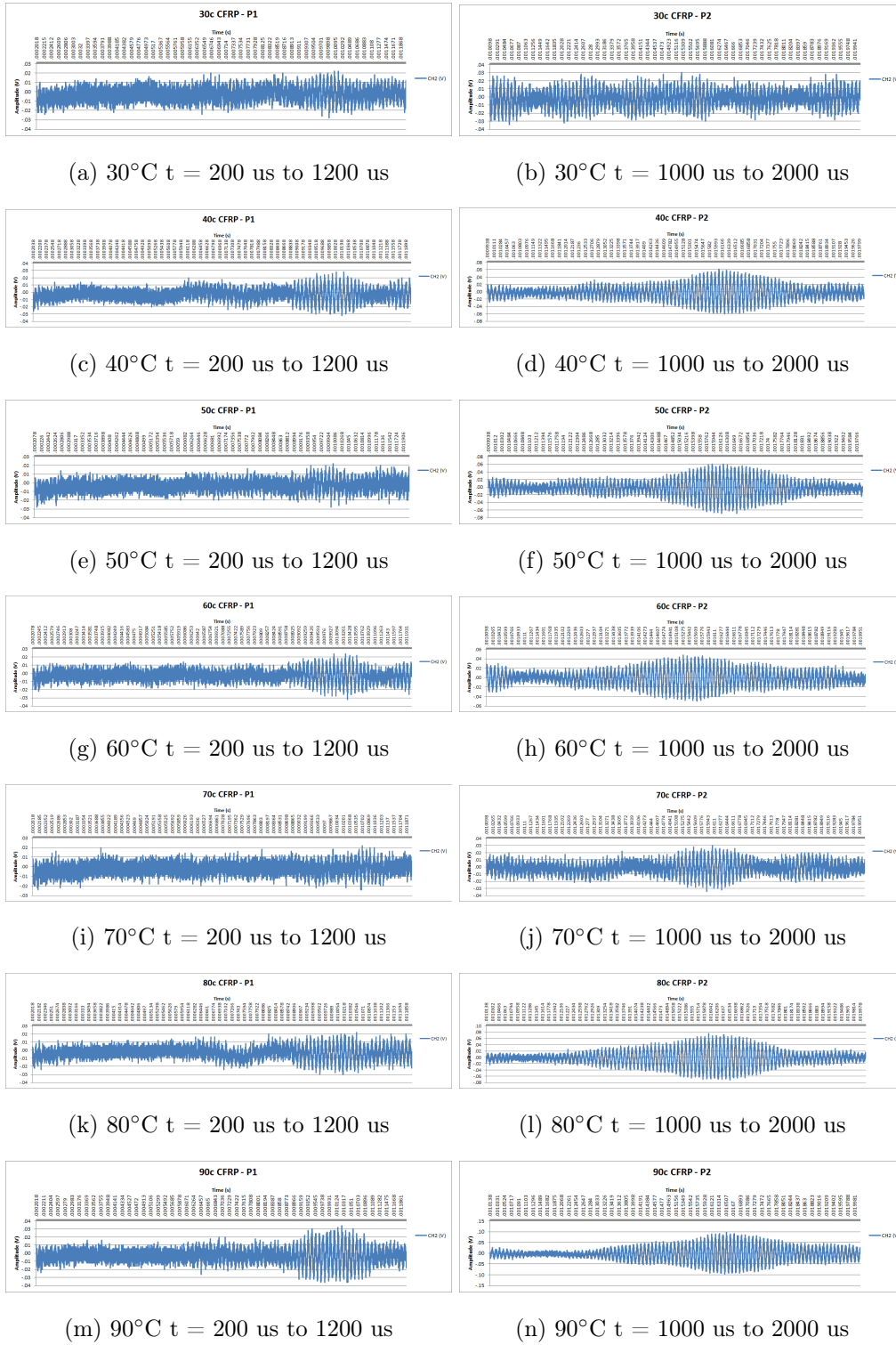


Figure 5.24: CFRP Lamb Wave Response Under Fire 30 to 90°C.

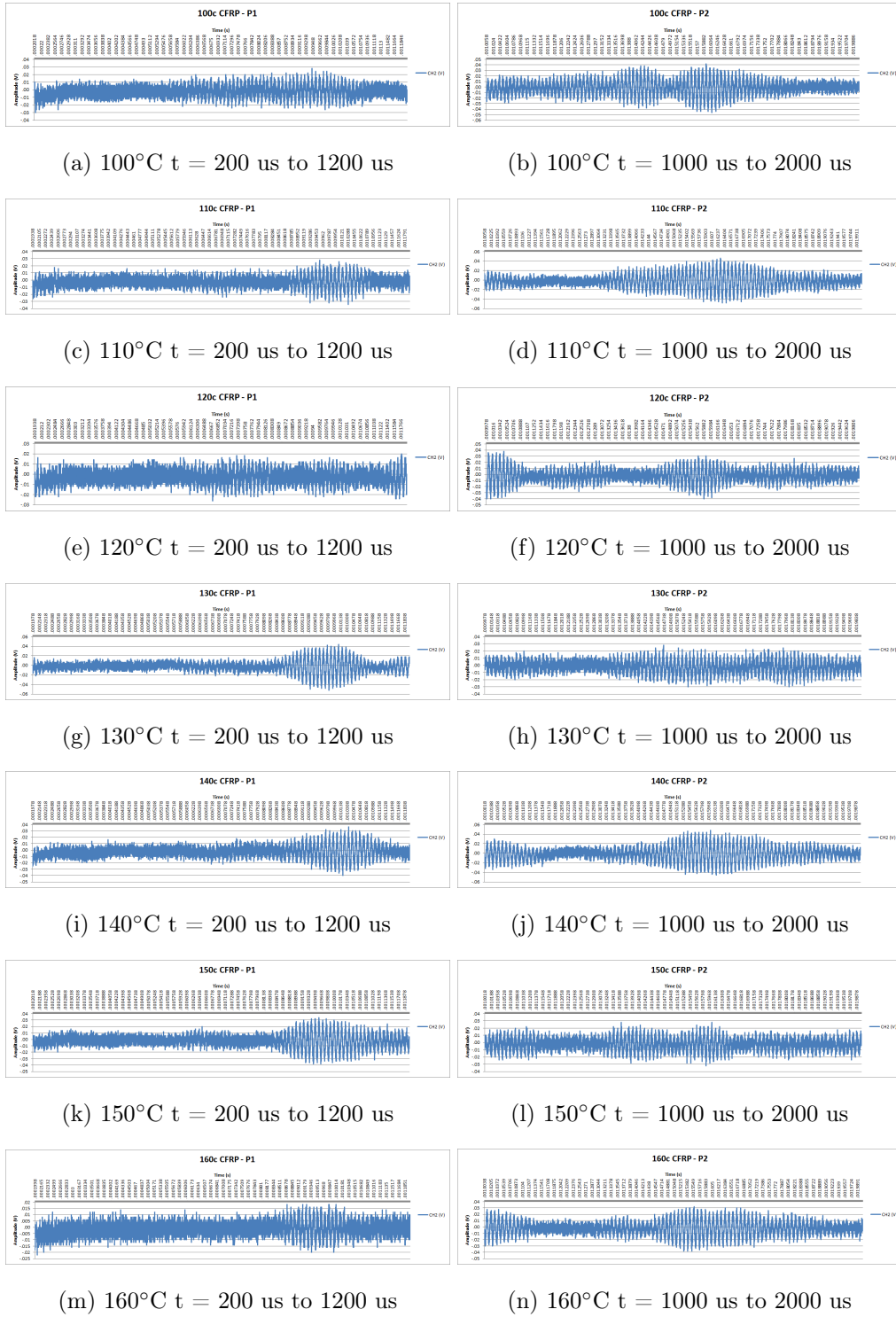


Figure 5.25: CFRP Lamb Wave Response Under Fire 100 to 160°C.

All signals underwent an FFT to determine the centre frequency. The FFT response at 30°C, 700°C and 140°C is shown at Figure 5.26. All FFT's showed a spike at 100 KHz and harmonics at 590 and 890 KHz. The code at Appendix O was used to undertake signal processing.

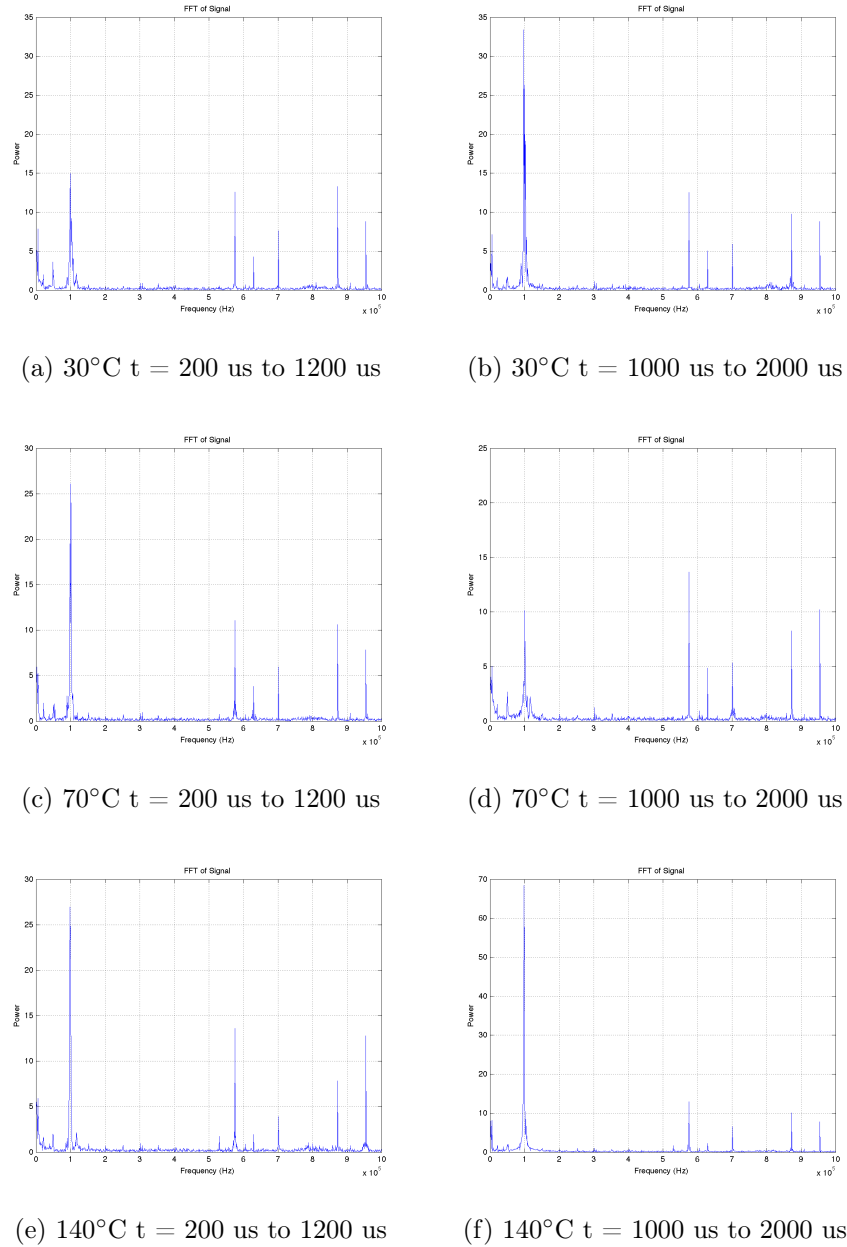


Figure 5.26: FFT CFRP Under Fire.

At room temperature the lamb wave response was a result of seven signals. As the plate underwent fire conditions the strongest lamb wave response received is similar to that at room temperature, with only a variance in the time domain. Unlike during the Aluminium and GFRP test, all tests resulted in a lamb wave response. This is due to how CFRP reacts under thermal loading, in that the layers of carbon fibre created a thermal barrier to the fire, as detailed in Chapter 3.4.

Temperature	Air Velocity	Plate Velocity	Frequency	Wavelength
17°C	343 m/s	2200 m/s	100 KHz	22 mm
30	343	2200	100	22
40	345	2200	100	22
50	345	2150	100	21.5
60	345	2150	100	21.5
70	345	2100	100	21
80	345	2050	100	20.5
90	345	2000	100	20
100	345	2000	100	20
110	345	1900	100	19
120	345	1900	100	19
130	345	1850	100	18.5
140	345	1850	100	18.5
150	350	1800	100	18
160	360	1800	100	18

Table 5.3: CFRP ACU Fire Test Results.

Similar to the GFRP test, the epoxy of the CFRP caught on fire. However, the flames produced from the epoxy burning were not as intense and did not impact the surrounding air through flame overshoot. This can be seen in Figure 5.27.

At an outer surface temperature of 60-70°C the epoxy caught fire and increased the

thermal load applied to the plate. Between room temperature and 70°C there was a 4% change in velocity. From 70°C to 160°C there was a 14% change. The resulting wavelength decreased from 22 mm at room temperature to 18 mm at 160°C. As noted in Table 4.6, the T_g for Ampregg 22 is 63.2°C, which was when the composite moves to glass transition. This sharp change in lamb wave velocity shows a correlation between the materials solid state moving to glass transition due to thermal loading. The lamb wave velocity is linear until the composite transitions to a new state.

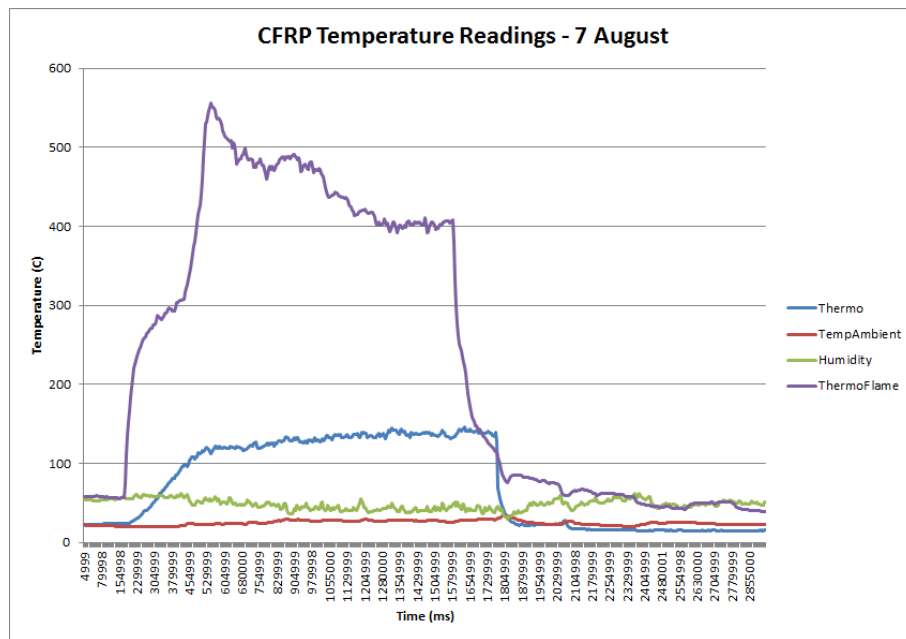


Figure 5.27: CFRP Temperature Readings.

A follow up test was conducted on the CFRP plate once it was cooled and the enclosure had returned to a room temperature of 17°C. The test was conducted on both the fire damage side and the non fire side of the plate. The results of this test are shown in Figure 5.28. The fire side of the plate has a low amplitude response which is difficult too analyse. The non fire damaged side of the plate had a resulting plate velocity of 1800 m/s, which equates to a wavelength of 18 mm. This shows that the CFRP plate has been damaged by the fire and has not returned to its original solid state. The non-fire surface of the CFRP plate is show in Figure 5.29a and the fire surface is shown in Figure

5.29b.

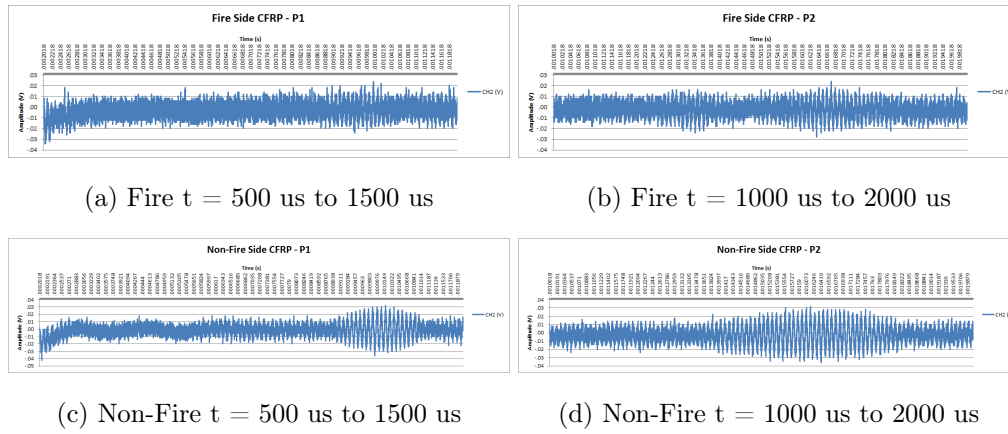


Figure 5.28: Burnt Lamb Wave Response CFRP.



(a) CFRP Non-Fire Surface.

(b) CFRP Fire Surface.

Figure 5.29: CFRP Post Fire

5.3 Discussion

The results show that ACU utilising commercially available components is feasible under fire conditions.

The results show that care must be taken when analysing the lamb wave response in an ACU system. This is due the secondary signals produced from the reflections off the large diameter transducers. If the air path, transducer angle, plate path and subsequent reflections are not well understood, then the signals could be misinterpreted as a transducer reflection or a plate edge reflection. This would lead to a great misrepresentation of velocities.

The pulsed waveform utilised, shown in Figure 4.5, has overlaps at room temperature due to the reflected lamb waves arriving at similar times. This makes it difficult to distinguish whether a lamb wave response is an edge plate reflection or a ultrasonic transducer reflection. A shorter pulsed waveform would provide greater separation between the consecutive pulses. This would provide greater accuracy in the feedback. A more suitable pulsed waveform would be of 100 us or 10 peaks at 100 KHz. This shorter pulsed waveform was not possible with the code utilised for the function generator. The procurement of a new waveform generator was outside the budget of the project.

Due to the large amount of noise that was received, the lamb wave symmetric mode response is not possible to analyse. If both the symmetric and antisymmetric modes were received this would allow greater analysis of the lamb wave response due to two modes being available, one wave due to bending and the other due to stretching. This would improving the feedback possible on the integrity of the material. To receive the symmetric mode response, the standing noise received must be removed. This noise was believed to be caused due to the internal noise of the oscilloscope, as stated in Chapter 4.2.3. Therefore, to be able to accurately analyse the lamb wave for a symmetric mode response the oscilloscope must be re-calibrated.

The results received during the two ACU tests under fire conditions were consistent for each material. There was no deviation in the lamb wave response received under fire conditions. This shows that ACU provides accurate and consistent information for aluminium, GFRP and CFRP.

As the plates were heated up, the received lamb wave antisymmetric response differed from that at room temperature. Not all reflections were received as the plates undergo thermal loading. This makes it difficult to distinguish whether a lamb wave response is a edge plate reflection or a ultrasonic transducer reflection. Extra care must be taken when analysing the differences in time domain between consecutive pulses. Further, any automation in signal analysis would need to account for the change in lamb wave responses. Automation would need to be able to calculate if the response was an edge plate reflection or an ultrasonic transducer reflection. Without being able to account for this, incorrect plate velocities would provide false reading about the materials integrity.

As the plates heat up under fire conditions, the elastic properties of the material began change as the material moves away from solid state. This material state change impacts the resulting lamb wave response. The lamb wave velocity and wavelength through the plate linearly decreases until the elastic properties drastically change due to smoothing, which results in a drastic changes the lamb wave response. It is this drastic change in lamb wave response that is of interest to the project. This drastic change in lamb wave response shows the material is moving away from solid state and the structural integrity of the material is compromised.

The change in lamb wave response was not as drastic for CFRP when compared to GFRP. Due to the multiple layers in the composite, the fire impacted layers created a thermal barrier due to the exposed carbon fibre. This resulted in the remaining layers undergoing less of a thermal load. It is these outer layers the lamb wave traveled along. A greater penetration in the thermal loading is required to change the elastic properties of the outer fibre layers. Therefore, the resulting change in lamb wave velocity for CFRP at 70°C showed the outer ply moving to glass transition. This did not occur in GFRP

to the extent of CFRP, due to the fire having greater penetration thereby impacting all layers of the composite. This can be seen through the charred outer surface of the plate.

As the fire impacted the plates, thermal energy is transmitted changing the surface mass density. This thermal energy impacted the transmission of the ultrasonic waveform form into the plate. This increase in thermal energy may result in a full reflection which can be seen in the results for Aluminium and GFRP. Furthermore, the thermal energy also impacted the amplitude of the lamb wave response, in that the waveform may only be transmitted with limited energy. This means that using the lamb wave response to examine attenuation was difficult. A change in amplitude is either a factor of the thermal loading limiting waveform transmission or attenuation in the plate.

It was expected that as the plates were impacted by the fire, due to thermal loading the lamb wave response would have undergone a frequency shift or thermal broadening. The FFT conducted on all the lamb wave responses showed that this did not occur. The ambiguity function was also unable to be correlated to confirm a Doppler shift. There are three possible reasons as to why the FFT has not showed a frequency shift. The first reasons is that even though the ultrasonic transducer has a centre frequency ± 8 KHz, the centre resonance frequency is a peak and not curvilinear resulting in being band width limited. The second reason was that due to the low frequency used, short timescale and quality of components, a shift in frequency would not be large enough to capture. The third reasons is that no frequency shift occurred and that the FFT is correct. To ensure the accuracy in the result, further testing is required to confirm which reason, if any is correct.

GFRP and CFRP behaved differently under fire conditions. Both materials were composed of Ampregg 22, however CFRP burns no where near the extent as that of GFRP. The difference in fire temperature can be seen in Figure 5.27 and 5.20. Fire temperatures in CFRP reached 550°C for only a brief period before it returned to 400°C . This spike in temperature occurred over a longer period in GFRP and reached 630°C . CFRP has a spike in temperature at the start in temperature rise due to having a thicker layer of

epoxy between the carbon fibre layers before formation of the thermal barrier. During the GFRP test the high temperature spike occurred towards the end of the temperature rise. Even though GFRP had less epoxy per layer of glass fibre, as the epoxy has higher COTE than GFRP this resulted in a de-lamination allowing more epoxy to burn overall. CFRP had a higher COTE to that of the epoxy thereby creating a barrier preventing the burning of further epoxy due to the high temperature resistance.

This difference in behaviour between GFRP and CFRP is also observed in the reason why testing was ceased. Even though both tests were ceased at 160°C, the GFRP test was stopped due to flame overshoot possibly causing damage to components. The CFRP test was stopped due to the temperature peaking and stabilising when a thermal barrier from the exposed carbon fibre was created.

When testing was stopped the LPG fuel source, was removed from the fire enclosure. For GFRP and CFRP once this fuel source was removed, the fire self-extinguished after a brief period of time. This occurs even though as the epoxy burned it provided a secondary fuel source for the fire. The fire self-extinguished due to material combustion not yet reaching self-sustaining. This is due to the thermal mass of the material not heating up enough to support combustion before the flame was removed. For a composite plate under fire to be self-sustaining, the fuel source would need to be applied for a longer period of time thereby raising the overall thermal mass to a point which was not reached during the project.

Chapter 6

Further Work

This chapter details further work required to ensure that the design is suitable for in-service applications. It also details other possible testing or design validation requirements for further improvements in the design.

The result showed there were a number of limitations due to design which require further research. These limitations requiring further work were categorised as either ACU design development or in-service application development.

6.1 Air Coupled Ultrasonics Test Method

6.1.1 Ultrasonic Transducer

It was expected that as the plates were impacted by the fire, due to thermal loading the lamb wave response would have undergone a frequency shift or thermal broadening. The FFT conducted on all the lamb wave responses showed that this did not occur. Chapter 5.3 summarised the possible reasons for this not occurring. To confirm the bandwidth

of the MCUSD40A100B17RS-70C, a broad bandwidth ultrasonic transducer should be set up to transmit an ultrasonic waveform over a number of frequencies. The waveform would be received on the MCUSD40A100B17RS-70C and compared to the transmitted signal. This would confirm the bandwidth of the transducer and allow confirmation if the received frequency was in-fact correct or if it was due to resonance at the ultrasonic transducers centre frequency.

6.1.2 Waveform Generator

Improvements to the ultrasonic waveform could be achieved through shortening the pulsed waveform to 100 us at 100 KHz. Further testing is required to ensure that this shorter pulsed waveform does not have a limitation on penetration or signal quality for response analysis.

6.1.3 Oscilloscope

Concerns regarding the accuracy of the oscilloscope raised in Chapter 4.2.3 and 5.3 should be investigated. The oscilloscope must be re-calibrated to remove internal noise. Once the oscilloscope has been re-calibrated, further testing will need to be undertaken to determine if the symmetric mode is able to be received.

Secondly, as the TDS3054C is not portable, an alternative oscilloscope should be sourced to meet the final requirement of the project specification. A portable oscilloscope that is suitable for a hazardous environment would meet the requirements of the project specification.

6.1.4 Depth of Penetration

Due to the multiple layers which are present in composite plates, further research is required into accounting for the change in penetration depth of the lamb wave. If the lamb wave response is able to analyse the depth of penetration of the signal, from this the number of layers which have been destroyed by the fire would be able to be determined and accounted for in determining the structural integrity.

6.2 In-Service Application

6.2.1 Distance

The current ACU test model described in Chapter 4.6, required the transmit ultrasonic transducer be placed 117 mm from the surface of the test material at a -5° angle from the vertical, and the receive ultrasonic transducer be placed 52 mm from the test material at an angle of 5° from the vertical. For the in-service application of ACU, such close distances to the test material may not be feasible. Such close distances may not be feasible due to obstructions from components, equipment, ship structure or extreme heat. To ensure testing of the fire affected bulkhead and/or deckhead is possible, the limitation on distance the ACU is able to be placed from the test material should be investigated. Investigating the possibility of conducting ACU at distances up to one meter from the test material should be examined.

The results in Chapter 5 highlighted that the distance from where the ultrasonic waveform enters the plate, to the edge of the plate is of vital importance. Without knowing this distance, the lamb wave velocity is difficult to determine. For in-service applications this distance becomes difficult to ascertain. The edge of the bulkhead and/or deckhead may be inaccessible, unknown or hidden. Further research needs to be undertaken into determining how best to ascertain this distance, thereby improving the accuracy in the

calculated lamb wave velocity.

6.2.2 Feedback

Currently the response received through ACU testing are examined using a computer and required multiple programs for analysis. This analysis method would not be possible for in-service applications. Determining the best way for the lamb wave response to be analysed, enabling feedback on the material state in a portable device requires investigation.

Chapter 7

Conclusion and Recommendations

This chapter summarises the project, analyses the results achieved, compares the results to the project specification, and provides recommendations.

Research was conducted into various non-invasive methods for testing integrity of materials during a fire. From this literature review it was determined that ACU was the most suitable non-invasive test method.

Through testing at room temperature a suitable ACU test method was constructed. The ACU test method was constructed utilising only components that are commercially available.

The ACU test method did not require contact with the material undergoing testing. Being non-contact ensured the safety of personnel conducting the testing by keeping them a safe distance from the hot material. In addition, ACU test method did not negatively impact or affect the test which ensured that the structural integrity was not reduced or impeded during testing.

Aluminium, GFRP and CFRP were ACU tested under fire conditions. The results re-

ceived during the two ACU tests conducted were consistent for each material. No deviation in the results were achieved.

The lamb wave response in composite plates was impacted by the multiple layers of composite. The lamb wave is able to travel along the outer layers of the composite which were less impacted by the fire. A greater penetration in the thermal loading is thereby required to change the elastic properties of the outer composite layers thereby, impacting the lamb wave response. This limits the feedback possible, thereby reducing the reliability in the results.

CFRP fared better when compared to GFRP under fire conditions. The exposed carbon fibres blocked ingress of the fire, whereas the glass fibres exposed a greater amount epoxy to fuel and increase the intensity of the fire.

The ACU response showed that there was a sharp change in the lamb wave velocity as the material underwent a sharp change in elastic properties. This change in elastic properties was due to the material moving away from solid state due to thermal loading.

The results showed that the lamb wave velocity greatly changed as the material underwent a significant change in elastic properties, however before ACU is suitable for in-service implementation, further research and development is required. Further research and development is required into ultrasonic transducer bandwidth, waveform generator pulse, oscilloscope, depth of penetration and portability to ensure accuracy and reliability in results.

Testing Aluminium, GFRP and CFRP under fire conditions showed that ACU is a viable non-invasive test method for testing the integrity of bulkheads and/or deckheads during a fire. Even though further research and development is required, the ACU test method is able to assess the integrity of the material under fire through the change in lamb wave response due to the change in elastic properties with temperature.

References

- A Popov, V. K. & Pashkouleva, D. (2013), 'Non-destructive evaluation of the yield stress of low carbon steel by ultrasound measurement', *Russian Journal of Nondestructive Testing* **49**(6), 328–333.
- Adafruit (2016*a*), 'Adafruit sensiron sht31-d temperature and humidity sensor breakout', <https://www.adafruit.com/product/2857>. [Online; accessed February-2016].
- Adafruit (2016*b*), 'Thermocouple amplifier max31855 breakout board', <https://www.adafruit.com/products/269>. [Online; accessed February-2016].
- Aerospace Specification Metals Inc (2016), 'Aluminum 5083-h116', <http://asm.matweb.com/search/SpecificMaterial.asp?bassnum=MA5083H116>. [Online; accessed July-2016].
- American Piezo (2016), 'Piezoelectricity', <https://www.americanpiezo.com/knowledge-center/piezo-theory/piezoelectricity.html>. [Online; accessed August-2016].
- Austal (2015), *Aluminium Delivering Speed and Strength in Naval Applications*, Austal.
- AZOM (2003), 'Carbon epoxy composite materials', <http://www.azom.com/article.aspx?ArticleID=1995>. [Online; accessed July-2016].
- Bai, Y. & Keller, T. (2013), *High Temperature Performance of Polymer Composites*, Wiley-VCH.

- Beatrice Faggiano, Gianfranco De Matteis, R. L. . F. M. M. (2004), ‘Behaviour of aluminium alloy structure under fire’, *Journal of Civil Engineering and Management* .
- Benck, R. & Filbey, G. (1976), Elastic constants of aluminum alloys, 2024-t3510, 5083-h131 and 7039-t64 as measured by a sonic technique, Technical report, USA Ballistic Research Laboratories.
- Blom, A. & Gradin, P. (1990), ‘Radiography’, *Non-Destructive testing of fibre-reinforced plastic composites* **1**, 1–24.
- Bourbigot, S. & Flambard, X. (2002), ‘Heat resistance and flammability of high performance fibres: a review’, *Fire and Materials* **26**, 155–168.
- Butrus Khuri-Yakub, Jun Pei, F. D. & Saraswat, K. (1996), ‘In situ simultaneous measurement of temperature and thin film thickness with ultrasonic techniques’, *Center for Integrated Systems* **2948**.
- Cheng, C. & Lu, C. (2011), ‘Temperature evaluated by ultrasonic technique during mixing process’, *Asia-Pacific Journal of Chemical Engineering* **7**, 755–760.
- Chimenti, D. (2014), ‘Review of air-coupled ultrasonic materials characterization’, *Ultrasonics* **54**.
- Chu, Y. & Rokhlin, S. (1994), ‘Comparative analysis of through-transmission ultrasonic bulk wave methods for phase velocity measurements in anisotropic materials’, *Journal of Acoustical Society of America* **95**.
- CIV8803 Mechanics and Technology of Fibre Composites: Study Book* (2008), University of Southern Queensland.
- Colan Australia (2007), *MX4500 E-glass composite reinforcement*, Colan Australia, Huntingwood NSW.
- David, J. & Cheeke, N. (2012), *Fundamentals and Applications of Ultrasonic Waves*, CRC Press.

- Dawson, A. (2010), High Frequency Ultrasonic Wave Propagation in Anisotropic Materials, PhD thesis, Victoria University of Wellington.
- Department of Justice & Attorney General (2015), 'The risks of exposure', <http://www.deir.qld.gov.au/asbestos/general/risks.htm>. [Online; accessed April-2016].
- ELGas (2016), 'Lpg gas', <http://www.elgas.com.au/blog/1585-why-does-a-gas-flame-burn-blue-lpg-gas-natural-propane-methane>. [Online; accessed August-2016].
- Elite Fire (2013), 'Back to basics with the fire triangle', <http://www.elitefire.co.uk/basics-fire-triangle/>. [Online; accessed August-2016].
- Engineers Handbook (n.d.), 'Radiography testing', www.engineershandbook.com/mfgmethods/ndtrt.htm. [Online; accessed March-2016].
- European Committee for Standardisation (2008), Non-destructive testing - ultrasonic examination - part 6: Time-of-flight diffraction techniques as a method for deflection and sizing discontinuities, Technical report, European Committee for Standardisation.
- F Cegla, P Cawley, J. A. & Davies, J. (2011), 'High-temperature wall thickness monitoring using dry-coupled ultrasonic waveguide transducers', *Transaction on Ultrasonics* **58**(1).
- Freetronics (2016), 'Ir temperature sensor', <http://www.freetronics.com.au/products/irtemp-ir-temperature-sensor-module#.V7kIUGPPZHg>. [Online; accessed February-2016].
- G Alleman, M. P. & Groves, R. (2014), 'Air-coupled ultrasound for damage detection in cfrp using lamb waves and ultrasonic verification', *International Conference on Adaptive Structures and Technologies*.
- Gandhi, S. (1999), 'Postcrash health hazards from burning aircraft composites', *Journal of Fire Sciences*.

- Garcia, M. (2009), 'Non destructive characterisation oin air of plates using ultrasonic lamb waves', *Research in Electronic Engineering* .
- Gardiner, C. & Mathys, Z. (2002), 'Tensile and compressive properties of frp composite with localised fire damage', *Applied Composite Materials* **9**, 353–367.
- Grainger (2016), 'Infrared thermometers', <https://www.grainger.com/content/qt-370-infrared-thermometers>. [Online; accessed February-2016].
- Green, R. & Joshi, N. (1972), 'Ultrasonic detection of fatigue damage', *Fracture Mechanics* **4**, 577–583.
- Gurit (2015), *Ampreg 22 - Epoxy Laminating System*, Gurit.
- H Blontrock, L. T. & Matthys, S. (1999), 'Properties of fibre reinforced plastics at elevated temperatures and regard to fire resistance of reinforced concrete mambers', *Fibre Reinforced Polymer Reinforcement for Reinforced Concrete Structures* pp. 43–54.
- Hashemite University, T. (n.d.), *Radiographic Testing*, The Hashemite University.
- Hosten, B. (1992), 'Stiffness matrix invariants to validate the characterization of composite materials with ultrasonic methods', *Ultrasonics* **30** pp. 365–371.
- Humphries, H. (n.d.), *Ultrasonic Testing - Part 6 Lamb Waves*, American Society for Nondestructive Testing.
- Inspection for Industry (2012), 'Magnetic particle inspection', <http://www.inspection-for-industry.com/magnetic-particle-inspection.html>. [Online; accessed February-2016].
- International, A. (2008), *E709-08 Standard Shuide for Magnetic Particle Testing*.
- International Atomic Energy Agency (1988), *Ultrasonic Testing of Materials at Level 2*, Vienna.

- International Atomic Energy Agency (2005), *Development of protocols for corrosion and deposits evaluation in pipes by radiography*.
- J Adamowski, M. A., Franco, E. & Buiocchi, F. (2007), ‘Ultrasonic through-transmission characterization of fibre reinforced composites using a large aperture receiver’, *Proceedings of the International COngress on Ultrasonics* .
- J Dobson, D. I. (2014), ‘Investigating the thermally induced acoustoelastic effect in isotropic media with lamb waves’, *Journal of Acoustical Society of America* pp. 2532–2543.
- Jobs, M. (2013), ‘Radiography testing x and gamma technique’, <http://www.mechjobs.in/2015/06/radiography-testing-x-and-gamma.html>. [Online; accessed March-2016].
- Joseph Johnson, K. K., Zhang, S., Wu, D. & Jiang, X. (2014), ‘High-temperature acoustic emission sensing tests using a yttrium calcium oxyborate sensor’, *Transactions on Ultrasonics, Ferroelectrics and Frequency Control* **61**.
- K Salma, J. W. & Barber, G. (1983), The use of the temperature dependence of ultrasonic velocity to measure residual stress, Technical report, University of Houston.
- Kapadia, A. (n.d.), *Non-Destructive Testing of Composite Materials*, National Composites Network.
- Khan, A. (1999), ‘Non-destructive testing applications in commercial aircraft maintenance’, *Non-Destructive testing* **4**.
- Kommareddy, V. (2003), Air-coupled ultrasonic measurements in composites, PhD thesis, Iowa State University.
- Kumar, D. & Pandey, S. (2010), ‘Ultrasonic: A technique of material characterization’, *Acoustic Waves* .
- L Nelson, R Dalton, E. B., Jones, L. & Smith, R. (2008), ‘A new low-frequency vibration technique for blind-side inspections’, *Insight* **48**(3).

- Lappe, V. (2013), *Infrared Temperature Sensors Operation and Selection*, Ircon.
- Lobkis, O., Chimenti, D., Zhang, H. & Rudolph, M. (2000), 'In-plane elastic property characterization in composite plates', *Review of Progress in Quantitative Nondestructive Evaluation* **17**.
- M Caslini, C. Z. & O'Brien, T. (1987), 'Study of matrix cracking and delamination in glass/epoxy composites', *Composites Technology* **9**, 121–130.
- M El-Badry, H. A. & Ghali, A. (2000), 'Effects of temperatures on the behaviour of fibre reinforced polymer concrete members: Experimental members', *Canadian Journal of Civil Engineering* .
- M Seale, B. S. & Prosser, W. (1998), 'Lamb wave assessment of fatigue and thermal damage in composites', *Acoustical Society of America* .
- McConaghy Boats (2016), 'Composite plates'.
- Metals, E. (2011), 'Aluminum oxide', www.espimetals.com/index.php/msds/321-aluminum-oxide. [Online; accessed March-2016].
- Mouritz, A. & Mathys, Z. (1999), 'Post-fire properties of marine composites', *Composite Structures* **47**, 643–653.
- Mouritz, A. & Mathys, Z. (2000), 'Mechanical properties of fire-damaged glass-reinforced phenolic composites', *Fire and Materials* **24**, 67–75.
- Mouritz, A. & Mathys, Z. (2001), 'Post-fire properties of glass-reinforced polyester composites', *Composites Science and Technology* **61**, 475–490.
- Multicomp (2010), *MCUSD40A100B17RS-70C Multicomp*, Multicomp.
- Nanekar, P. & Shah, B. (2003), 'Characterization of material properties by ultrasonics', *National Seminar on Non-Destructive Evaluation* .

- Non Destructive Testing Database (2000), ‘Nondestructive material testing with ultrasonics - introduction to the basic principles’, <http://www.ndt.net/article/v05n09/berke/berke2.htm>. [Online; accessed February-2016].
- Non Destructive Testing Resource Center (2016), ‘Acoustic emissions’, https://www.nde-ed.org/EducationResources/CommunityCollege/Other20Methods/AE/AE_Intro.php. [Online; accessed February-2016].
- Oliveira, R. (2004), Health Monitoring of FRP using Acoustic Emission and Fibre Optic Techniques, PhD thesis, University of Porto.
- Olympus (2016), ‘Introduction to eddy current testing’, <http://www.olympus-ims.com/en/eddycurrenttesting/>. [Online; accessed February-2016].
- P Summers, Y Chen, C. R., Allen, B., Mouritz, A., Case, S. & Lattimer, B. (2015), ‘Overview of aluminum alloy mechanical properties during and after fires’, *Fire Science Reviews* .
- Pant, S. (2014), Lamb Wave Propagation and Material Characterization of Metallic and Composite Aerospace Structures for Improved Structural Health Monitoring (SHM), PhD thesis, Carleton University.
- Piezo Drive (2016), *MX200 - High Performance Piezo Driver*, Piezo Drive, Callaghan, NSW.
- R Kazys, R Sliteris, R. R., Zukauskas, E. & Mazeika, L. (2015), ‘Ultrasonic technique for density measurement of liquids in extreme conditions’, *Sensors* **15**, 19393–19415.
- R Nishanth, K Lingadurai, V. M. & Babu, M. (n.d.), ‘An experimental study on defect detection on thin aluminum plates using guided lamb waves’, *Non Destructive Testing* .
- Ramesh, K. (2009), *Nanomaterials: Mechanics and Mechanisms*, Springer.

- Resource Center, N. (n.d.), 'Basic principles of ultrasonic testing', <https://www.nde-ed.org/EducationResources/CommunityCollege/Ultrasonics/Introduction/description.htm>. [Online; accessed February-2016].
- Robinson, M. (2009), *10 Things You Need To Know About Infrared Windows*, IRISS.
- Rodrigo, M. (2013), The Ultrasonic Pulse-Echo Immersion Technique and Attenuation Coefficient of Particulate Composites, PhD thesis, University of Rhode Island.
- Rose, J. (2004), *Ultrasonic Waves in Solid Media*, Cambridge, Cambridge University Press.
- Rose, W., Rokhlin, S. & Adler, L. (1987), 'Evaluation of anisotropic properties of graphite-epoxy composites using lamb waves', *Review of Progress in Quantitative Nondestructive Evaluation* **6B**.
- Rouse, M. (2005), 'Nyquist theorem', <http://whatis.techtarget.com/definition/Nyquist-Theorem>. [Online; accessed April-2016].
- Royal Australian College of General Practitioners (2012), 'Metal fume fever', <http://www.racgp.org.au/afp/2012/march/metal-fume-fever/>. [Online; accessed April-2016].
- S Buxbaum, C Friant, S. F. & Green, R. (1979), 'Ultrasonic and acoustic emission detection of fatigue damage', *International Advances in Nondestructive Testing* **6**(125-177).
- Safe Work Australia (2012), Guidance on the interpretation of workplace exposure standards for airborne contaminants, Technical report, Safe Work Australia.
- Salma, K. & Ling, C. (1979), Nondestructive evaluation of bulk stresses in aluminum and copper, Technical report, University of Houston.
- Silicon Chip Magazine (1994), *PreChamp Pre-Amplifier*, 1.2 edn, Jaycar.

- Summers, P. (2014), Microstructure-based constitutive models for residual mechanical behavior of aluminum alloys after fire exposure., PhD thesis, Virginia Polytechnic Institute and State University.
- Summerscales, J. (1990), *Non-Destructive Testing of Fibre-Reinforced Plastics Composites*, Vol. 2, Springer Science and Business Media.
- Svab, E. & Balasko, M. (n.d.), ‘Non-destructive testing: Neutron radiography’, *Physical Methods, Instruments and Measurements IV*.
- Testing, A. T. & Research (2016), ‘Acoustic emissions monitoring’, url<http://www.attar.com.au/Asset-Testing-RBI-Programs/Acoustic-Emission-Monitoring/155/catmenu.aspx>. [Online; accessed February-2016].
- Texas Instruments (2013), Lm138/lm338 5-amp adjustable regulators, Technical Report SNVS771B, Texas Instruments.
- University of Colorado (2016), ‘Line shapes’, <http://www.colorado.edu/chemistry/volkamer/teaching/lectures/Lecture%203%20-%20Line%20shapes>. [Online; accessed July-2016].
- W Wright, D Schindel, D. H., Carpenter, P. & Jansen, D. (1998), ‘Ultrasonic tomographic imaging of temperature and flow fields in gases using air-coupled capacitance transducers’, *Acoustical Society of America* **104**.
- Wang, L. & Rokhlin, S. (2002), ‘Ultrasonic waves in layered anisotropic media: characterization of multidirectional composites’, *International Journal of Solids and Structures* .
- Y Bai, T. K. & Vallee, T. (2008), ‘Modelling of stiffness of frp composites under elevated and high temperatures’, *Composites Science and Technology* .
- Z Zhang, H. F. & Zhao, W. (2016), ‘The ndt methods under high temperature service environment’, *Suzhou Nuclear Power Research Institute* .

Appendix A

Project Specification

ENG 4111/2 Research Project

Project Specification

For: **Michael Gall**
Topic: Non-invasive methods for testing the integrity of bulkheads and/or deckheads during a fire
Supervisors: John Billingsley - USQ
Ian Raymond - NTB
Sponsorship: Faculty of Health, Engineering & Sciences
Naval Technical Bureau (NTB) - Department of Defence
Project Aim: To investigate and evaluate a possible non-invasive test method to evaluate the integrity of bulkheads and/or deckheads during a fire.

Program: Issue A, 15 March 2015

1. Research non-invasive methods for testing integrity of materials during a fire.
2. Design a potential non-invasive test method to determine integrity of a material.
3. Test the chosen non-invasive method on Aluminium and Glass Fibre Reinforced Plastics (GRP) under fire conditions up to 200C.
4. Evaluate the results achieved from the chosen non-invasive test.
5. Evaluate the feasibility of this chosen non-invasive test method.

As time and resources permit:

1. Test the chosen non-invasive method against Carbon Fibre and evaluate results.
2. Re-design the chosen non-invasive test method to be fully portable and suitable for a fire hazardous environment.

Agreed:

Student Name: Michael Gall
Date: 15 March 2015
Supervisor Name: John Billingsley
Date: 15 March 2015

Appendix B

Risk Assessment

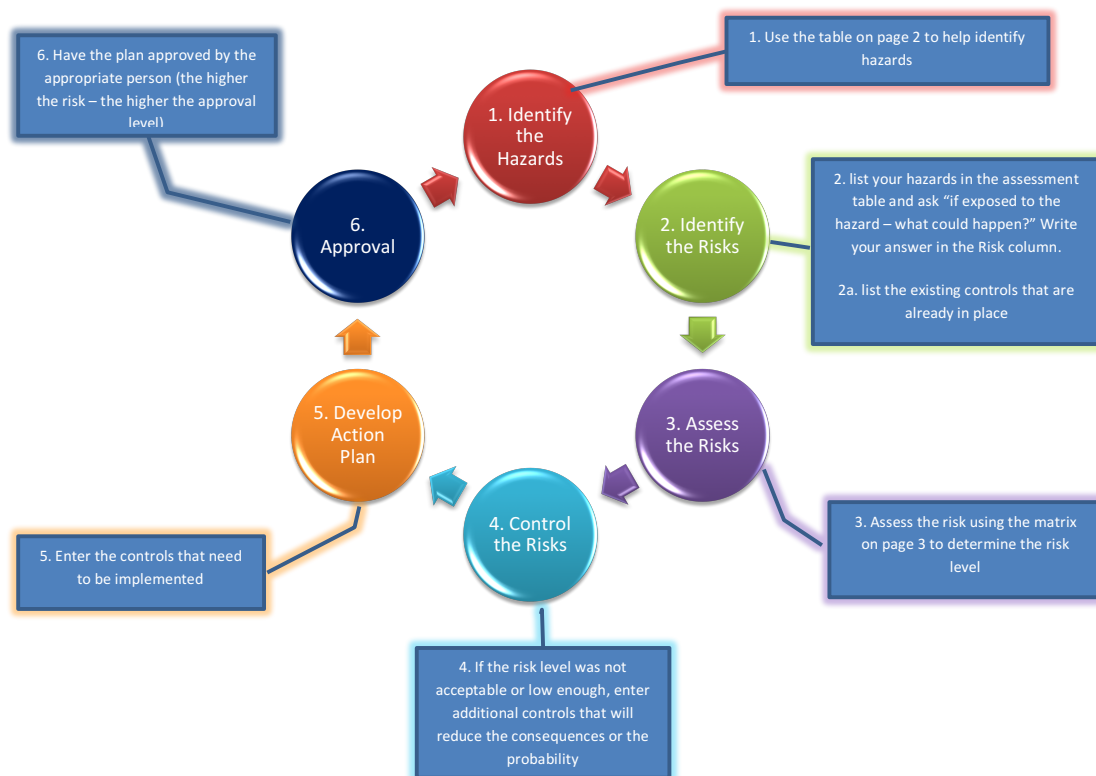


University of Southern Queensland

Risk Management Plan

Workplace (Division/Faculty/Section): Faculty of Health, Engineering & Sciences		
Assessment No (if applicable): ERP16 – ENG4111 & ENG4112	Assessment Date: 29/04/2016	Review Date: 01/10/2016
Context: What is being assessed? Describe the item, job, process, work arrangement, event etc: Non-invasive methods for testing the integrity of bulkheads and/or deckheads during a fire		
Assessment Team – who is conducting the assessment?		
Assessor(s): Michael Gall Others consulted: Ian Raymond (Fire and Safety Manager), Keith Mackie (Mechanical Technician) and Mathew Ryan (Electrical Technician)		

The Risk Management Process

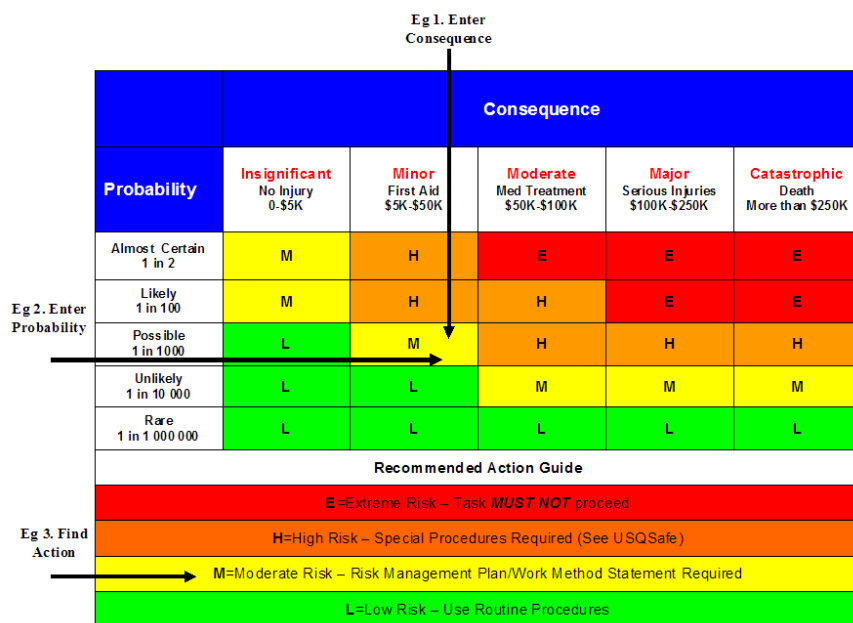


Step 1 - Identify the hazards (use this table to help identify hazards then list all hazards in the risk table)		
General Work Environment		
<input checked="" type="checkbox"/> Sun exposure	<input type="checkbox"/> Water (creek, river, beach, dam)	<input checked="" type="checkbox"/> Sound / Noise
<input type="checkbox"/> Animals / Insects	<input type="checkbox"/> Storms / Weather/Wind/Lightning	<input checked="" type="checkbox"/> Temperature (heat, cold)
<input checked="" type="checkbox"/> Air Quality	<input checked="" type="checkbox"/> Lighting	<input type="checkbox"/> Uneven Walking Surface
<input type="checkbox"/> Trip Hazards	<input type="checkbox"/> Confined Spaces	<input type="checkbox"/> Restricted access/egress
<input type="checkbox"/> Pressure (Diving/Altitude)	<input checked="" type="checkbox"/> Smoke	<input type="checkbox"/>
Other/Details:		
Machinery, Plant and Equipment		
<input type="checkbox"/> Machinery (fixed plant)	<input type="checkbox"/> Machinery (portable)	<input checked="" type="checkbox"/> Hand tools
<input type="checkbox"/> Laser (Class 2 or above)	<input type="checkbox"/> Elevated work platforms	<input type="checkbox"/> Traffic Control
<input type="checkbox"/> Non-powered equipment	<input checked="" type="checkbox"/> Pressure Vessel	<input checked="" type="checkbox"/> Electrical
<input type="checkbox"/> Vibration	<input type="checkbox"/> Moving Parts	<input type="checkbox"/> Acoustic/Noise
<input checked="" type="checkbox"/> Vehicles	<input type="checkbox"/> Trailers	<input checked="" type="checkbox"/> Hand tools
Other/Details:		
Manual Tasks / Ergonomics		
<input checked="" type="checkbox"/> Manual tasks (repetitive, heavy)	<input type="checkbox"/> Working at heights	<input type="checkbox"/> Restricted space
<input type="checkbox"/> Vibration	<input type="checkbox"/> Lifting Carrying	<input type="checkbox"/> Pushing/pulling
<input type="checkbox"/> Reaching/Overstretching	<input checked="" type="checkbox"/> Repetitive Movement	<input checked="" type="checkbox"/> Bending
<input checked="" type="checkbox"/> Eye strain	<input type="checkbox"/> Machinery (portable)	<input checked="" type="checkbox"/> Hand tools
Other/Details:		
Biological (e.g. hygiene, disease, infection)		
<input type="checkbox"/> Human tissue/fluids	<input type="checkbox"/> Virus / Disease	<input type="checkbox"/> Food handling
<input type="checkbox"/> Microbiological	<input type="checkbox"/> Animal tissue/fluids	<input type="checkbox"/> Allergenic
Other/Details:		
Chemicals Note: Refer to the label and Safety Data Sheet (SDS) for the classification and management of all chemicals.		
<input type="checkbox"/> Non-hazardous chemical(s)	<input type="checkbox"/> 'Hazardous' chemical (Refer to a completed <u>hazardous chemical risk assessment</u>)	
<input type="checkbox"/> Engineered nanoparticles	<input type="checkbox"/> Explosives	<input checked="" type="checkbox"/> Gas Cylinders
Name of chemical(s) / Details:		
Critical Incident – resulting in:		
<input type="checkbox"/> Lockdown	<input type="checkbox"/> Evacuation	<input type="checkbox"/> Disruption
<input type="checkbox"/> Public Image/Adverse Media Issue	<input type="checkbox"/> Violence	<input type="checkbox"/> Environmental Issue
Other/Details:		
Radiation		
<input type="checkbox"/> Ionising radiation	<input type="checkbox"/> Ultraviolet (UV) radiation	<input type="checkbox"/> Radio frequency/microwave
<input type="checkbox"/> Infrared (IR) radiation	<input type="checkbox"/> Laser (class 2 or above)	<input type="checkbox"/>
Other/Details:		
Energy Systems – incident / issues involving:		
<input type="checkbox"/> Electricity (incl. Mains and Solar)	<input type="checkbox"/> LPG Gas	<input type="checkbox"/> Gas / Pressurised containers
Other/Details:		
Facilities / Built Environment		
<input checked="" type="checkbox"/> Buildings and fixtures	<input type="checkbox"/> Driveway / Paths	<input checked="" type="checkbox"/> Workshops / Work rooms
<input type="checkbox"/> Playground equipment	<input type="checkbox"/> Furniture	<input type="checkbox"/> Swimming pool
Other/Details:		
People issues		
<input checked="" type="checkbox"/> Students	<input checked="" type="checkbox"/> Staff	<input checked="" type="checkbox"/> Visitors / Others
<input type="checkbox"/> Physical	<input type="checkbox"/> Psychological / Stress	<input type="checkbox"/> Contractors
<input type="checkbox"/> Fatigue	<input type="checkbox"/> Workload	<input type="checkbox"/> Organisational Change
<input type="checkbox"/> Workplace Violence/Bullying	<input type="checkbox"/> Inexperienced/new personnel	<input type="checkbox"/>
Other/Details:		

Step 1 (cont) Other Hazards / Details (enter other hazards not identified on the table)

Fire exposure hazard due to the heating of the plates.

Risk Matrix



Risk register and Analysis

Step 1 (cont)		Step 2		Step 2a		Step 3			Step 4			
Hazards: From step 1 or more if identified	The Risk: What can happen if exposed to the hazard with existing controls in place?	Existing Controls: What are the existing controls that are already in place?	Risk Assessment: (use the Risk Matrix on p3) Consequence x Probability = Risk Level			Additional controls: Enter additional controls if required to reduce the risk level	Risk assessment with additional controls: (use the Risk Matrix on p3 – has the consequence or probability changed?)	Controls Implemented? Yes/No				
			Consequence	Probability	Risk Level							
Sun exposure during experiment	Sun exposure leading to heat stress/heat stroke/exhaustion and sun burn leading to serious personal injury	Regular breaks, chilled water, sun screen and appropriate clothing.	Catastrophic	Possible	High	Limit exposure time, buddy system and temporary shade	Catastrophic Unlikely	Moderate	Yes			
Air quality during experiment	Exposure to microfibers leading to respiratory problems	Ventilation is appropriate, limit exposure proximity to experiment area.	Major	Likely	Extreme	Experiment to be conducted in a well-ventilated area. Experiment to be conducted outside. Appropriate respiratory PPE to be worn.	Major Possible	High	Yes			
Smoke and fumes from metals exposure during experiment and soldering	Exposure to smoke and fumes leading to respiratory problems and metal fume fever	Ventilation is appropriate, limit exposure proximity to experiment area.	Major	Likely	Extreme	Experiment to be conducted in a well-ventilated area. Experiment to be conducted outside. Appropriate respiratory PPE to be worn.	Major Possible	High	Yes			
Lighting	Low or extreme light exposure leading to strain on eyes	Ensure that lighting is appropriate for the activity. Use desk lamps to ensure activities are appropriately lit.	Minor	Possible	Moderate	Ensure that lighting is appropriate for the activity. Use desk lamps to ensure activities are appropriately lit.	Minor Unlikely	Low	Yes			
Working with ultrasonics	Extended exposure to ultrasonics leading to health issues with body tissue.	Minimise exposure time to ultrasonics and avoid direct path between piezo.	Moderate	Unlikely	Moderate	Minimise exposure time to ultrasonics and avoid direct path between piezo.	Moderate Unlikely	Moderate	Yes			
Working with tools at high temperature	High temperature exposure leading to serious burns	Tools are handled and stored in the correct manner. Allow sufficient cooling time.	Major	Possible	High	Components are held in place using mechanical means while using high temperature tools.	Major Unlikely	Moderate	Yes			
Working with materials at high temperature	High temperature exposure leading to serious burns	No direct contact with high temperature materials. Allow sufficient cooling time.	Major	Possible	High	Appropriate material handling techniques are in place to avoid contact with high temperature i.e. use of grips while wearing gloves.	Major Unlikely	Moderate	Yes			
Ignition of materials at high temperatures	High temperature materials igniting causing an uncontrolled leading to serious burns	Ensure materials are stored in an appropriate manner.	Major	Possible	High	All materials to be kept at temperatures below 200°C during experiment.	Major Unlikely	Moderate	Yes			
Vehicles	Use of a vehicle leading to car accident causing serious personal injury/death	Drive according to the road conditions and in accordance with road rules.	Catastrophic	Possible	High	Drive according to the road conditions and in accordance with road rules.	Catastrophic Possible	High	Yes			
Pressure Vessels	Improper handling/use of gas bottle leading to explosion causing serious personal injury/death	Gas bottles are suitably stored, transported and valves are not tampered with.	Catastrophic	Possible	High	Gas bottles are only used with appropriately fitted components. Gas bottles are not in close proximity to the flame that is produced.	Catastrophic Unlikely	Moderate	Yes			
High voltage electrical	Electric shock leading to serious personal injury/death	Ensure high voltage devices are suitably tagged out before any contact is made.	Catastrophic	Possible	High	Ensure that devices are disconnected from power before they are touched.	Catastrophic Unlikely	Moderate	Yes			

Step 1 (cont)		Step 2	Step 2a	Step 3			Step 4			
Hazards: From step 1 or more if identified	The Risk: What can happen if exposed to the hazard with existing controls in place?	Existing Controls: What are the existing controls that are already in place?	Risk Assessment: (Use the Risk Matrix on p3) Consequence x Probability = Risk Level			Additional controls: Enter additional controls if required to reduce the risk level	Risk assessment with additional controls: (Use the Risk Matrix on p3 – has the consequence or probability changed?)			Controls Implemented? Yes/No
			Consequence	Probability	Risk Level		Consequence	Probability	Risk Level	
exposure										
Manual handling of heavy objects	Manual handling of heavy plates leading to serious back injury	Ensure that a maximum of one plate is carried at a time. Maximum weight allowed to be carried by one person is 10kg.	Major	Unlikely	High	Ensure that a maximum of one plate is carried at a time. Maximum weight allowed to be carried by one person is 10kg.	Major	Unlikely	Moderate	Yes
Bending while carrying objects	Bending during manual handling leading to serious personal injury	Back is kept straight and knees bent while carrying any object.	Major	Almost Certain	Extreme	Ensure a buddy system or mechanical means in place while carrying any object over 10kg.	Major	Unlikely	Moderate	Yes
Working with micro fibres	Contact with micro fibres leading to skin and eye irritation.	Use protective clothing, gloves and eye wear when handling damage composite plates.	Major	Almost Certain	Extreme	Use water to wet down composite to avoid microfiber spreading through air	Major	Unlikely	Moderate	Yes
Fire hazard while conducting experiment	Fire exposure leading to serious burns.	No direct contact with flames and ensure unobstructed access to gas bottle to control flame	Major	Possible	High	Clothing is appropriate for high temperatures and access to fire extinguishers.	Major	Unlikely	Moderate	Yes
Gas bottle leak during transportation	Gas leak leading explosion during transportation	Gas bottles must be stored upright and secured during transportation.	Catastroph ic	Rare	Moderate	Gas bottles must not be stored against each other.	Catastroph ic	Rare	Moderate	Yes

Page 6 of 6

Appendix C

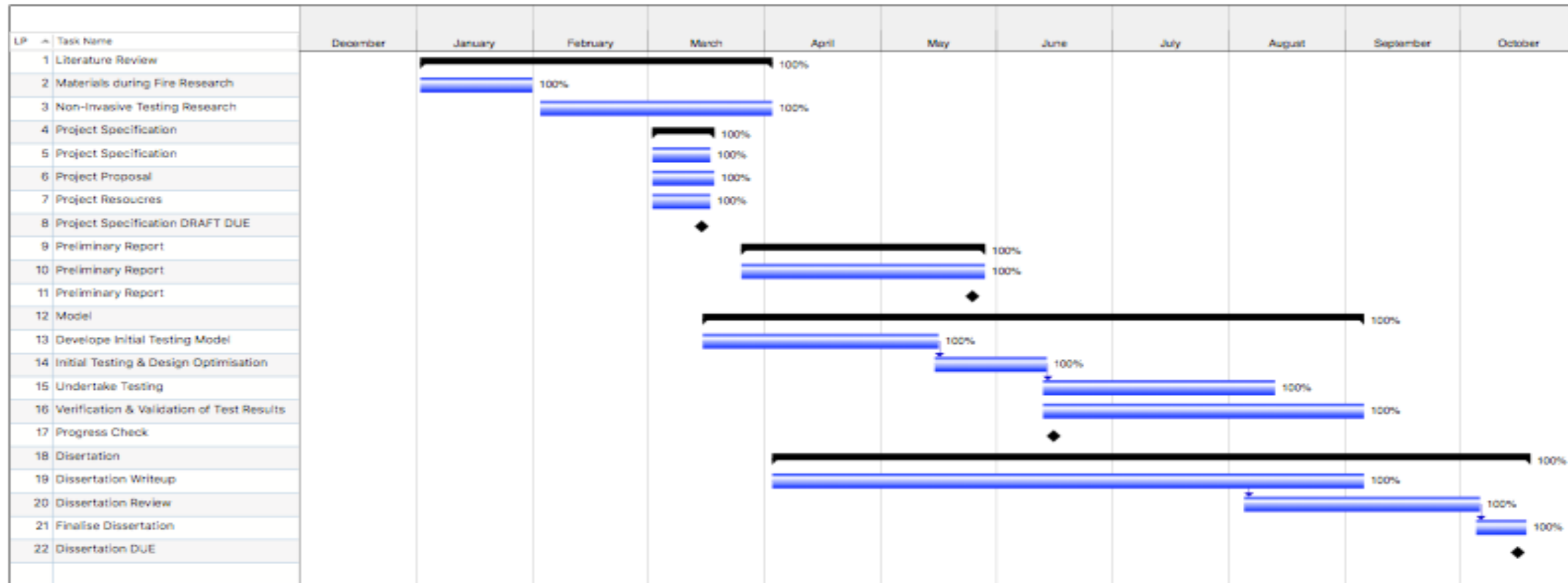
Timeline

The duration required to complete each task for the project is provided in Table C.1.

Tasks	Start Date	Time (days)	End Date
Literature Review	01/01/2016	90	31/03/2016
Project Specification	01/03/2016	15	16/03/2016
Preliminary Report	24/03/2016	62	25/05/2016
Develop Initial Test Model	14/03/2016	60	13/05/2016
Initial Testing & Design Optimisation	13/05/2016	28	10/06/2016
Undertake Testing	10/06/2016	61	10/08/2016
Verification & Validation of Test	10/06/2016	36	01/08/2016
Dissertation Writeup	01/04/2016	92	01/08/2016
Dissertation Review	01/08/2016	60	30/09/2016
Finalise Dissertation	30/09/2016	7	07/10/2016

Table C.1: Project Timeline.

Project Timeline



Appendix D

Resource Requirements Cost

A listing of all relevant resources utilised to undertake the project is included within the Tables D.1 to D.7. Prices marked [*] denotes conversion from USD to AUD using a multiplier of 1.39.

Indirect resources required for the undertaking of the project have not been included in the tables.

Product	Product Number	Supplier	Qty	Cost
Arduino Zero	2843	Adafruit	1	76.38*
Arduino M0 Pro	865-9004	RS	1	54.04
Piezo Transceiver 175KHz	MVUSD19A17B11.5RS	Element14	2	79.75
Piezo Transceiver 100KHz	MCUSD40A100B17RS	Element14	2	84.85
High Performance Piezo Drive	MX200	PiezoDrive	1	548.90
Pre-Amplifier Champ	KC5166	Jaycar	1	9.95
Cable HU RND H/D 10M RED	WH3045	Jaycar	1	4.70
Cable HU RND H/D 10M BLK	WH3046	Jaycar	1	4.70
Cable Audio SCRN L/D GRY	WB1500	Jaycar	3m	1.65
PLG Banana 4MM Piggyback RED	PP0390	Jaycar	2	3.50
PLG Banana 4MM Piggyback BLK	PP0391	Jaycar	2	3.50
CAP CER Y5P 330P 50V	RC5530	Jaycar	1	0.64
CAP CER Y5P 180P 50V	RC5527	Jaycar	1	0.64
RES 0.5W MTL 1K0	RR0572	Jaycar	1	0.55
Heatsink T0220 Clip	ZV1505	Jaycar	2	2.40
			Total Cost	876.15

Table D.1: Non-Invasive Test Method Resource Costing.

Product	Product Number	Supplier	Qty	Cost
ATMEGA 328 Uno R3	XC4410	Duinodech	1	26.95
Thermocouple Amplifier	MAX31855	Adafruit	3	62.34*
Thermocouple K-Type	XX	Adafruit	1	13.83*
Thermocouple K-type	QM1282	Jaycar	2	29.90
Temperature & Humidity Sensor	SHT31-D	Adafruit	1	19.39*
IRTemp Sensor	XC4260	Freetronics	1	40.45
Data Logging Shield	1411	Adafruit	1	27.73*
TFT Touch Shield	1947	Adafruit	1	62.48*
Module LCD 2 X 16 Controller	XC4454	Jaycar	1	13.45
Shield Stacking Headers	85	Adafruit	2	5.42*
Lead Jumper 90 PC	WC6029	Jaycar	1	8.75
SD Memory Card	XG4961	Dicksmith	1	10.00
Breadboard 170 Points	PB8817	Jaycar	1	12.85
Breadboard half-size	AF-64	Little Bird Electronics	1	7.75
Lead USB PLG A - PLG Micro B	WC7724	Jaycar	1	9.95
Lead USB PLG A - PLG B	WC7772	Jaycar	1	13.35
			Total Cost	364.74

Table D.2: Temperature Evaluation Resource Costing.

Product	Product Number	Supplier	Qty	Cost
Aluminium	5083 H116	Capral	3	232.41
Glass Fibre Reinforce Plastic	E-Glass Epoxy	McConaghy Boats	3	2860.00
Carbon Fibre Reinforced Plastic	C Epoxy	McConaghy Boats	3	
			Total Cost	3092.41

Table D.3: Test Materials Costing

Product	Product Number	Supplier	Qty	Cost
Gas Bottle - 8.5kg		Bunnings	1	28.90
Cast Iron Stove Burner		Bunnings	1	49.98
Gas Hose/Regulator - 1.2m		Bunnings	1	28.87
Masonry Brick		Bunnings	6	21.00
Universal Clay Commons Brick		Bunnings	6	5.10
Grill		Bunnings	1	44.50
			Total Cost	178.35

Table D.4: Fire Resource Costing.

Product	Product Number	Supplier	Qty	Cost
Wireless Keyboard & Mouse	MK270r	CX Com- puters	1	39.00
Mini Display Port to DVI adapter	WQ7444	Jaycar	1	29.95
Fire Extinguisher		Bunnings	1	87.00
Protector Respirator Kit	5822368	Bunnings	1	46.98
			Total Cost	202.93

Table D.5: WHS Resources Costing.

Product	Product Number	Supplier	Qty	Cost
Soldering Station 240VAC 48W	TS1564	Jaycar	1	89.95
Solder 60/40 0.71mm	NS3008	Jaycar	1	1.75
Tool Set Cut/Plier 5PCE S/S	TH1812	Jaycar	1	27.95
INCA - Card Reader	601274	JB HI-FI	1	23.00
CAT III Digital Multimeter	QM1323	Jaycar	1	39.95
			Total Cost	182.60

Table D.6: Miscellaneous Resources Costing.

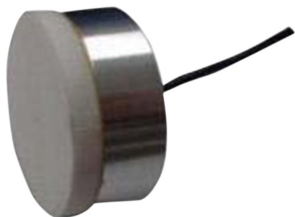
Product	Product Number	Supplier
Oscilloscope	TDS3054C	Tektronix
Dual Power Supply	246A	BWD Electronics

Table D.7: Calibrated Test Equipment.

Appendix E

Ultrasonic Transducer Data Sheet

MCUSD40A100B17RS-70C



Applications:

- Level measurement
- Automation control
- Proximity
- Obstacle avoidance
- Robotics

Features:

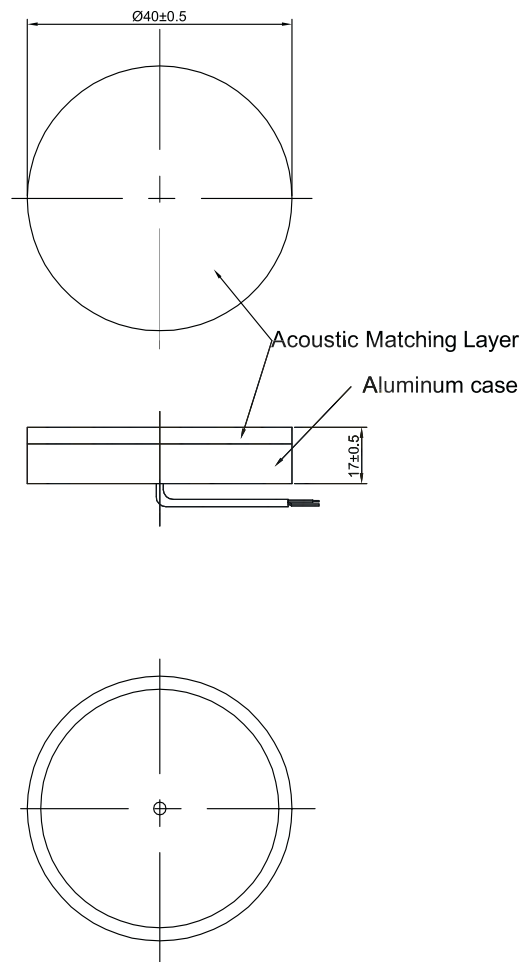
- Rugged sealed construction
- Cylindrical design allows for installation in various applications
- Short-range measurement capabilities

Technical Terms:

No	Item	Specification
1	Part Number	MCUSD40A100B17RS-70C
2	Construction	Water Proof
3	Using Method	Dual Use
4	Centre Frequency	100 ± 8kHz
5	Receive Sensitivity Echo (V)	≥1.5 (driver signal:200Vp-p, 100kHz, at 70cm)
6	Capacitance (pF)	900 ± 25%
7	Max. Input Voltage	600Vp-p
8	Directivity (-3dB)	9 ± 2
9	Distance of Detection	0.2m to 4m
10	Protection Class	IP65
11	Material	Aluminium
12	Operating Temperature Range	-20°C to +80°C
13	Storage Temperature Range	-35°C to +85°C

MCUSD40A100B17RS-70C

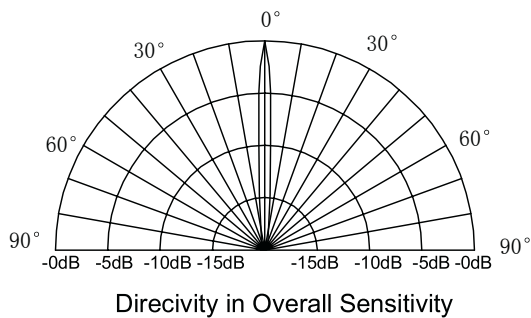
Drawing:



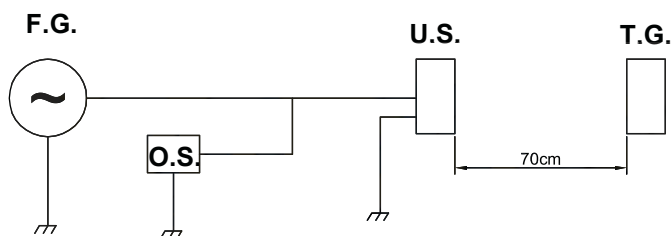
Dimensions : Millimetres

MCUSD40A100B17RS-70C

Beam Pattern:



Test Circuit:

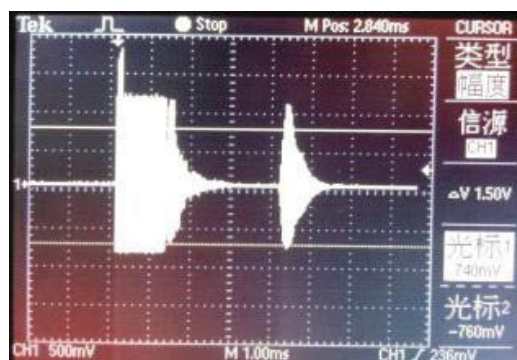


F.G. : Function Generator
 U.S. : Ultrasonic Sensor
 T.G. : Target
 O.S. : Oscilloscope

MCUSD40A100B17RS-70C

Echo sensitivity / Ringing

driver signal: 200Vp-p, 100kHz, at 70cm



Part Number Table

Description	Part Number
Transceiver, 100kHz, 40mm, Metal	MCUSD40A100B17RS-70C

Important Notice : This data sheet and its contents (the "Information") belong to the members of the Premier Farnell group of companies (the "Group") or are licensed to it. No licence is granted for the use of it other than for information purposes in connection with the products to which it relates. No licence of any intellectual property rights is granted. The Information is subject to change without notice and replaces all data sheets previously supplied. The Information supplied is believed to be accurate but the Group assumes no responsibility for its accuracy or completeness, any error in or omission from it or for any use made of it. Users of this data sheet should check for themselves the Information and the suitability of the products for their purpose and not make any assumptions based on information included or omitted. Liability for loss or damage resulting from any reliance on the Information or use of it (including liability resulting from negligence or where the Group was aware of the possibility of such loss or damage arising) is excluded. This will not operate to limit or restrict the Group's liability for death or personal injury resulting from its negligence. Multicomp is the registered trademark of the Group. © Premier Farnell plc 2012.

www.element14.com
www.farnell.com
www.newark.com



Appendix F

Oscilloscope Certificate of Calibration

CELEMETRIX
the art of measurement

 Celemetrix Australia Pty Ltd
 Unit 1, 6 Anella Ave
 Castle Hill, NSW 2154

 NATA Accredited
 Laboratory Number 19397

Certificate of Calibration

Calibration Certificate Number: M410769/3AL



UNIT UNDER TEST:	Tektronix TDS3034C Oscilloscope	TEMPERATURE:	23°C ± 5°C
SERIAL NUMBER:	C014478	HUMIDITY:	50% ± 30% RH
OPTIONS:		CALIBRATED BY:	Kevin Fraser
PROCEDURE NAME:	Tek_TDS3054C_Cal_V1.32_D_SydAcc_ClosedLoop_140 92015	PROCEDURE REV:	V1.32
CUSTOMER:	Department of Defence Building L474-2ND floor RAAF Williams Laverton, VIC 3028	ASSET NUMBER:	A74086
		CMX BARCODE:	CMX107980
		CAL DATE:	29/02/2016
		DUE DATE:	28/02/2017

REPORT TYPE: AS-LEFT

This Certificate of Calibration applies only to the item being calibrated, identified above and shall not be reproduced, except in full, unless written permission for an approved abstract is obtained from Celemetrix Australia Pty Ltd.

Accredited for compliance with ISO/IEC 17025. NATA is a signatory to the ILAC mutual recognition agreement for the mutual recognition of the equivalence of testing, calibration and inspection reports.

Measurements in this calibration are traceable to the International System of Units (SI) via national metrology institutes that are signatories to the CIPM Mutual Recognition Agreement.

The report may contain data that is not within the Scope of Accreditation. The unaccredited material is indicated by an Asterisk (*) in the Expanded Measurement Uncertainty field (Exp Uncert) adjacent to the affected parameter. NATA accreditation does not cover the performance of this service.

Measurement uncertainties at the time of test, expressed in SI units, are given on the following pages, where applicable. They are calculated in accordance with the methods described in applicable Guides to the Uncertainty in Measurement (GUM), using a coverage factor $k=2.0$, corresponding to a confidence level of 95%.

Evaluation of Results:

One or more test result values are within specification but when including the measurement uncertainty range may exceed the specification limits - **One or more test points has a result of Pass Indeterminate**

As-Left Data Type Definition: Calibration data collected after adjustment or repair. For As-Found condition results please refer to Calibration Certificate number M410769/3AF, unless otherwise noted in remarks.

Result Definitions:

- Pass: The measured test result value (including the uncertainty range when the test point is within the Scope of Accreditation) is within the specification limits.
- Pass Indeterminate: The measured test result value is within the specification limit, but when including the uncertainty range the measurement may exceed the specification limit.
- Fail Indeterminate: The measured test result value is outside the specification limit, but when including the uncertainty range the measurement may be within the specification limit.
- Fail: The measured test result value including the uncertainty range is outside the specification limits.

Remarks: After repair:

Signed:

☒ Jason Dortmans
Technical Director

Date Of Issue:

9/3/2016

☐ Aarthi Sriram
Senior Technician

SERIAL NUMBER: C014478

Calibration Certificate Number: M410769/3AL

Model: TDS3034C

Standards Used

<u>Asset #</u>	<u>Description</u>	<u>Cal Date</u>	<u>Due Date</u>
Instrument 62	Fluke 5520A Multi-Product Calibrator	8/12/2015	8/12/2016

SERIAL NUMBER: C014478

Calibration Certificate Number: M410769/3AL

Model: TDS3034C

Test Results

Test Description	Test Result	Lower limit	Upper limit	Units	Result	Exp Uncert ±
IDENTIFICATION						
Serial Number:	Not available					
Firmware Level:	CF:91.1CT FV:v4.26 TDS3GV:v1.00 TDS3FFT :v1.00 TDS3TRG:v1.00					
SIGNAL PATH COMPENSATION					Pass	*
SELF TEST					Pass	*
DC VOLTAGE MEASUREMENT ACCURACY						
Channel 1						
1 mV/div, 100 mV input	99.96	99.25	100.80	m V	Pass	1.03E-004 V
2 mV/div, -7 mV input	-7.125	-7.540	-6.460	m V	Pass	4.96E-005 V
5 mV/div, -100 mV input	-100.15	-101.80	-98.24	m V	Pass	1.03E-004 V
50 mV/div, 1 V input	0.9984	0.9824	1.0180	V	Pass	6.22E-004 V
50 mV/div, 650 mV input	649.1	632.4	667.6	m V	Pass	4.22E-004 V
50 mV/div, 350 mV Delta	349.4	340.5	359.5	m V	Pass	*
90 mV/div, -315 mV input	-317.2	-339.3	-290.7	m V	Pass	2.33E-004 V
200 mV/div, 10 V input	9.995	9.900	10.100	V	Pass	6.00E-003 V
1 V/div, -10 V input	-9.943	-10.300	-9.698	V	Pass	6.00E-003 V
Channel 2						
1 mV/div, 100 mV input	99.93	99.25	100.80	m V	Pass	1.03E-004 V
2 mV/div, -7 mV input	-7.091	-7.540	-6.460	m V	Pass	4.96E-005 V
5 mV/div, -100 mV input	-100.05	-101.80	-98.24	m V	Pass	1.03E-004 V
50 mV/div, 1 V input	0.9984	0.9824	1.0180	V	Pass	6.22E-004 V
50 mV/div, 650 mV input	649.7	632.4	667.6	m V	Pass	4.22E-004 V
50 mV/div, 350 mV Delta	348.6	340.5	359.5	m V	Pass	*
90 mV/div, -315 mV input	-316.6	-339.3	-290.7	m V	Pass	2.33E-004 V
200 mV/div, 10 V input	9.995	9.900	10.100	V	Pass	6.00E-003 V
1 V/div, -10 V input	-9.932	-10.300	-9.698	V	Pass	6.00E-003 V
Channel 3						
1 mV/div, 100 mV input	100.01	99.25	100.80	m V	Pass	1.03E-004 V
2 mV/div, -7 mV input	-7.041	-7.540	-6.460	m V	Pass	4.96E-005 V
5 mV/div, -100 mV input	-100.10	-101.80	-98.24	m V	Pass	1.03E-004 V
50 mV/div, 1 V input	0.9988	0.9824	1.0180	V	Pass	6.22E-004 V
50 mV/div, 650 mV input	649.5	632.4	667.6	m V	Pass	4.22E-004 V
50 mV/div, 350 mV Delta	349.4	340.5	359.5	m V	Pass	*
90 mV/div, -315 mV input	-316.4	-339.3	-290.7	m V	Pass	2.33E-004 V
200 mV/div, 10 V input	9.995	9.900	10.100	V	Pass	6.00E-003 V
1 V/div, -10 V input	-9.966	-10.300	-9.698	V	Pass	6.00E-003 V
Channel 4						
1 mV/div, 100 mV input	100.12	99.25	100.80	m V	Pass	1.03E-004 V
2 mV/div, -7 mV input	-7.013	-7.540	-6.460	m V	Pass	4.96E-005 V
5 mV/div, -100 mV input	-100.06	-101.80	-98.24	m V	Pass	1.03E-004 V
50 mV/div, 1 V input	0.9993	0.9824	1.0180	V	Pass	6.22E-004 V
50 mV/div, 650 mV input	649.7	632.4	667.6	m V	Pass	4.22E-004 V
50 mV/div, 350 mV Delta	349.4	340.5	359.5	m V	Pass	*
90 mV/div, -315 mV input	-315.6	-339.3	-290.7	m V	Pass	2.33E-004 V
200 mV/div, 10 V input	10.002	9.900	10.100	V	Pass	6.00E-003 V

Date Printed: 08/03/2016

DATA TYPE: AS-LEFT

Page 3 of 4

SERIAL NUMBER: C014478

Calibration Certificate Number: M410769/3AL

Model: TDS3034C

Test Results

<u>Test Description</u>	<u>Test Result</u>	<u>Lower limit</u>	<u>Upper limit</u>	<u>Units</u>	<u>Result</u>	<u>Exp Uncert ±</u>
1 V/div, -10 V input	-9.973	-10.300	-9.698	V	Pass	6.00E-003 V
BANDWIDTH						
Channel 1						
212.0 mV @ 500 MHz	157.7	150.0	212.0 m V	Pass	Indeterminate	1.06E-002 V
Channel 2						
212.0 mV @ 500 MHz	151.7	150.0	212.0 m V	Pass	Indeterminate	1.06E-002 V
Channel 3						
212.0 mV @ 500 MHz	156.6	150.0	212.0 m V	Pass	Indeterminate	1.06E-002 V
Channel 4						
212.0 mV @ 500 MHz	155.8	150.0	212.0 m V	Pass	Indeterminate	1.06E-002 V
TRIGGER SENSITIVITY AT FULL BANDWIDTH						
Channel 1						
Rising Slope, Stable Trigger				Pass		*
Falling Slope, Stable Trigger				Pass		*
Channel 2						
Rising Slope, Stable Trigger				Pass		*
Falling Slope, Stable Trigger				Pass		*
Channel 3						
Rising Slope, Stable Trigger				Pass		*
Falling Slope, Stable Trigger				Pass		*
Channel 4						
Rising Slope, Stable Trigger				Pass		*
Falling Slope, Stable Trigger				Pass		*
TRIGGER SENSITIVITY AT 50 MHZ						
Channel 1						
Rising Slope, Stable Trigger				Pass		*
Falling Slope, Stable Trigger				Pass		*
Channel 2						
Rising Slope, Stable Trigger				Pass		*
Falling Slope, Stable Trigger				Pass		*
Channel 3						
Rising Slope, Stable Trigger				Pass		*
Falling Slope, Stable Trigger				Pass		*
Channel 4						
Rising Slope, Stable Trigger				Pass		*
Falling Slope, Stable Trigger				Pass		*
SAMPLE RATE AND DELAY TIME ACCURACY						
Limit : ±2 div @1 µs/div, 100 ms delay time				Pass		*

***** End of Certificate *****

Date Printed: 08/03/2016

DATA TYPE: AS-LEFT

Page 4 of 4

Appendix G

Piezo Driver Data Sheet

PiezoDrive

MX200 200V 1A Piezo Driver



The MX200 is a complete power supply and high-performance linear amplifier module for driving piezoelectric actuators. The MX200 can drive stack actuators; standard piezoelectric actuators; two wire benders; and three-wire piezoelectric benders requiring a bias voltage. Output currents of up to 1 Amp are developed at frequencies up to 100 kHz with less than 100 μ V noise (10Hz to 10kHz).

The MX200 is protected against short-circuit, average current overload, and supply under-voltage. The MX200 can be used as a stand-alone module or mounted to a base with four M3 screws. The PCB mounting version (MX200-PCB) is supplied with headers for direct mounting onto a host motherboard.

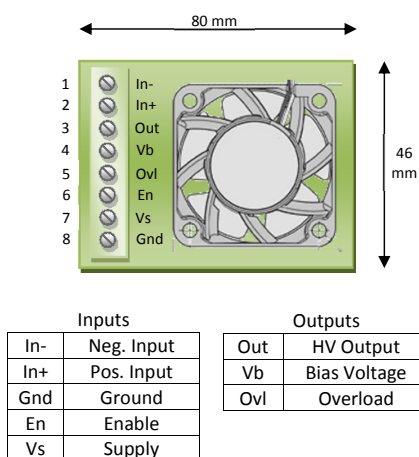


Figure 1. Connection diagram

Specifications

Power Supply	24V (18V to 36V)
Voltage Range	+100V, +150V, or +200 V
Peak Current	1 Amp
RMS Current	550 mA, 330 mA, 220 mA
Power Bandwidth	106 kHz (180 Vp-p)
Signal Bandwidth	200 kHz (100nF Load)
Slew Rate	60 V/ μ s
Gain	20 V/V
Input Impedance	33 $k\Omega$ (In+), 1.6 $k\Omega$ (In-)
Input Offset	± 5 mV
Load	Unlimited
Output Noise	<100 μ V RMS (10Hz to 10kHz)
Protection	Short-circuit, average current, and under-voltage protection
Quiescent Current	0.3 A (30 mA in Shutdown)
Dimensions	80 x 46 x 40 mm (L x W x H)
Environment	-40 to 60°C (-40 to 140°F) Non-condensing humidity
Weight	95 g

Operation

The system block diagram is illustrated in Figure 2. A boost converter generates the high voltage supply and negative rail. The output voltage range can be set to either +100V, +150V, or +200V. Configuration options are discussed in "Configuration".

The high-voltage amplifier has differential inputs with a gain of 20 and an input voltage range of 10 V. The negative input can be connected to ground or to a differential source. It should not be left floating.

The load is connected between the output and ground. The bias voltage output is for three wire bimorph bender actuators.

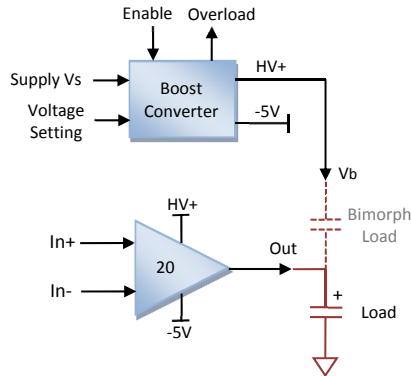


Figure 2. MX200 Block Diagram

Configuration

The output voltage range can be set to either +100V, +150V or +200V using the two jumpers LK1 and LK2. Greater output current is available in the lower voltage ranges, as described in Table 1. Incorrect jumper combinations will damage the amplifier.

Output Voltage	Peak Current	RMS Current	Average Current	LK1	LK2
100 V	1 A	550 mA	250 mA	A	Out
150 V	1 A	330 mA	150 mA	B	B
200 V	1 A	220 mA	100 mA	Out	A

Table 1. Voltage Range Jumper Settings

Output Current

The peak output current is 1 Amp for all voltage ranges but the maximum continuous RMS current is dependent on the voltage range, as described in Table 1. The average positive output current is also useful for calculating power dissipation and the average supply current. For a sine wave, the average positive output current is equal to

$$I_{av} = \frac{\sqrt{2}}{\pi} I_{rms} = \frac{1}{\pi} I_{pk}.$$

Supply Current

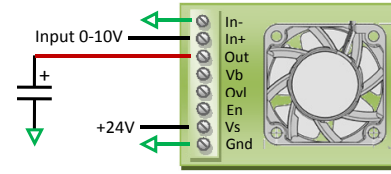
The quiescent power for the amplifier and fan is approximately 8 W. Therefore, the quiescent supply current at 24 V is 0.3 A. This can be reduced to <30 mA by applying a logic zero to the Enable pin. The supply current is related to the average positive output current by

$$I_s = \frac{1.1 \times V_{out} \times I_{av} + 8}{V_s}.$$

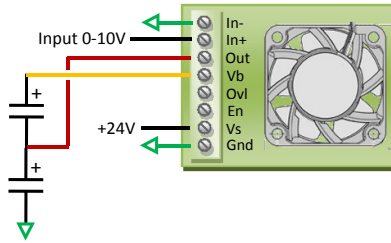
where V_{out} is the output voltage range, and I_{av} is the average output current. Therefore, the maximum supply current is 1.25 A with a 24 V supply at the full rated power ($I_{av} = 100$ mA).

The power supply must be sufficient for the amplifier, a rating of at least 1.5 Amps is recommended. Note that when power is first applied or when the amplifier is enabled, full current will be required for a brief period to charge the storage capacitors.

Applications Circuits



200 V Piezo stack driver.

200 V Bimorph Bender Driver with bias.
Also suitable for benders with +100V and -100V bias.

Bias Output for Piezo Bimorphs

The bias output (Vb) provides a fixed voltage for driving three-wire piezoelectric benders. The bias voltage is approximately 5V above the selected voltage range. The effective capacitance when using bimorph actuators is the sum of both layers.

Actuators that require a symmetrical bias voltage, e.g. ± 100 V can also be driven since this configuration is electrically identical to the unipolar configuration, e.g. 0V to 200V.

Power Bandwidth

The nominal slew-rate of the MX200 is 60 V/us. Therefore, the maximum frequency sine-wave is

$$f_{max} = \frac{60 \times 10^6}{\pi V_{L(p-p)}}$$

The unloaded power bandwidth for each voltage range is listed in Table 2.

Voltage Range	Power Bandwidth
200 V	95 kHz
150 V	127 kHz
100 V	190 kHz

Table 2. Unloaded power bandwidth

With a capacitive load, the power bandwidth is limited by the output current. The maximum frequency sine wave is

$$f_{pwr} = \frac{I_{av}}{V_{L(p-p)}C_L}$$

where I_{av} is the average current limit, $V_{L(p-p)}$ is the peak-to-peak output voltage, and C_L is the effective load capacitance. The power bandwidth for a range of load capacitance values is listed in Table 3.

Load (uF)	Voltage Range		
	100 V	150 V	200 V
0.01	190000	100000	50000
0.03	83333	33333	16667
0.1	25000	10000	5000
0.3	8333	3333	1667
1	2500	1000	500
3	833	333	167
10	250.0	100.0	50.0
30	83.3	33.3	16.7

Table 3. Power bandwidth (in Hz) with a capacitive load

In the following figures, the maximum peak-to-peak voltage is plotted against frequency for each voltage range.

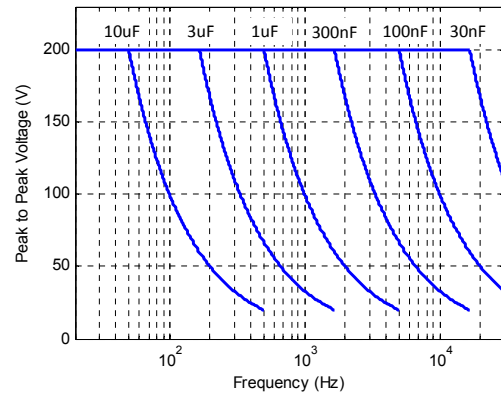


Figure 3. Power Bandwidth (200V Range)

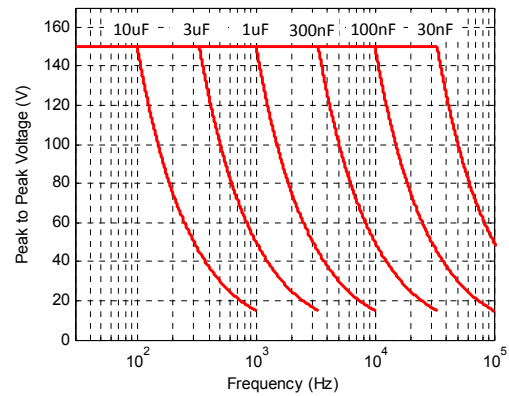


Figure 4. Power Bandwidth (150V Range)

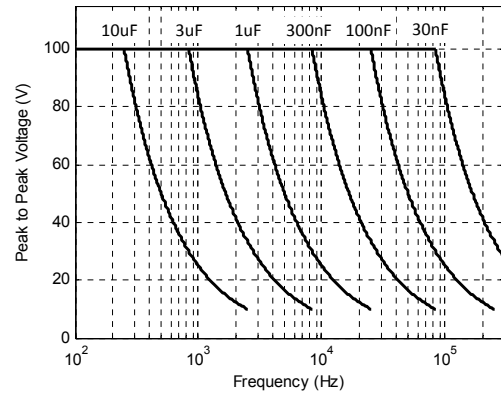


Figure 5. Power Bandwidth (100V Range)

Signal Bandwidth

The small-signal bandwidth for a range of capacitive loads is listed in Table 4. The small-signal frequency responses are plotted in Figure 6.

Load Capacitance	Signal Bandwidth
10 nF	180 kHz
30 nF	283 kHz
100 nF	275 kHz
300 nF	160 kHz
1 uF	78 kHz
3 uF	30 kHz
10 uF	8.3 kHz
30 uF	3.0 kHz

Table 4. Small signal bandwidth (-3 dB)

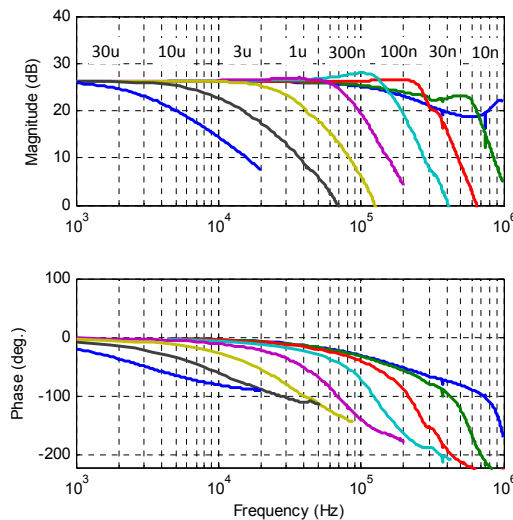


Figure 6. Small signal frequency response

Noise

The output noise contains a low frequency component (0.03 Hz to 10 Hz) that is independent of the load capacitance; and a high frequency component (10 Hz to 1 MHz) that is inversely related to the load capacitance.

Note that many manufacturers quote only the AC noise measured by a multimeter (20 Hz to 100 kHz) which is usually a gross underestimate.

The noise is measured with an SR560 low-noise amplifier (Gain = 1000), oscilloscope, and Agilent 34461A Voltmeter. The low-frequency noise is plotted

in Figure 7. The RMS value is 360 μ V with a peak-to-peak voltage of 1.8 mV.

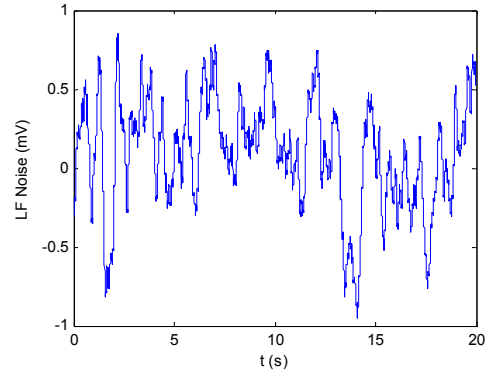


Figure 7. Low frequency output noise (0.03 Hz to 10 Hz)

The high frequency noise (10 Hz to 1 MHz) is listed in the table below versus load capacitance. The total noise from 0.03 Hz to 1 MHz is found by summing the RMS values, that is $\sigma = \sqrt{\sigma_{LF}^2 + \sigma_{HF}^2}$.

Load Capacitance	HF Noise	Total Noise
10 nF	1.5 mV	1.5 mV
30 nF	2.6 mV	2.6 mV
100 nF	3.5 mV	3.5 mV
300 nF	1.2 mV	1.3 mV
1 uF	306 μ V	470 μ V
3 uF	129 μ V	380 μ V
10 uF	100 μ V	370 μ V
30 uF	120 μ V	380 μ V

Table 5. HF Noise (10 Hz to 1 MHz) and total noise

The majority of high-frequency noise is due to ripple from the boost converter (at 170 kHz). In ultra-low noise applications, the output bandwidth can be restricted to 10 kHz which reduces the noise to less than 100 μ V RMS in the 10 Hz to 1 MHz frequency range. This can be achieved with the RLC filter shown below.

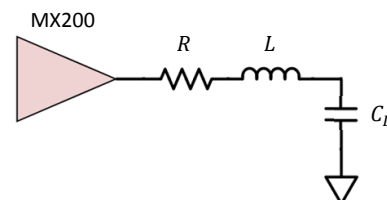


Figure 8. Output noise filter

The required inductance and resistance is

$$L = \frac{1}{4\pi^2 f_c^2 C_L} \quad \text{and} \quad R = 1.4\sqrt{L/C_L}$$

where f_c is the cut-off frequency (10 kHz) and C_L is the load capacitance. The inductor should be rated for at least 1 A with a self-resonance frequency of greater than 1 MHz.

A first-order resistive filter can also be effective, although it must be rated for the expected RMS current. The required value is

$$R = \frac{1}{2\pi f_c C_L}$$

Overload Protection / Shutdown

The MX200 is protected against short-circuit and average current overload. The module is also disabled when the input supply voltage is less than 12 V. Current overload conditions are signalled by +5 V on the Overload pin.

The amplifier can be shutdown manually by pulling the Enable pin low with an open-collector, or open-drain circuit. The Enable pin normally floats at 6.2V and should not be driven directly.

Bridge Configuration

The output voltage range can be doubled to ± 200 V by driving the load in a bridged configuration as shown in Figure 9. In this configuration, the output voltage is

$$V_{out} = 40(V_{in} - 5)$$

That is, a 0V to 10V input produces ± 200 V at the load. Zero volts across the load occurs when the input voltage is +5V. However, note that the absolute voltage of each terminal is still +100V.

The power bandwidth for this configuration can be calculated by considering only one amplifier and doubling the effective capacitance.

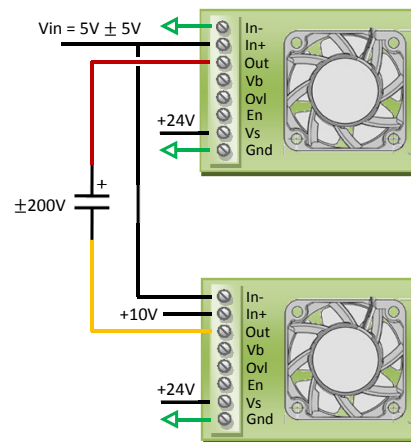


Figure 9. Bridge configuration achieving ± 200 V

Safety

This device produces hazardous potentials and should be used by suitably qualified personnel. Do not operate the device when there are exposed conductors.



Parts of the circuit may store charge so precautions must also be taken when the device is not powered.

Dimensions

The mounting posts accept M3 screws. For the PCB mounting version (MX200-PCB), a schematic and footprint library is available for Altium Designer, contact info@piezodrive.com to receive the file.

Contact / Support

info@piezodrive.com

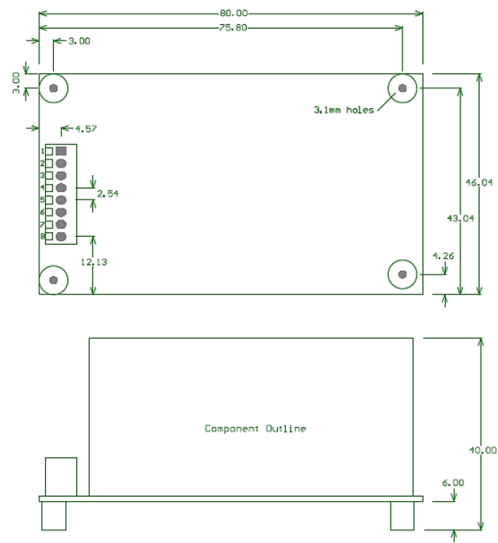


Figure 10. Dimensions (mm)

Appendix H

Glass Fibre Data Sheet



6 WOODS CLOSE
HUNTINGWOOD NSW
AUSTRALIA 2148



TEL: +(61 2) 9672 7888
FAX: +(61 2) 9672 7666
WEB: www.colan.com.au

PRODUCT INFORMATION

ENGINEERED TEXTILES WOVEN IN AUSTRALIA BY
COLAN PRODUCTS, AN AUSTRALIAN COMPANY

MX4500

E-glass composite reinforcement

Typical Properties

TOTAL WEIGHT :	457 g/m ² (nominal) (including polyester stitching yarn 8 g/m ²)	
FABRIC TYPE:	Double Bias ±45°	
YARN TYPE:	E-glass	
CONSTRUCTION:	<u>Angle°</u>	<u>g/m²</u>
	90°	7
	+45°	221
	-45°	221
WIDTH:	1270 mm (nominal)	
THICKNESS:	0.5 mm (nominal)	
ROLL SIZE:	82m/47.6kg (nominal)	
MOISTURE CONTENT:	0.2% (maximum)	
LOSS ON IGNITION:	4.5% (maximum)	
COMPATIBILITY:	suitable for use with polyester, vinyl ester and epoxy laminating resins	

E-glass typical properties

TENSILE STRENGTH:	3400 MPa
TENSILE MODULUS:	80-81 GPa
ELONGATION AT BREAK:	4.6%
DENSITY:	2.54 g/cm ³
COEFFICIENT OF THERMAL EXPANSION:	+5.0 X 10 ⁻⁶ m/mK

Options

Other weights, constructions, coloured tracers, edge taper and roll lengths. Limited stock or minimum quantities required

Features & Benefits

* High quality laminates with minimum resin content are able to be manufactured

* Det Norske Veritas certified

Issue Date 29/05/07

All information contained in this publication is based upon tests carried out by Colan Products, independent testing authorities or other suppliers. This information is believed to be correct and reliable at time of printing. Colan requires that users establish the suitability of all products for their applications and assume all risks.

Appendix I

Carbon Fibre Data Sheet

CERTIFICATE OF CONFORMITY

FORMAX
MULTIAXIAL REINFORCEMENTS

FORMAX STYLE: [C24k, 400, -45/+45]

FORMAX CODE: FCIM296-V8

REINFORCING FIBRE SPECIFICATION

FIBRE TYPE: Carbon
AREAL WEIGHT: 410 gsm +/- 5%
SIZE COMPATABILITY: Multi-Compatible
WIDTH: 1270 +/- 5mm

PLY CONSTRUCTIONS

-45° Ply

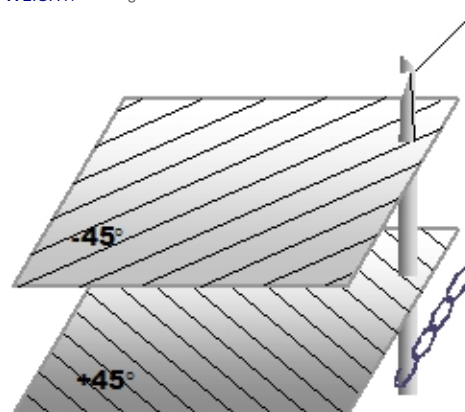
FIBRE SPECIFICATION: A-42 24K
FIBRE TEX: 1600
GAUGE: 2.23 gg
PLY WEIGHT: 199 gsm

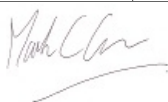
+45° Ply

FIBRE SPECIFICATION: A-42 24K
FIBRE TEX: 1600
GAUGE: 2.23 gg
PLY WEIGHT: 199 gsm

STITCHING FIBRE SPECIFICATION

STITCHING THREAD: 78 DTEX Texturised Polyester
STITCH GAUGE: 6 gg
STITCH LENGTH: 2.2 mm
STITCH TYPE: Pillar
STITCH WEIGHT: 9 gsm



DATE:	25/08/2015	FIBRE TEST CERTIFICATE REF:	DN 35967 FTC
FORMAX DELIVERY REF:	DN 35967	APPROVAL:	M. Greaves
QUANTITY:	307.80 KG	POSITION:	QHSE DIRECTOR
CUSTOMER PRODUCT CODE:	6251A	SIGNED / DATED:  25/08/2015	
CUSTOMER DESCRIPTION:	[C24k, 400, -45/+45]		
CUSTOMER ORDER NUMBER:	P109102		



Certificate No:
EMS 600776



Certificate No:
FM 594167

FORMAX
Cutters Close
Narborough
Leicester, UK
LE19 2FZ

T +44 116 275 2200
F +44 116 284 1912
E info@formax.co.uk
W www.formax.co.uk

A LEADING GLOBAL MANUFACTURER OF CARBON FIBRE AND SPECIALITY COMPOSITE REINFORCEMENTS.

CERTIFICATE OF CONFORMITY

FORMAX
MULTIAXIAL REINFORCEMENTS

FORMAX STYLE: [C24k, 400, -45/+45]

FORMAX CODE: FCIM296-V11

REINFORCING FIBRE SPECIFICATION

FIBRE TYPE: Carbon
AREAL WEIGHT: 410 gsm +/- 5%
SIZE COMPATABILITY:
WIDTH: 1270 +/- 5mm

PLY CONSTRUCTIONS

-45° Ply

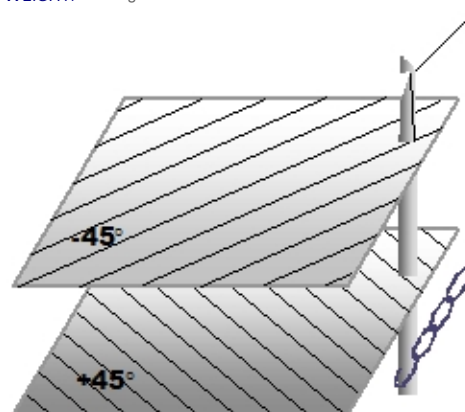
FIBRE SPECIFICATION: Tairafil TC 35R 24K
FIBRE TEX: 1600
GAUGE: 2.23 gg
PLY WEIGHT: 199 gsm

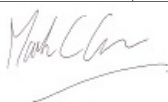
+45° Ply

FIBRE SPECIFICATION: Tairafil TC 35R 24K
FIBRE TEX: 1600
GAUGE: 2.23 gg
PLY WEIGHT: 199 gsm

STITCHING FIBRE SPECIFICATION

STITCHING THREAD: 78 DTEX Texturised Polyester
STITCH GAUGE: 6 gg
STITCH LENGTH: 2.2 mm
STITCH TYPE: Pillar
STITCH WEIGHT: 9 gsm



DATE:	25/08/2015	FIBRE TEST CERTIFICATE REF:	DN 35967 FTC
FORMAX DELIVERY REF:	DN 35967	APPROVAL:	M. Greaves
QUANTITY:	523.60 KG	POSITION:	QHSE DIRECTOR
CUSTOMER PRODUCT CODE:	6251A	SIGNED / DATED:  25/08/2015	
CUSTOMER DESCRIPTION:	[C24k, 400, -45/+45]		
CUSTOMER ORDER NUMBER:	P109102		



Certificate No:
EMS 600776



Certificate No:
FM 594167

FORMAX
Cutters Close
Narborough
Leicester, UK
LE19 2FZ

T +44 116 275 2200
F +44 116 284 1912
E info@formax.co.uk
W www.formax.co.uk

A LEADING GLOBAL MANUFACTURER OF CARBON FIBRE AND SPECIALITY COMPOSITE REINFORCEMENTS.

Appendix J

Epoxy Resin Data Sheet



Ampreg 22

EPOXY LAMINATING SYSTEM

- Optimised for open-mould laminating of large structures
- Germanischer Lloyd approved*

INTRODUCTION

Ampreg 22 is an established and widely used laminating system. It is intended for both wet lay-up and vacuum bagging processes and uses the most up-to-date epoxy chemistry available. Its long working time, low exotherm and low viscosity make it ideal for the manufacture of large, high performance composite structures.

The Ampreg 22 system consists of a resin and a choice of five hardeners to provide a complete range of working properties. With its extra slow hardener Ampreg 22 can provide laminate working times of over 5 hours at 20°C whilst having low exothermic reactions even when used in thick sections. The Fast hardener has such rapid through-cure at 25-30°C that it can be used to produce small mouldings that are demouldable in just a few hours.

The low initial viscosity allows laminates to be produced by contact pressure, vacuum or pressure bag techniques, filament winding, or vacuum assisted resin injection. Thorough wetting of reinforcement fibres is ensured by the low viscosity and excellent air release properties of the resin / hardener mixture. This, in particular, assists with the impregnation of aramid and carbon fibres.

Ampreg 22 resin is coloured bright yellow, with the hardeners having a range of different colours. This makes component identification easier and facilitates thorough mixing of resin and hardener. For example, the Extra Slow Hardener is coloured blue leading to a clearly identifiable green colour when thoroughly mixed with the resin.

Ampreg 22 resin has one of the lowest diluent contents of any epoxy resin system available today. Together with the use of some unique chemistry in the hardeners, the overall system shows marked improvements in handling safety over other products. The system is formulated without DDM, which is particularly important for those using the product in open-mould, hand lay-up situations, where skin contact and exposure to vapours can be difficult to avoid completely.

*High Tg Hardener excluded

INSTRUCTIONS FOR USE

WORKSHOP CONDITIONS

Ampreg 22 is optimised for use between 18 - 25°C. At lower temperatures the product thickens and may become unworkable. At higher temperatures working times will be significantly reduced. Maximum relative humidity for use is 70%.

MIXING AND HANDLING

Ampreg 22 resin is combined with either Ampreg 22 Fast, Standard, Slow and Extra-Slow hardener in the following ratio:

Ampreg 22 resin : Ampreg 22 hardener	
100 : 28 (by weight)	All hardeners
100 : 32 (by volume)	Fast
100 : 33 (by volume)	Standard or Slow
100 : 34 (by volume)	Extra Slow
100 : 29 (by volume)	High Tg

It is important that the resin and hardener components are measured out accurately. Measurement by weight and electronic scales are recommended for this purpose. The resin / hardener mixture should be well mixed, paying particular attention to the sides and bottom of the mixing vessel. The mixture should then be transferred to a shallow tray in order to reduce the exothermic heat build up, which would reduce pot life and working time. Accurate measurement of the components and thorough mixing are essential. Deviating from the prescribed mix ratio will not accelerate or inhibit the cure and can seriously degrade the properties of the system.

Ampreg 22 resin and hardeners are pigmented as a visual aid for the user - see component properties table. The colours are primarily a quick and easy guide to help distinguish the resin and different hardener speeds in the workshop. In addition, when mixing the chosen hardener with the resin, its colour blends with the yellow colour of the resin to help indicate that the two components have been mixed.

Ampreg 22 resin and hardeners will lose their colour tint strength with time. This is a natural function of the pigments used and does not affect the product performance. In the case of Ampreg 22 Slow Hardener and Ampreg 22 Resin, the pigment can settle to the bottom of the container with time - if this should happen they may be returned to their original uniform colour by stirring before use.

MOULD RELEASE

From smooth metal or grp moulds tests have shown that suitable release can be obtained by use of 5-6 waxings of a carnauba based wax e.g. Polywax. Use PVA for less well prepared or complex surfaces. Whichever mould release is proposed it is recommended that a test laminate is laid up in the mould to be used, with the mould release proposed, in order to ensure an adequate and effective part release. Semi permanent agents such as Frecote or Chemlease are also suitable.

APPLICATION

The mixed system is usually applied by foam roller from a roller tray (which also serves to increase exothermic heat release, as described above). High and accurate fibre volume fractions can be obtained by applying known weight of mixed resin / hardener to each fabric / fibre layer. As a general rule of thumb, resin weight per square metre must be no more than, and preferably less than, the area weight of the fabric being wet out. If the laminate is particularly thick, it is recommended that slower hardeners are used for the first layers put down and faster hardeners in the later layers. In this way the whole thickness laid down remains workable for approximately the same time.

PREGEL

Ampreg Pregel is a thixotropic resin which, when used with the appropriate hardener, can be added to, or used in place of, Ampreg 22 resin/hardener mixes. Mix Ampreg Pregel resin with any of the Ampreg 22 Hardeners at the ratio indicated in the Ampreg Pregel datasheet. Mixed Ampreg Pregel / Ampreg 22 Hardener can be added to an Ampreg 22 resin/hardener mix to make it more thixotropic. A separate data sheet is available describing this product's use in more detail.

- As a resin modifier to reduce drainage in laminates.
- As an adhesive mix for bonding core materials to Ampreg 22 laminate skins.
- For the secondary bonding of pre-formed Ampreg 22 laminate components.

BONDING TECHNIQUES & PEEL PLY

Where it is necessary for a bonding operation to be carried out following the cure of the Ampreg 22 laminate, a suitable Peel Ply can be applied to the surface to be bonded during the lay-up process. After curing and just prior to bonding, the Peel Ply is stripped off leaving a clean, dust and grease free surface, with an already 'textured' surface which makes the 'keying' process less time consuming.

Peel Ply is used on laminate surfaces which need to be left to cure or partially cure before further laminating or bonding operations. The peel ply serves two functions - preventing the surface from becoming contaminated and / or damaged, and providing a 'textured' surface that can reduce the level of preparation required for the secondary laminating or bonding operations.

Gurit recommends the use of its Stitch Ply A peel ply, or suitable alternative product. Any proposed peel ply should be tested prior to use to ensure that it not only releases adequately from the laminated surface but also does not leave any residues behind which may impair adhesion. If in doubt please contact Technical Services.

VACUUM BAG TECHNIQUES

Consolidation of the laminate can be obtained either by hand using paddle rollers or by vacuum or pressure bags. A typical vacuum bag arrangement is shown in figure 1. It is important when using high vacuums and using the slower hardeners that vacuum is not applied until at least 50% into the laminate working time, as excessive flow and resin starved laminates may result (see working properties). Heating can be economically and effectively achieved with either space heaters under an insulation tent or heated blankets with insulation over. If vacuum is applied earlier only 30-50% vacuum should be used. Details of the various types of system are available from Technical Services.

Ampreg 22 resin with either Slow or Extra Slow hardener is best suited. Do not expose wet laminates to excessive vacuum pressures - keep below 0.8 bar (80% vacuum). Gurit supplies a range of Tygavac vacuum bag materials and ancillaries. For details of effective vacuum bag consolidation, please contact Technical Services.

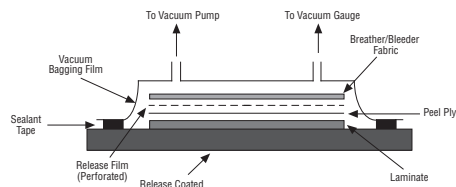


Figure 1

CORE MATERIALS

Gurit supplies Corecell™ SAN closed cell foam for sandwich laminate construction. Other core materials such as PVC foam, Nomex honeycomb and end grain balsa, are also suitable for use with Ampreg 22 system. For further information on the use of core materials with Ampreg 22 system, please contact Technical Services.

CURING SCHEDULE

AMBIENT TEMPERATURE CURE

The system has been developed to return good mechanical properties after cure at ambient temperatures, the minimum recommended temperature being 18°C, and excellent properties after a slightly elevated temperature post-cure. An initial cure of at least 48 hours (with slow and extra slow hardener) or 16 hours (with fast or standard hardener) at 18°C is recommended before demoulding. Laminates moulded with Fast, Standard or Slow hardener and subjected to an ambient temperature cure should be allowed 14 days before the system can be considered to be adequately cured (see working properties). Such mouldings should be kept in a warm dry environment during this period. When using the Slow, Extra Slow and High Tg Hardeners exclusively, an elevated temperature cure is strongly recommended. Ideally the postcure should be undertaken prior to demoulding.

ELEVATED TEMPERATURE CURE

Post curing the laminate will greatly increase mechanical properties. The system will achieve similar properties with a cure of 5 hours at 70-80°C or 16 hours at 50°C. The latter temperature is easily achievable with low cost heating and insulation techniques. The tables in the datasheet show that these cure cycles improve the properties considerably.

The post cure need not be carried out immediately after laminating. It is possible to assemble several composite components and post-cure the entire assembly together. It is recommended, however, that elevated temperature curing should be completed before any further painting / finishing operations. Furthermore, care should be taken to adequately support the laminate if it is to be post cured after demoulding, and the laminate must be allowed to cool before the support is removed.

PROPERTIES

Component Properties						
	Resin	Hardener				
		Fast	Std.	Slow	Extra Slow	High Tg
Mix Ratio (by weight)	100	28	28	28	28	28
Mix Ratio (by volume)	100	32	33	33	34	29
Viscosity @ 15°C (cP)	9270	420	67	43	34	110
Viscosity @ 20°C (cP)	3915	270	40	36	22	80
Viscosity @ 25°C (cP)	2396	164	24	28	14	60
Viscosity @ 30°C (cP)	1312	105	15	21	9	40
Shelf Life (months)	24	24	24	24	24	24
Colour	yellow	(6)*	red	green	blue	*6
Mixed Colour	-	yellow	pink	green	green	yellow
Component Dens. (g/cm ³)	1.147	0.958	0.950	0.947	0.940	0.96
Mixed Density (g/cm ³)	-	1.108	1.101	1.099	1.097	1.10
Hazard Definition	Please refer to SDS information.					

*Hardener is not pigmented - Hardener colour stated.

Working Properties																	
	Resin/ Fast Hardener				Resin/ Standard Hardener				Resin/ Slow Hardener				Resin/ Extra Slow Hardener				Resin/ High Tg Hardener
	15°C	20°C	25°C	30°C	15°C	20°C	25°C	30°C	15°C	20°C	25°C	30°C	15°C	20°C	25°C	30°C	20°C
Initial Mixed Viscosity (cP)	4132	1995	1265	881	2848	1529	805	431	1610	950	579	361	1402	722	461	294	1110
†Gel Time - 150g Mix in water (hrs:mins)	0:31	0:26	0:22	0:18	2:18	1:31	1:00	0:40	9:10	5:44	3:35	2:12	14:00	9:10	7:00	4:50	5:40
†Pot Life - 500g Mix in air (hrs:mins)	-	0:25	-	0:15	-	0:26	-	0:20	-	2:12	-	1:10	-	5:35	-	2:00	2:20
†Earliest Time To Apply Vacuum (hrs:mins)	1:30	1:10	1:00	0:50	2:00	1:50	1:30	1:20	5:30	4:40	4:00	3:20	8:40	7:00	5:50	4:45	4:40
†Latest Time To Apply Vacuum (hrs:mins)	3:10	2:15	1:40	1:10	3:20	2:45	2:20	2:00	7:45	6:40	5:30	4:20	11:30	9:10	7:20	5:50	6:40
†Earliest Time To Turn Off Vacuum (hrs:mins)	5:00	3:30	2:30	1:40	5:00	4:00	3:15	2:40	18:30	15:30	12:30	9:30	48:00	30:00	18:00	11:20	15:30
†Demould Time (hrs:mins)	6:00	4:00	3:00	2:00	8:20	5:20	4:00	3:00	36:00	30:00	25:00	19:00	100:00	62:00	37:00	22:00	30:00

NOTES: For an explanation of test methods used see 'Formulated Products Technical Characteristics'. Please refer to the "Intro to Form Prds".pdf, which can be found in the Formulated product section on the website. www.gurit.com

All figures quoted are indicative of the properties of the product concerned. Some batch to batch variation may occur.

†All times are measured from when resin and hardener are first mixed together

PROPERTIES (CONT'D)

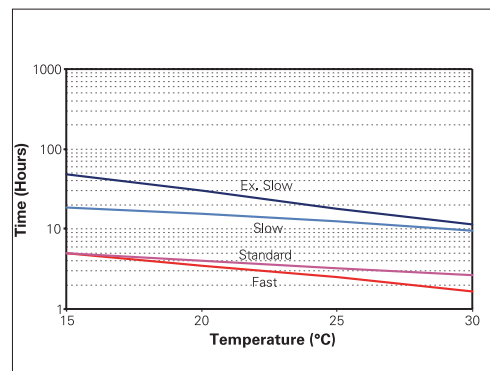
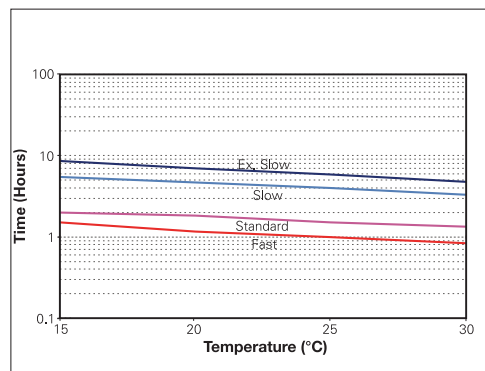
Cured System Properties									
	Room Temperature Cure (28 days @ 21°C)				Post Cured (24 hours @ 21°C +16 hours @ 50°C)				
	Fast	Std.	Slow	Extra Slow*	Fast	Std.	Slow	Extra Slow	High Tg
Tg DMTA (Peak Tan δ)(°C)	71.5	70.9	71.1	60.8	91.6	78.8	83.6	82.2	-
Tg Ult - DMTA (°C)	102.7	106.4	108.7	110.3	102.7	106.4	108.7	110.3	115
ΔH - DSC (J/g)	50	44	65	59	13	0	15	27	0
Tg1 - DMTA (°C)	61.5	58.3	63.2	50.4	79.7	73.6	73.6	72.7	77
Est. HDT (°C)	57	56	56	46	77	64	69	67	73
Moisture Absorption (%)	2.31	2.25	1.41	1.46	1.92	-	0.62	1.22	1.1
Cured Density (g/cm ³)	1.16	1.13	1.14	1.14	1.16	1.14	1.14	1.14	1.14
Linear Shrinkage (%)	1.7	1.4	1.6	1.7	1.7	1.5	1.5	1.6	1.2
Barcol Hardness	21	22	18	27	25	23	18	20	20
Cast Tensile Strength (MPa)	70.3	50.7	54.6	- *	878	72.2	75.0	73.3	74
Cast Tensile Mod. (GPa)	3.78	3.65	3.89	- *	3.64	3.74	3.51	3.36	3.4
Cast Strain to Failure (%)	3.0	2.3	3.4	- *	4.50	4.04	4.00	4.50	4.5
Lam. Comp. Strength (MPa)	503	410	429	515	437	462	441	516	430
Laminate T.V.M. Strain (%)	2.2	-	2.0	1.9	2.15	-	2.00	2.50	-
Laminate ILSS (MPa)	52	52	50	45	48.0	53.3	54.0	46.0	57
ILSS Wet Retention (%)	79	81	90	92	87	84	82	98	-

*Ambient temperature cure alone is not recommended with this hardener.

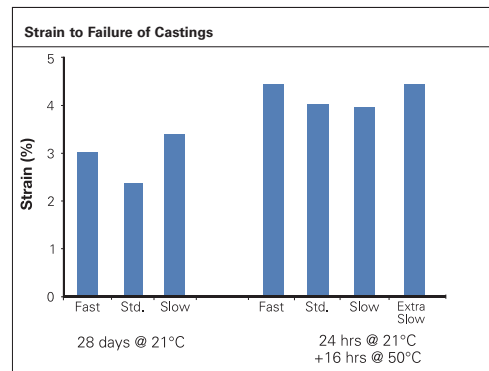
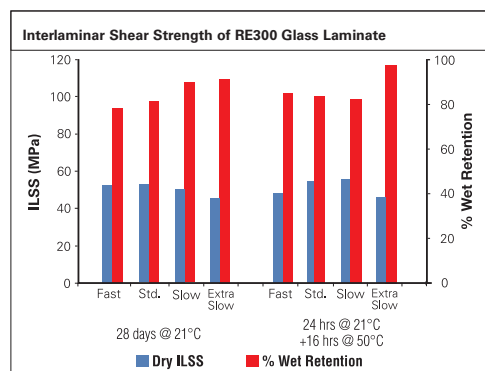
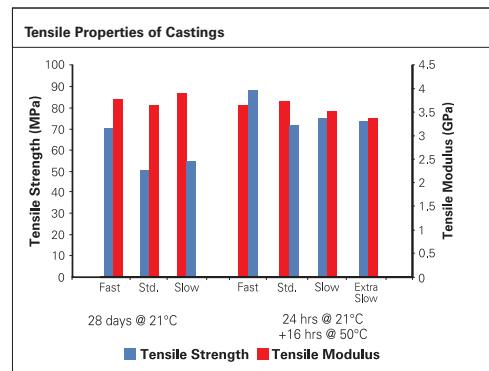
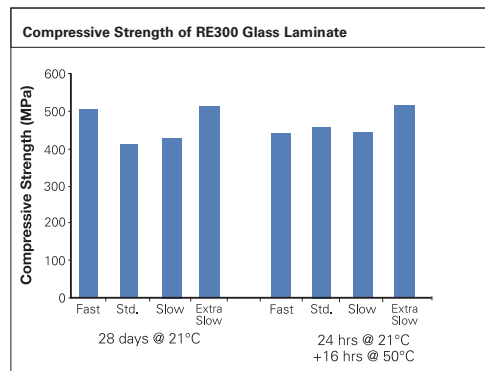
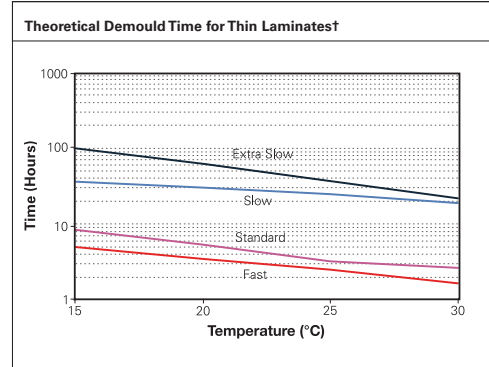
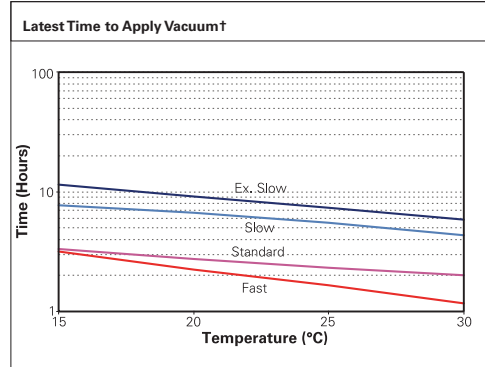
Notes: For an explanation of test methods used see "Formulated Products Technical Characteristics". Please refer to the "Intro to Form Prods".pdf, which can be found in the Formulated product section on the website. www.gurit.com

All figures quoted are indicative of the properties of the product concerned. Some batch to batch variation may occur.

† All times are measured from when resin and hardener are first mixed together.



PROPERTIES (CONT'D)



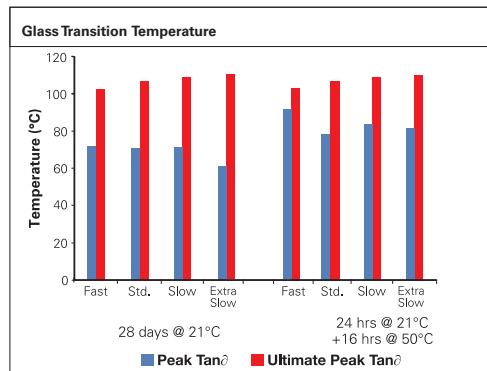
**Data generated from 16 hours @ 55°C Postcure

NOTES: For an explanation of test methods used see 'Formulated Products Technical Characteristics'.

All figures quoted are indicative of the properties of the product concerned. Some batch to batch variation may occur.

†All times are measured from when resin and hardener are first mixed together

PROPERTIES (CONT'D)



**Data generated from 16 hours @ 55°C Postcure

NOTES: For an explanation of test methods used see 'Formulated Products Technical Characteristics'.

All figures quoted are indicative of the properties of the product concerned. Some batch to batch variation may occur.

†All times are measured from when resin and hardener are first mixed together

HEALTH AND SAFETY

The following points must be considered:

1. Skin contact must be avoided by wearing protective gloves. Gurit recommends the use of disposable nitrile gloves for most applications. The use of barrier creams is not recommended, but to preserve skin condition a moisturising cream should be used after washing.
2. Overalls or other protective clothing should be worn when mixing, laminating or sanding. Contaminated work clothes should be thoroughly cleaned before re-use.
3. Eye protection should be worn if there is a risk of resin, hardener, solvent or dust entering the eyes. If this occurs flush the eye with water for 15 minutes, holding the eyelid open, and seek medical attention.
4. Ensure adequate ventilation in work areas. Respiratory protection should be worn if there is insufficient ventilation. Solvent vapours should not be inhaled as they can cause dizziness, headaches, loss of consciousness and can have long term health effects.
5. If the skin becomes contaminated, then the area must be immediately cleansed. The use of resin-removing cleansers is recommended. To finish, wash with soap and warm water. The use of solvents on the skin to remove resins etc must be avoided.

Washing should be part of routine practice:

- before eating or drinking
- before smoking
- before using the lavatory
- after finishing work

6. The inhalation of sanding dust should be avoided and if it settles on the skin then it should be washed off. After more extensive sanding operations a shower/bath and hair wash is advised.

Gurit produces a separate full Safety Data Sheet (SDS) for all hazardous products. Please ensure that you have the correct SDS to hand for the materials you are using before commencing work. A more detailed guide for the safe use of Gurit resin systems is also available from Gurit, and can be found at www.gurit.com

APPLICABLE RISK & SAFETY PHRASES

Please refer to product SDS for up to date information specific to this product.



TRANSPORT & STORAGE

The resin and hardeners should be kept in securely closed containers during transport and storage. Any accidental spillage should be soaked up with sand, sawdust, cotton waste or any other absorbent material. The area should then be washed clean (see appropriate Safety Data Sheet).

Adequate long term storage conditions will result in a shelf life of two years for both the resin and hardeners. Storage should be in a warm dry place out of direct sunlight and protected from frost. The storage temperature should be kept constant between 10°C and 25°C, cyclic fluctuations in temperature can cause crystallization. Containers should be firmly closed. Hardeners, in particular, will suffer serious degradation if left exposed to air.

For more information on crystallization please refer to the Laminating section on the Gurit website. (www.gurit.com)

NOTICE

All advice, instruction or recommendation is given in good faith but Gurit AG (the company) only warrants that advice in writing is given with reasonable skill and care. No further duty or responsibility is accepted by the Company. All advice is given subject to the terms and conditions of sale (the Conditions) which are available on request from the Company or may be viewed at the Company's Website: <http://www.gurit.com/terms-and-conditions.aspx>

The Company strongly recommends that Customers make test panels and conduct appropriate testing of any goods or materials supplied by the Company to ensure that they are suitable for the Customer's planned application. Such testing should include testing under conditions as close as possible to those to which the final component may be subjected. The Company specifically excludes any warranty of fitness for purpose of the goods other than as set out in writing by the Company. The Company reserves the right to change specifications and prices without notice and Customers should satisfy themselves that information relied on by the Customer is that which is currently published by the Company on its website. Any queries may be addressed to the Technical Services Department.

Gurit are continuously reviewing and updating literature. Please ensure that you have the current version, by contacting Gurit Marketing Communications or your sales contact and quoting the revision number in the bottom right-hand corner of this page.

E gurit@gurit.com
W www.gurit.com

Appendix K

Arduino M0 Pro Function Generator Code

```
/*
*****
Title: Arduino M0 Pro Function Generator Code
Student: Michael Gall
Student ID: 0061009722
Frequency: 100 KHz
Cycle Rate: 50%
Based off code written by MartinL
Found at: http://forum.arduino.cc/index.php?topic=346731.0
*****
*/

void setup()
{
  pinMode(7, OUTPUT); // Makes Pin 7 an Output
  Pin // Makes Pin 7 Active
  digitalWrite(7, HIGH);

  REG_GCLK_GENDIV = GCLK_GENDIV_DIV(1) | // Divide the 48MHz clock
    source by divisor 1: 48MHz/1=48MHz
    GCLK_GENDIV_ID(4); // Select Generic Clock (
  GCLK) 4
  while (GCLK->STATUS.bit.SYNCBUSY); // Wait for
    synchronization

  REG_GCLK_GENCTRL = GCLK_GENCTRL_IDC | // Set the duty cycle to
    50/50 HIGH/LOW
    GCLK_GENCTRL_GENEN | // Enable GCLK4
    GCLK_GENCTRL_SRC_DFL48M | // Set the 48MHz clock
    source
    GCLK_GENCTRL_ID(4); // Select GCLK4
}
```

```
void loop() {
```

```
}
```

Listing K.1: M0 Pro Function Generator Code.

Appendix L

Arduino Zero Function Generator Code

```
/******  
  Title : Arduino Zero Function Generator Code  
  Student : Michael Gall  
  Student ID: 0061009722  
  Frequency : 100 KHz  
  Cycle Rate : 50%  
*****/  
  
void setup() {  
  tone(13,100000);    // Produces 100 KHz Tone on Pin 13  
  delayMicroseconds(100); // Creates 100 Microsecond delay before next  
    function  
  noTone(7);          // Ends Tone on Pin 13  
}  
  
void loop() {  
  
}
```

Listing L.1: Arduino Zero Function Generator Code.

Appendix M

Temperature Calibration Code

```
/******  
  Title: Arduino Temperature Calibration Code  
  Student : Michael Gall  
  Student ID: 0061009722  
  Code to test the difference in Temperature  
  readings between the thermocouple and the InfraRed Sensor  
*****/  
  
#include <Arduino.h>  
#include <SD.h>  
#include <Wire.h>  
#include "RTClib.h"  
#include "IRTemp.h"  
#include "Adafruit_MAX31855.h"  
#include "Adafruit_SHT31.h"  
  
// how many milliseconds between grabbing data and logging it.  
#define LOG_INTERVAL 5000 // mills between entries  
  
// how many milliseconds before writing the logged data permanently to disk  
#define SYNC_INTERVAL 5000 // mills between calls to flush() - to write  
  data to the card  
uint32_t syncTime = 0; // time of last sync()  
  
#define ECHO_TO_SERIAL 1 // echo data to serial port  
#define WAIT_TO_START 0 // Wait for serial input in setup()  
  
// Example creating a thermocouple instance with software SPI on any three  
// digital IO pins.  
#define thermoDO_1 2  
#define thermoCLK_1 3  
#define thermoCS_1 4
```

```

// initialize the Thermocouple
Adafruit_MAX31855 thermocouple_1(thermoCLK_1, thermoCS_1, thermoDO_1);

static const byte PIN_DATA    = 14; // Choose any pins you like for these
static const byte PIN_CLOCK   = 15;
static const byte PIN_ACQUIRE = 16;

static const TempUnit SCALE=CELSIUS; // Options are CELSIUS, FAHRENHEIT

IRTemp irTemp(PIN_ACQUIRE, PIN_CLOCK, PIN_DATA);

RTC_DS1307 RTCDL; // define the Real Time Clock object

Adafruit_SHT31 sht31 = Adafruit_SHT31();

// for the data logging shield, we use digital pin 10 for the SD cs line
const int chipSelect = 10;

// the logging file
File logfile;

void error(char *str)
{
    Serial.print("error: ");
    Serial.println(str);

    while(1);
}

void setup(void)
{
    Serial.begin(9600);
    Serial.println();

    #if WAIT_TO_START
        Serial.println("Type any character to start");
        while (!Serial.available());
    #endif //WAIT_TO_START

    // initialize the SD card
    Serial.print("Initializing SD card...");
    // make sure that the default chip select pin is set to
    // output, even if you don't use it:
    pinMode(10, OUTPUT);

    // see if the card is present and can be initialized:
    if (!SD.begin(10)) {
        error("Card failed, or not present");
    }
    Serial.println("card initialized.");

    // create a new file
    char filename[] = "LOGGER00.CSV";
    for (uint8_t i = 0; i < 100; i++) {

```

```

    filename[6] = i/10 + '0';
    filename[7] = i%10 + '0';
    if (! SD.exists(filename)) {
        // only open a new file if it doesn't exist
        logfile = SD.open(filename, FILE_WRITE);
        break; // leave the loop!
    }
}

if (! logfile) {
    error("couldnt create file");
}

Serial.print("Logging to: ");
Serial.println(filename);

// connect to RTC
Wire.begin();
if (!RTC.DL.begin()) {
    logfile.println("RTC failed");
#ifdef ECHO_TO_SERIAL
    Serial.println("RTC failed");
#endif //ECHO_TO_SERIAL
}

logfile.println(" millis ,stamp ,datetime ,Thermo,IRTemp,IRAmbient ,
    TempAmbient,Humidity");
#ifdef ECHO_TO_SERIAL
    Serial.println(" millis ,stamp ,datetime ,Thermo,IRTemp,IRAmbient ,TempAmbient
        ,Humidity");
#endif //ECHO_TO_SERIAL

    if (! sht31.begin(0x44)) { // Set to 0x45 for alternate i2c addr
        Serial.println("Couldn't find SHT31");
        while (1) delay(1);
    }
}

void loop(void)
{
    DateTime now;

    // delay for the amount of time between readings
    delay((LOG_INTERVAL -1) - (millis() % LOG_INTERVAL));

    // log milliseconds since starting
    uint32_t m = millis();
    logfile.print(m);           // milliseconds since start
    logfile.print(", ");
#ifdef ECHO_TO_SERIAL
    Serial.print(m);           // milliseconds since start
    Serial.print(", ");
#endif
    #endif

```

```

// fetch the time
now = RTCDL.now();
// log time
logfile.print(now.unixtime()); // seconds since 1/1/1970
logfile.print(", ");
logfile.print(' ');
logfile.print(now.year(), DEC);
logfile.print("/");
logfile.print(now.month(), DEC);
logfile.print("/");
logfile.print(now.day(), DEC);
logfile.print(" ");
logfile.print(now.hour(), DEC);
logfile.print(":");
logfile.print(now.minute(), DEC);
logfile.print(":");
logfile.print(now.second(), DEC);
logfile.print(' ');
#ifdef ECHO_TO_SERIAL
Serial.print(now.unixtime()); // seconds since 1/1/1970
Serial.print(", ");
Serial.print(' ');
Serial.print(now.year(), DEC);
Serial.print("/");
Serial.print(now.month(), DEC);
Serial.print("/");
Serial.print(now.day(), DEC);
Serial.print(" ");
Serial.print(now.hour(), DEC);
Serial.print(":");
Serial.print(now.minute(), DEC);
Serial.print(":");
Serial.print(now.second(), DEC);
Serial.print(' ');
#endif //ECHO_TO_SERIAL

// Activate InfraRed Sensor
float irTemperature = irTemp.getIRTemperature(SCALE);
float ambientTemperature = irTemp.getAmbientTemperature(SCALE);
delay(10);
// Activate Thermocouple
double c = thermocouple_1.readCelsius();
delay(10);
// Activate Air Temperature and Humidity Sensor
float t = sht31.readTemperature();
float h = sht31.readHumidity();

// Log readings to data logger
logfile.print(", ");
logfile.print(c);
logfile.print(", ");
logfile.print(irTemperature);
logfile.print(", ");
logfile.print(ambientTemperature);

```

```

    logfile.print(", ");
    logfile.print(t);
    logfile.print(", ");
    logfile.print(h);
    #if ECHO_TO_SERIAL
// Print readings in Serial Monitor
    Serial.print(", ");
    Serial.print(c);
    Serial.print(", ");
    Serial.print(irTemperature);
    Serial.print(", ");
    Serial.print(ambientTemperature);
    Serial.print(", ");
    Serial.print(t);
    Serial.print(", ");
    Serial.print(h);
#endif //ECHO_TO_SERIAL

    logfile.println();
    #if ECHO_TO_SERIAL
        Serial.println();
    #endif // ECHO_TO_SERIAL

    // Now we write data to disk!
    if ((millis() - syncTime) < SYNC_INTERVAL) return;
    syncTime = millis();

    logfile.flush();
}

```

Listing M.1: Arduino Temperature Calibration Code.

Appendix N

Temperature Readings Code

```
/******  
  Title : Arduino Temperatrue Sensing Code  
  Student : Michael Gall  
  Student ID: 0061009722  
  Code reads the temperature from three thermocouples and an air  
  temperature and humidity sensor.  
  Temperature readings are saved to a data logger  
*****/  
  
#include <Arduino.h>  
#include <SD.h>  
#include <Wire.h>  
#include "RTClib.h"  
#include "IRTemp.h"  
#include "Adafruit_MAX31855.h"  
#include "Adafruit_SHT31.h"  
  
// how many milliseconds between grabbing data and logging it. 1000 ms is  
// once a second  
#define LOG_INTERVAL 5000 // mills between entries (reduce to take more/  
// faster data)  
  
// how many milliseconds before writing the logged data permanently to disk  
#define SYNC_INTERVAL 5000 // mills between calls to flush() - to write  
// data to the card  
uint32_t syncTime = 0; // time of last sync()  
  
#define ECHO_TO_SERIAL 1 // echo data to serial port  
#define WAIT_TO_START 0 // Wait for serial input in setup()  
  
// Creating thermocouple instances with software SPI on  
// digital IO pins for each thermocouple.  
#define thermoDO_1 2
```

```

#define thermoCLK_1 3
#define thermoCS_1 4
#define thermoDO_2 5
#define thermoCLK_2 6
#define thermoCS_2 7
#define thermoDO_3 16
#define thermoCLK_3 15
#define thermoCS_3 14

// initialize the Thermocouple
Adafruit_MAX31855 thermocouple_1(thermoCLK_1, thermoCS_1, thermoDO_1);
Adafruit_MAX31855 thermocouple_2(thermoCLK_2, thermoCS_2, thermoDO_2);
Adafruit_MAX31855 thermocouple_3(thermoCLK_3, thermoCS_3, thermoDO_3);

RTC_DS1307 RTCDL; // define the Real Time Clock object

Adafruit_SHT31 sht31 = Adafruit_SHT31();

// Set pin for the data logging shield
const int chipSelect = 10;

// the logging file
File logfile;

void error(char *str)
{
    Serial.print("error: ");
    Serial.println(str);

    while(1);
}

void setup(void)
{
    Serial.begin(9600);
    Serial.println();

    #if WAIT_TO_START
        Serial.println("Type any character to start");
        while (!Serial.available());
    #endif //WAIT_TO_START

    // initialize the SD card
    Serial.print("Initializing SD card...");
    // Default chip select pin is set to output:
    pinMode(10, OUTPUT);

    // see if the card is present and can be initialized:
    if (!SD.begin(10)) {
        error("Card failed , or not present");
    }
    Serial.println("card initialized.");

    // create a new file

```

```

char filename[] = "LOGGER00.CSV";
for (uint8_t i = 0; i < 100; i++) {
    filename[6] = i/10 + '0';
    filename[7] = i%10 + '0';
    if (! SD.exists(filename)) {
        // only open a new file if it doesn't exist
        logfile = SD.open(filename, FILE_WRITE);
        break;
    }
}

if (! logfile) {
    error("couldnt create file");
}

Serial.print("Logging to: ");
Serial.println(filename);

// connect to RTC
Wire.begin();
if (!RTCSDL.begin()) {
    logfile.println("RTC failed");
}
#ifdef ECHO_TO_SERIAL
    Serial.println("RTC failed");
#endif //ECHO_TO_SERIAL
}

logfile.println(" millis ,stamp,datetime ,Thermo,TempAmbient,Humidity ,
    ThermoFlame,ThermoOuter");
#ifdef ECHO_TO_SERIAL
    Serial.println(" millis ,stamp,datetime ,Thermo,TempAmbient,Humidity ,
        ThermoFlame,ThermoOuter");
#endif //ECHO_TO_SERIAL

    if (! sht31.begin(0x44)) {
        Serial.println("Couldn't find SHT31");
        while (1) delay(1);
    }
}

void loop(void)
{
    DateTime now;

    // delay for the amount of time between readings
    delay((LOG_INTERVAL -1) - (millis() % LOG_INTERVAL));

    // log milliseconds since starting
    uint32_t m = millis();
    logfile.print(m);           // milliseconds since start
    logfile.print(", ");

    #ifdef ECHO_TO_SERIAL
        Serial.print(m);       // milliseconds since start
        Serial.print(", ");
    #endif

```

```

#endif

    // fetch the time
    now = RTCDL.now();
    // log time
    logfile.print(now.unixtime()); // seconds since 1/1/1970
    logfile.print(", ");
    logfile.print(' ');
    logfile.print(now.year(), DEC);
    logfile.print("/");
    logfile.print(now.month(), DEC);
    logfile.print("/");
    logfile.print(now.day(), DEC);
    logfile.print(" ");
    logfile.print(now.hour(), DEC);
    logfile.print(":");
    logfile.print(now.minute(), DEC);
    logfile.print(":");
    logfile.print(now.second(), DEC);
    logfile.print(' ');
#ifecho ECHO_TO_SERIAL
    Serial.print(now.unixtime()); // seconds since 1/1/1970
    Serial.print(", ");
    Serial.print(' ');
    Serial.print(now.year(), DEC);
    Serial.print("/");
    Serial.print(now.month(), DEC);
    Serial.print("/");
    Serial.print(now.day(), DEC);
    Serial.print(" ");
    Serial.print(now.hour(), DEC);
    Serial.print(":");
    Serial.print(now.minute(), DEC);
    Serial.print(":");
    Serial.print(now.second(), DEC);
    Serial.print(' ');
#endif //ECHO_TO_SERIAL

    // Activate thermocouple readings
    double c = thermocouple_1.readCelsius();
    delay(10);
    double d = thermocouple_2.readCelsius();
    delay(10);
    double e = thermocouple_3.readCelsius();
    delay(10);
    // Activate air temperature and humidity reading
    float t = sht31.readTemperature();
    float h = sht31.readHumidity();

    // Save readings to data logger
    logfile.print(", ");
    logfile.print(c);
    logfile.print(", ");
    logfile.print(t);

```

```

    logfile.print(", ");
    logfile.print(h);
    logfile.print(", ");
    logfile.print(d);
    logfile.print(", ");
    logfile.print(e);
    #if ECHO_TO_SERIAL
    // Display readings on Serial Monitor
    Serial.print(", ");
    Serial.print(c);
    Serial.print(", ");
    Serial.print(t);
    Serial.print(", ");
    Serial.print(h);
    Serial.print(", ");
    Serial.print(d);
    Serial.print(", ");
    Serial.print(e);
    #endif //ECHO_TO_SERIAL

    logfile.println();
    #if ECHO_TO_SERIAL
    Serial.println();
    #endif // ECHO_TO_SERIAL

    // Now we write data to disk!
    if ((millis() - syncTime) < SYNC_INTERVAL) return;
    syncTime = millis();

    logfile.flush();
}

```

Listing N.1: Arduino Temperature Sensor Code.

Appendix O

Signal Processing Code

```
%%%%
% Title: Lamb Wave Signal Processing
% Student: Michael Gall
% Student ID: 0061009722
% Date: August 2016
% Description: Code reads the lamb wave response from the excel file and
% plots it as a signal, FFT, phase shift and zoomed FFT.
%%%%

%% Data Clear

clc
clear all
close all

%% Signal

Fs = 10000000;           % Sampling frequency
t = 0:1/Fs:0.001;        % Time vector

m = xlsread('CFRP20JulyTestcopy.xlsx',1,'B:B'); % Load Excel File

m2 = reshape(m,1,10000); % Reshape signal to appropriate vector

m_segment = m2;%(3404:5103); % To analyse single pulse of signal

nfft = length(m_segment); % Length of FFT

figure(1)                % Plot Wave
plot(m_segment);
title('Wave Signal');
xlabel('Time (s)');
ylabel('Amplitude');
```

```

print( 'WaveW1', '-dpng' )

%% FFT

X1 = fft( m_segment, nfft );           % FFT of signal

X2 = X1(1:nfft/2);

mx = abs(X2);

f1 = (0:nfft/2-1)*Fs/nfft;

figure(2);                             % Plot FFT
plot(f1,mx);
set(gca,'XTick',[0:1e5:5e6]);
grid on
title('FFT of Signal');
xlabel('Frequency (Hz)');
ylabel('Power');
print('FFTW1', '-dpng')

%% Phase Shift

p = unwrap(angle(X1));                  % Signal Phase

f2 = (0:length(X1)-1)/length(X1)*Fs;   % Frequency vector

figure(3)                               % Plot Phase Shift
plot(f2,p)
grid on
set(gca,'XMinorTick','on','XTick',[0:1e5:10e6]);
title('Phase of Signal');
xlabel('Frequency (Hz)');
ylabel('Phase (rad)');
print('PhaseW1', '-dpng')

%% FFT Small

figure(4);                              % Plot Zoomed FFT
plot(f1(1:1000),mx(1:1000));
grid on
title('FFT of Signal');
xlabel('Frequency (Hz)');
ylabel('Power');
print('FFTRW2short', '-dpng')

```

Listing O.1: MATLAB Signal Processing Code.

Appendix P

Ambiguity Function

```
%%%%
% Title: Ambiguity Function Signal Processing
% Student: Michael Gall
% Student ID: 0061009722
% Date: August 2016
% Description: Undertakes a signal correlation and runs the lamb wave
% response through the ambiguity fuinction
%%%%

%% Data Clear
clc;
clear all;
close all;

%%

fs = 10000000;           % Sampling frequency
t = 0:1/(fs):0.001;      % Time vector

f = 100000;              % Wave frequency

Max_f = 1;
%Max_t = 0.001;
Max_t = 0.00017;

m = sin(2*pi*f*t);

S1 = m;%(1:1700);
OS1 = S1;

t = t;%(1:1700);

n = xlsread('Aluminium7AugTest.xlsx',21,'E:E');
```

```

n_segment = n;%(4044:5743);

S2 = reshape(n_segment,1,10000);
OS2 = S2;

%fs = 1700;

%% DETERMINE WINDOW CORRELATION

[acorr,lag]=xcorr(S1,S2);

[~,I] = max(abs(acorr));
lagDiff = lag(I);
timeDiff = lagDiff/fs;
fprintf(1, 'Lag: %d Samples, %d Seconds\n', lagDiff, timeDiff);

%% DETERMINE TOTAL NUMBER OF SAMPLES IN EACH VECTOR
ReferenceSigLength = length(S1);
SurveillanceSigLength = length(S2);

%% DETERMINE OVERALL VECTOR SIZE
if ReferenceSigLength <= SurveillanceSigLength
    OverallLength = ReferenceSigLength;
else if SurveillanceSigLength < ReferenceSigLength
    OverallLength = SurveillanceSigLength;
end
end

%% TRUNCATE VECTORS TO EQUAL LENGTH
S1(OverallLength+1:end)=[];
S2(OverallLength+1:end)=[];

S1nl = S1;
S2nl = S2;

%% CROSS-CORRELATION
if lagDiff >= 0.1
    lagDiffnew = abs(lagDiff);
    S2al = S2(1:(end-lagDiffnew));
    S2al = [zeros(1,lagDiffnew),S2al];
else if lagDiff <= -0.1
    lagDiffnew = abs(lagDiff);
    S2al = S2((lagDiffnew):end);
    S2al(numel(S1)) = 0;
else
    S2al = S2;
end
end

S2 = S2al;

%% Check

```

```
[acorr, lag]=xcorr(S1,S2);

[~,I] = max(abs(acorr));
lagDiff = lag(I);
timeDiff = lagDiff/fs;
fprintf(1, 'Lag: %d Samples, %d Seconds\n', lagDiff, timeDiff);
```

```
%% Amibuity FUnction
```

```
[TDOA, FDOA] = CAF(S1, S2, Max_f, fs, Max_t);
```

Listing P.1: MATLAB Ambiguity Function Code.

```
function [TDOA, FDOA] = CAF(S1, S2, Max_f, fs, Max_t);
```

```
% Reference: Johnson, L. (2001). CAF.m. Monterey, California: NAVAL  
POSTGRADUATE SCHOOL.
```

```
% *****  
% CAF takes as inputs two sampled signal vectors (S1 & S2) in analytic  
% signal format, the maximum expected FDOA in Hertz (Max_f), the  
% sampling frequency used to generate S1 & S2 (fs), and the maximum  
% expected TDOA in seconds (Max_t). The function then utilizes  
% Stein's method in [1] to compute coarse estimations of TDOA and  
% FDOA between S1 & S2. Finally, "fine mode" calculations are made  
% to compute the final TDOA and FDOA, which are returned to the  
% user via the output arguments.  
% Written by: LCDR Joe J. Johnson, USN  
% Last modified: 17 September 2001  
% *****
```

```
clc;
```

```
N = length(S1);  
S1 = reshape(S1,N,1);  
S2 = reshape(S2,N,1);
```

```
S1_orig = S1;  
S2_orig = S2;
```

```
% Ensures signals are column vectors due to % Matlab's better efficiency on  
columns  
% Want to preserve original input signals % for later use; S1 & S2 will be  
% manipulated in the fine mode below.  
% The following while loop ensures that the sub-block size, N1, is  
% large enough to ensure proper resolution. If Max_f/fs*N1 were  
% less than 1, then the Freq calculated at the end would always be  
% + or - 1/N1! 2^19 = 524288 is about the limit for efficient  
% processing speed.
```

```
N1=1024;  
while (Max_f/fs*N1 < 2) & (N1 < 2^19)
```

```

N1 = 2*N1;
end
N2=N1/2;

if N1 > N
S1 = [S1;zeros(N1-N,1)];
S2 = [S2;zeros(N1-N,1)];
N = N1;
end

% For cases where resolution calls for % a sub-block size larger than the
% signal vectors, pad the vectors with % zeros so that they have a total of
% N1 elements.

% Want magnitude of Max_f, since +&- will be used below
Max_f = abs(Max_f);
Number_of_Blocks = length(S1)/N1;
Min_v = floor(-Max_f/fs*N1);
Max_v = -Min_v;
v_values = Min_v : Max_v;
Max_samples = Max_t * fs;

% Number of sub-blocks to break % the signal into
% Smallest freq bin to search % Largest freq bin to search % Vector of all
% bins to search
% Maximum number of samples to search
% Finds max number of block shifts (q) that must occur for each % R and v
% below.
if Max_samples > N2
q_max = min(ceil((Max_samples - N2)/N1),Number_of_Blocks-1);
else q_max = 0;
end

x=0;
divisors = Number_of_Blocks:-1:1; % Used to scale "temp" below...

% *****
% COARSE MODE computations.
% *****
for v = 1:length(v_values)
temp(1:N1,1:q_max+1)=0; % Initializing — saves time...
for R = 0:Number_of_Blocks-1
% temp1 is the FFT of the R'th block of S1, shifted by "v" bins.
temp1 = fftshift(fft(S1(1+R*N1 : N1*(R+1))));
temp1 = shiftud(temp1,v_values(v),0);
for q = 0:q_max
% R+q cannot exceed the number of sub-blocks
if R + q > Number_of_Blocks-1 break
end

% FFT of the (R+q)'th block of S2
temp2 = fftshift(fft([S2(1+(R+q)*N1 : N2 + N1*(R+q));...
zeros(N2,1)]));

```

```

% Multiplies temp1 & temp2, FFTs the product, then adds to
% previous values for the same value of q (but different R)
temp(:,q+1) = temp(:,q+1) + ...
abs(fftshift(fft(temp1.*conj(temp2))));
end
end

% Each value of q was used a different # of times, so they must be
% scaled properly.
for q_index = 1:q_max+1
temp(:,q_index) = temp(:,q_index) / divisors(q_index);
end

% If combination of current v and any q provides a greater value
% than the previous max, then remember m, Q, & V.
if max(max(temp))>x
x = max(max(temp));
[m Q] = find(temp == max(max(temp)));
% Must do this since q starts at 0, but Matlab doesn't allow for
% zero indexing.
Q = Q - 1;
V = v_values(v);
end
end

% Coarse estimate of TDOA (in # of samples)
TDOA_Coarse = Q * N1 + (-N2+1 + m);

% Coarse estimate of FDOA (in Freq Bin #)
FDOA_Coarse = V/N1*N;

% The following 3 lines can be used to display the coarse estimates,
% if desired.
%disp(['The coarse TDOA estimate is: ', num2str(TDOA_Coarse), ...
% ' samples.']);
%disp(['The coarse FDOA estimate is: ', num2str(FDOA_Coarse/N), ...
% ' (digital frequency).']);

% *****
% FINE MODE computations.
% *****

S2 = conj(S2); % S2 is conjugated in basic CAF definition

% Vector of freq "bins" to use (DON'T have to be integers!!)
k_val = FDOA_Coarse-10 : FDOA_Coarse+10;

% Vectors of TDOAs to use (must be integers)
tau_val = TDOA_Coarse-10 : TDOA_Coarse+10;

done = 0;
multiple = 1;
decimal = 0;

```

```

while ~done % Fine mode iterations continue until user is done.

    % Initialize to make later computations faster
    amb(length(k_val),length(tau_val))=0;
    Ntemp = N * multiple;

    for k = 1:length(k_val) % Must loop through all values of k

        % Vector of complex exponentials that will be used
        exponents = exp(-j*2*pi*k_val(k)/Ntemp*(0:Ntemp-1)');

        % Must loop through all potential TDOAs
        for t = 1:length(tau_val)

            % S2 is shifted "tau" samples
            S2temp = shiftud(S2,tau_val(t),0);

            % Definition of CAF summation
            temp = abs(sum(S1.*S2temp.*exponents));

            % Save CAF magnitude for the values of k & t
            amb(k,t)=temp;
        end
    end

    [k, t]=find(amb==max(max(amb))); % Find the peak of the CAF matrix

    TDOA = tau_val(t); % TDOA and FDOA associated with the peak of the

    FDOA = k_val(k); % CAF plane. These represent the final TDOA
    % & FDOA estimates.

    % The results are displayed.
    disp(' ');disp(' ');disp(' ');
    disp(['The TDOA is ', num2str(TDOA/multiple), ' samples']);
    disp([' or ', num2str(TDOA/(multiple*fs)), ' seconds.']);
    disp(' ');
    disp(['The resolution is ', num2str(0.5/...
    (multiple*fs)), ' seconds.']);
    disp(' ');disp(' ');
    disp(['The FDOA is ', num2str(FDOA/N) ,...
    ' in digital frequency (k/N)']);
    disp([' or ', num2str(FDOA/N*fs), ' Hz.']);
    disp(' ');
    disp(['The resolution is ', num2str(0.5*...
    (10^decimal)/N*fs), ' Hz.']);
    disp(' ');
    disp(' ');
    disp(' ');

    % If the signal length exceeds 524288 elements, max processing
    % capability has been achieved, and the user will not be given
    % the option of refining TDOA any further.
    if Ntemp >= 2^19

```

```

disp('Maximum TDOA processing capability has been achieved.')
doneT = 1;
else doneT = 0;
end

% User chooses whether to compute more accurate TDOA &/or % FDOA, or to
  stop fine mode computations.
disp('Do you desire a solution with finer resolution?');
disp('Select one of the following:'); disp(' ');

if ~doneT
disp('1. Finer resolution for TDOA. ');
else disp(' ');
end
disp('2. Finer resolution for FDOA. ');
if ~doneT
disp('3. Finer resolution for both TDOA and FDOA. ');
else disp(' ');
end
disp('4. The TDOA and FDOA resolutions are fine enough. '); disp(' ');

choice = input('What is your selection? ');

switch choice

% TDOA is refined by resampling the signals at twice the
% previous sampling rate. Increases resolution two-fold.
    case 1
        if ~doneT
            multiple = multiple*2;
            S1 = interp(S1, 2);
            S2 = interp(S2, 2);
            tau_val = TDOA*2 - 1 : TDOA*2 + 1;
            else done = 1;
        end
        clc;

% FDOA resolution is improved by a factor of 10.
    case 2
        decimal = decimal - 1;
        k_val = FDOA - 5*10^decimal : 10^decimal : FDOA + 5*10^decimal;
        clc;

% Both TDOA and FDOA resolutions are improved.
    case 3
        if ~doneT
            multiple = multiple*2;
            S1 = interp(S1, 2);
            S2 = interp(S2, 2);
            tau_val = TDOA*2 - 1 : TDOA*2 + 1;

        decimal = decimal - 1;
        k_val = FDOA - 5*10^decimal : 10^decimal : FDOA + ...
            5*10^decimal;

```

```

else done = 1;
end
clc;
otherwise
done = 1;
end

if done
disp(' '); disp(' '); disp('TDOA & FDOA estimation complete. ');
end
end

5*10^decimal;
% If user wants to see the CAF surface graphically, a call to % CAF_peak is
  made.
disp(' '); %disp(' '); disp(' ');
choice = input...
('Would you like to see the CAF peak graphically (Y or N)? ', 's'); choice =
  upper(choice);
switch choice
  case 'Y'
caf_peak(S1_orig, S2_orig, floor(TDOA/multiple) - 50, ...
  floor(TDOA/multiple) + 50, (FDOA-20)/N, (FDOA+20)/N, fs);
end
TDOA = TDOA/(multiple*fs); % Returns TDOA in seconds.
FDOA = FDOA/N*fs; % Returns FDOA in Hertz.
disp('Program Complete. ');

```

Listing P.2: MATLAB Ambiguity Function CAF Code.

```

function [TDOA, FDOA, MaxAmb, Amb] = ...
  caf_peak(S1, S2, Tau_Lo, Tau_Hi, Freq_Lo, Freq_Hi, fs);

% Reference: Johnson, L. (2001). CAFpeak.m. Monterey, California: NAVAL
  POSTGRADUATE SCHOOL.

% *****
% CAF_peak(S1, S2, Tau_Lo, Tau_Hi, Freq_Lo, Freq_Hi) takes as input:
% two signals (S1, S2) that are row or column vectors; a range of
% time delays (in samples) to search (Tau_Lo, Tau_Hi must be
% integers between -N & +N); a range of digital frequencies (in
% fractions of sampling frequency) to search (Freq_Lo, Freq_Hi must
% be between -1/2 and 1/2, or -(N/2)/N and (N/2)/N, where N is the
% length of the longer of the two signal vectors); and the sampling
% frequency, fs. %
% The function computes the Cross Ambiguity Function of the two
% signals. Four plots are produced which represent four different
% views of the Cross Ambiguity Function magnitude versus the input
% Tau and Frequency Offset ranges. %
% The function returns the scalars TDOA, FDOA, and MaxAmb, where
% TDOA & FDOA are the values of Time Delay and Frequency Offset
% that cause the Cross Ambiguity Function to peak at a magnitude
% of MaxAmb. Amb is the matrix of values representing the CAF

```

```

% surface.

% Written by: LCDR Joe J. Johnson, USN
% Last modified: 26 August 2001
% *****

% Ensures that the user enters all SIX required arguments.
if (nargin < 6)
    error...
    ('6 arguments required: S1, S2, Tau_Lo, Tau_Hi, Freq_Lo, Freq_Hi');
end

% Ensures that both S1 & S2 are row- or column-wise vectors.
if ((size(S1,1)~=1)&(size(S1,2)~=1)) | ((size(S2,1)~=1)&...
    (size(S2,2)~=1))
    error('S1 and S2 must be row or column vectors. ');
end

N1 = length(S1);
N2 = length(S2);
S1 = reshape(S1,N1,1);
S2 = reshape(S2,N2,1);

S1 = [S1;zeros(N2-N1,1)];
S2 = [S2;zeros(N1-N2,1)];
% S1 & S2 are reshaped into column-wise % vectors since MATLAB is more
    efficient % when manipulating columns.
% Ensure that S1 & S2 are the same size ,
% padding the smaller one w/ 0s as needed.
% This WHILE loop simply ensures that the length of S1 & S2 is a power
% of two. If not, the vectors are padded with 0s until their length
% is a power of two. This is not required, but it takes advantage of
% the fact that MATLAB's FFT computation is significantly faster for
% lengths which are powers of two!

while log(length(S1))/log(2) ~= round(log(length(S1))/log(2))
    S1(length(S1)+1) = 0;
    S2(length(S2)+1) = 0;
end

N = length(S1);

% Ensures that the Tau values entered are in the valid range.
if abs(Tau_Lo)>N | abs(Tau_Hi)>N
    error('Tau_Lo and Tau_Hi must be in the range -N to +N. ');
end

% Ensures that Tau values entered by the user are integers.
if (Tau_Lo ~= round(Tau_Lo)) | (Tau_Hi ~= round(Tau_Hi))
    error('Tau_Lo and Tau_Hi must be integers. ')
end

% Ensures that the Frequency values entered are in the valid range.
if abs(Freq_Lo)>1/2 | abs(Freq_Hi)>1/2

```

```

error('Freq_Lo and Freq_Hi must be in the range -0.5 to +0.5');
end

% Ensures that the lower bounds are less than the upper bounds.
if (Tau_Lo > Tau_Hi) | (Freq_Lo > Freq_Hi)
    error('Lower bounds must be less than upper bounds.')
end

% Freq values converted into integers for processing.
Freq_Lo = round(Freq_Lo*N);
Freq_Hi = round(Freq_Hi*N);

% Creates vectors for the Tau & Freq values entered by the user. Used % for
    plotting...
TauValues = [Tau_Lo:Tau_Hi];
FreqValues = [Freq_Lo:Freq_Hi]/N;

% The IF statement calculates the indices required to isolate the % user-
    defined frequencies from the FFT calculations below.
if Freq_Lo < 0 & Freq_Hi < 0
    Neg_Freq = (N+Freq_Lo+1:N+Freq_Hi+1);
    Pos_Freq = [];
elseif Freq_Lo < 0 & Freq_Hi >= 0
    Neg_Freq = (N+Freq_Lo+1:N);
    Pos_Freq = (1:Freq_Hi+1);
else
    Neg_Freq = [];
    Pos_Freq = (Freq_Lo+1:Freq_Hi+1);
end

% This FOR loop actually calculates the Cross Ambiguity Function for % the
    given range of Taus and Frequencies. Note that an FFT is
% performed for each Tau value and then the frequencies of interest
% are isolated using the Neg_Freq and Pos_Freq vectors obtained above. %
    For each value of Tau, the vector S2 is shifted Tau samples using a
% call to the separate function "SHIFTUD". Samples shifted out are %
    deleted and zeros fill in on the opposite end.

% Initializing Amb with 0s makes computations much faster.

Amb=zeros(length(Neg_Freq)+length(Pos_Freq),length(TauValues));
for t = 1:length(TauValues)
    temp = fft((S1).*conj(shiftud(S2,TauValues(t),0)));
    Amb(:,t) = [temp(Neg_Freq);temp(Pos_Freq)];
end

% Only interested in the Magnitude of the Cross Ambiguity Function.
Amb = abs(Amb);

% The following will remove any spike that occurs at Tau = FreqOff = 0.
% This may be desired in some cases, especially when the spike at (0,0)
% is due to correlation of the two signals' noise components. The
% spike, of course, could also indicate that the two signals have no
% TDOA or FDOA between them.

```

```

% if find(TauValues == 0) & find(FreqValues == 0)
% Amb(find(FreqValues==0),find(TauValues==0)) = 0;
% end
%clc; %Clears the MATLAB command window.
% The four different views of the Cross Ambiguity Function plots are %
%   created here.

figure % This one is the 3-D view
mesh(TauValues/fs , FreqValues*fs , Amb);
xlabel('TDOA (Seconds)');
ylabel('FDOA (Hertz)');
zlabel('Magnitude');
title('Cross Ambiguity Function');

figure
subplot(2,1,1) % This one is the 2-D view along the TDOA axis
mesh(TauValues/fs , FreqValues*fs , Amb);
xlabel('TDOA (Seconds)');
zlabel('Magnitude'); view(0,0);
subplot(2,1,2) % This one is the 2-D view along the FDOA axis
mesh(TauValues/fs , FreqValues*fs , Amb);
ylabel('FDOA (Hertz)'); zlabel('Magnitude'); view(90,0);

%This one is a 2-D view looking down on the plane
figure
mesh(TauValues/fs , FreqValues*fs , Amb);
xlabel('TDOA (Seconds)');
ylabel('FDOA (Hertz)');
zlabel('Magnitude');
title('Cross Ambiguity Function');
view(0,90);

% Finds the indices of the peak value.
[DFO, DTO] = find(Amb==max(max(Amb)));

TDOA = TauValues(DTO);
FDOA = FreqValues(DFO);
MaxAmb = max(max(Amb));

% Finds the actual value of the TDOA.
% Finds the actual value of the FDOA.
% Finds the actual Magnitude of the peak.

% The remaining lines will display the numerical results of the
% TDOA & FDOA, if desired. Since the FFT method was used for the
% calculations, the TDOA is accurate only to within +/- 0.5 samples,
% and the FDOA is accurate to within +/- 0.5/N in digital frequency.

% disp(' '); disp(' ');
% disp(['The TIME LAG (TDOA) is: ', num2str(TDOA), ' Samples.']);
% disp(' ');
% disp(['The FREQ OFFSET (FDOA) is: ', num2str(FDOA), ...
% ' (Fraction of Fs).']);
% disp(' '); disp(['Maximum Magnitude = ', num2str(MaxAmb)]);

```

```
% disp(' '); disp('_____');
% disp('NOTE: If the CAF plot has secondary peaks whose magnitudes');
% disp('are within about 80% of the Main Peak's magnitude,');
% disp('then the above results may be unreliable. Likely');
% disp('reasons: The true peak is not within the range of,');
% disp('Taus & Freq Offsets that you entered or the signals');
% disp('may be too noisy to detect the peak.');
```

Listing P.3: MATLAB Ambiguity Function CAF_Peak Code.

```
function y=shiftud(a,n,cs)

% Reference: Johnson, L. (2001). IMPLEMENTING THE CROSS AMBIGUITY FUNCTION
% AND GENERATING GEOMETRY-SPECIFIC SIGNALS. NAVAL POSTGRADUATE SCHOOL.

% ***** %
% SHIFTUD Shift or Circularly Shift Matrix Rows
% SHIFTUD(A,N) with N<0 shifts the rows of A DOWN N rows.
% The first N rows are replaced by zeros and the last N
% rows of A are deleted. %
% SHIFTUD(A,N) with N>0 shifts the rows of A UP N rows.
% The last N rows are replaced by zeros and the first N
% rows of A are deleted. %
% SHIFTUD(A,N,C) where C is nonzero performs a circular
% shift of N rows, where rows circle back to the other
% side of the matrix. No rows are replaced by zeros. %
% Copyright (c) 1996 by Prentice-Hall, Inc. ? Reference [9]
% *****

if nargin<3, cs=0; end
cs=cs(1);
[r,c]=size(a);
dn=(n<=0);
n=min(abs(n),r);

if n==0|(cs&n==r)
    y=a;
% If no third argument, default is False % Make sure third argument is a
% scalar % Get dimensions of input
% dn is True if shift is down
% Limit shift to less than rows
% Simple no shift case
elseif ~cs&dn
    y=[zeros(n,c); a(1:r-n,:)] ;
elseif ~cs&~dn
    y=[a(n+1:r,:); zeros(n,c)] ;
elseif cs&dn
    y=[a(r-n+1:r,:); a(1:r-n,:)] ;
elseif cs&~dn
    y=[a(n+1:r,:); a(1:n,:)] ;
end
% No circular and down % No circular and up
% Circular and down
```

```
% Circular and up
```

Listing P.4: MATLAB Ambiguity Function Shifted Code.

